



Universitat Autònoma de Barcelona

ADVERTIMENT. L'accés als continguts d'aquesta tesi queda condicionat a l'acceptació de les condicions d'ús establertes per la següent llicència Creative Commons:  http://cat.creativecommons.org/?page_id=184

ADVERTENCIA. El acceso a los contenidos de esta tesis queda condicionado a la aceptación de las condiciones de uso establecidas por la siguiente licencia Creative Commons:  <http://es.creativecommons.org/blog/licencias/>

WARNING. The access to the contents of this doctoral thesis it is limited to the acceptance of the use conditions set by the following Creative Commons license:  <https://creativecommons.org/licenses/?lang=en>

UNIVERSITAT AUTÒNOMA DE BARCELONA

DOCTORAL THESIS

**Understanding color vision:
from psychophysics to computational
modeling**

Author:
Xim CERDA-COMPANY

Supervisor:
Dr. Xavier OTAZU

*A thesis submitted in fulfillment of the requirements
for the degree of Doctor of Philosophy*

in the

NeuroComputation and Biological Vision Team (Neurobit)
Centre de Visió per Computador / Departament de Ciències de la
Computació

January 24, 2019



**Universitat Autònoma
de Barcelona**



neuroBIT

Director	<p>Dr. Xavier Otazu Computer Vision Center Universitat Autònoma de Barcelona, Spain</p>
Thesis committee	<p>Dr. Arash Akbarinia Abteilung Allgemeine Psychologie Justus-Liebig-Universität Gießen, Germany</p> <p>Dr. Matthias S. Keil Dept. de Cognició, Desenvolupament i Psicologia de l'Educació Universitat de Barcelona, Spain</p> <p>Dr. Sophie Wuerger Dept. of Psychological Sciences University of Liverpool, UK</p>
International evaluators	<p>Dr. Sérgio MC Nascimento Departamento de Física University of Minho, Portugal</p> <p>Dr. Javier Vazquez-Corral School of Computing Sciences University of East Anglia, UK</p>

The research described in this book was carried out at the Centre de Visió per Computador, Universitat Autònoma de Barcelona. Copyright ©2019 by Xim Cerda-Company. All rights reserved. No part of this publication may be reproduced or transmitted in any form or by any means, electronic or mechanical, including photocopy, recording, or any information storage and retrieval system, without permission in writing from the author.

ISBN: 978-84-948531-4-2

Printed by Ediciones Gráficas Rey, S.L.

Declaration of Authorship

I, Xim CERDA-COMPANY, declare that this thesis titled, "Understanding color vision:

from psychophysics to computational modeling" and the work presented in it are my own. I confirm that:

- This work was done wholly or mainly while in candidature for a research degree at this University.
- Where I have consulted the published work of others, this is always clearly attributed.
- Where I have quoted from the work of others, the source is always given. With the exception of such quotations, this thesis is entirely my own work.
- I have acknowledged all main sources of help.
- Where the thesis is based on work done by myself jointly with others, I have made clear exactly what was done by others and what I have contributed myself.

Signed: Xim Cerda Company

Date: January 24, 2019

"I know that I know nothing."

Socrates

"A person who never made a mistake never tried anything new."

Albert Einstein

"The harder I practice, the luckier I get."

Gary Player

UNIVERSITAT AUTÒNOMA DE BARCELONA

Abstract

Escola d'Enginyeria
Centre de Visió per Computador / Departament de Ciències de la Computació

Doctor of Philosophy

**Understanding color vision:
from psychophysics to computational modeling**

by Xim CERDA-COMPANY

In this PhD we have approached the human color vision from two different points of view: psychophysics and computational modeling. First, we have evaluated 15 different tone-mapping operators (TMOs). We have conducted two experiments that consider two different criteria: the first one evaluates the local relationships among intensity levels and the second one evaluates the global appearance of the tone-mapped images w.r.t. the physical one (presented side by side). We conclude that the rankings depend on the criterion and they are not correlated. Considering both criteria, the best TMOs are *KimKautz* (Kim and Kautz, 2008) and *Krawczyk* (Krawczyk, Myszkowski, and Seidel, 2005). Another conclusion is that a more standardized evaluation criteria is needed to do a fair comparison among TMOs.

Secondly, we have conducted several psychophysical experiments to study the color induction. We have studied two different properties of the visual stimuli: temporal frequency and luminance spatial distribution. To study the temporal frequency we defined equiluminant stimuli composed by both uniform and striped surrounds and we flashed them varying the flash duration. For uniform surrounds, the results show that color induction depends on both the flash duration and inducer's chromaticity. As expected, in all chromatic conditions color contrast was induced. In contrast, for striped surrounds, we expected to induce color assimilation, but we observed color contrast or no induction. Since similar but not equiluminant striped stimuli induce color assimilation, we concluded that luminance differences could be a key factor to induce color assimilation. Thus, in a subsequent study, we have studied the luminance differences' effect on color assimilation. We varied the luminance difference between the target region and its inducers and we observed that color assimilation depends on both this difference and the inducer's chromaticity. For red-green condition (where the first inducer is red and the second one is green), color assimilation occurs in almost all luminance conditions. Instead, for green-red condition, color assimilation never occurs. Purple-lime and lime-purple chromatic conditions show that luminance difference is a key factor to induce color assimilation. When the target is darker than its surround, color assimilation is stronger in purple-lime, while when the target is brighter, color assimilation is stronger in lime-purple ('mirroring' effect). Moreover, we evaluated whether color assimilation is due to luminance or brightness differences. Similarly to equiluminance condition, when the stimuli are equibrightness no color assimilation is induced. Our results support the hypothesis that mutual-inhibition plays a major role in color perception, or at least in color induction.

Finally, we have defined a new firing rate model of color processing in the V1 parvocellular pathway. We have modeled two different layers of this cortical area: layers $4C\beta$ and $2/3$. Our model is a recurrent dynamic computational model that considers both excitatory and inhibitory cells and their lateral connections. Moreover, it considers the existent laminar differences and the cells' variety. Thus, we have modeled both single- and double-opponent simple cells and complex cells, which are a pool of double-opponent simple cells. A set of sinusoidal drifting gratings have been used to test the architecture. In these gratings we have varied several spatial properties such as temporal and spatial frequencies, grating's area and orientation. To reproduce the electrophysiological observations, the architecture has to consider the existence of non-oriented double-opponent cells in layer $4C\beta$ and the lack of lateral connections between single-opponent cells. Moreover, we have tested our lateral connections simulating the center-surround modulation and we have reproduced physiological measurements where for high contrast stimulus, the result of the lateral connections is inhibitory, while it is facilitatory for low contrast stimulus.

UNIVERSITAT AUTÒNOMA DE BARCELONA

Abstract

Escola d'Enginyeria
Centre de Visió per Computador / Departament de Ciències de la Computació

Doctor of Philosophy

**Understanding color vision:
from psychophysics to computational modeling**

by Xim CERDA-COMPANY

En aquest doctorat, hem estudiat la visió del color dels humans des de dos punts de vista diferents: la psicofísica i la modelització computacional. Primer, hem avaluat 15 "tone-mapping operators" (TMOs) diferents en dos experiments que consideren criteris diferents: el primer té en compte les relacions locals entre nivells d'intensitat i el segon avalua l'aparença global de la imatge resultant respecte l'escena física (presentades una al costat de l'altra). La conclusió és que els rankings depenen del criteri utilitzat i que no estan correlacionats. Considerant els dos criteris, els millors TMOs són el *KimKautz* (Kim and Kautz, 2008) i el *Krawczyk* (Krawczyk, Myszkowski, and Seidel, 2005). Tot i això, s'han de definir criteris estàndards per a poder fer una comparació justa entre els diferents TMOs.

Després, hem realitzat diferents experiments psicofísics per estudiar la inducció del color. Bàsicament, hem estudiat dues propietats diferents dels estímuls: la freqüència temporal i la distribució espacial de la lluminància. Per a estudiar la freqüència temporal, vam definir uns estímuls equiluminants compostos per voltants uniformes i ratllats, els quals els vam mostrar durant un flash. En els voltants uniformes, els resultats mostren que la inducció del color depèn de la duració del flash i de la cromaticitat del inductor. Tal com esperàvem, en totes les diferents condicions cromàtiques, es va induir contrast cromàtic. Per contra, en els voltants ratllats, esperàvem induir assimilació cromàtica, però vam observar contrast o no inducció. Com que estímuls ratllats similars, que no són equiluminants, indueixen assimilació del color, vam concloure que les diferències llumíniques podien ser un factor clau per a la inducció. Per tant, hem analitzat l'efecte de les diferències llumíniques en l'assimilació. Vam variar les diferències de lluminància entre la regió d'interès i els seus inductors i vam veure que l'assimilació cromàtica depèn d'aquestes diferències i de la cromaticitat del inductor. En la condició vermell-verd (quan el primer inductor és vermell i el segon és verd), l'assimilació de color es produeix en gairebé totes les condicions llumíniques. En canvi, en el cas del verd-vermell, mai s'observa assimilació del color. Les condicions lila-llima i llima-lila mostren clarament que la diferència llumínica és un factor clau per induir assimilació del color. Quan la regió d'interès és més fosca que el seu voltant, l'efecte és més fort en la condició lila-llima, mentre que quan la regió d'interès és més brillant, l'efecte és més fort en la condició llima-lila (efecte mirall). A més a més, vam avaluar si l'assimilació del color ve donada per diferències llumíniques o de brillantor. De manera similar a la condició equiluminant, no s'observa assimilació del color quan l'estímul és equibrillant. Els nostres resultats donen suport a la hipòtesis que la inhibició mútua juga un rol important en la percepció del color, o com a mínim en la inducció del color.

Finalment, hem definit un nou model del processament del color (del "parvocel·lular pathway") a V1. Hem modelitzat dues capes diferents: les capes $4C\beta$ i $2/3$. El nostre model és una xarxa dinàmica recurrent que considera neurones excitadores i inhibidores i les seves connexions laterals. A més, també considera les diferències laminars existents i les diferents cèl·lules que les componen. Per tant, hem modelitzat les neurones simples "single-" i "double-opponent" i les neurones complexes, les quals es consideren un conjunt de neurones simples "double-opponent". Per testejar l'arquitectura, hem utilitzat un conjunt de "drifting gratings" sinusoidals i hem variat algunes de les seves propietats com la freqüència temporal i espacial, la seva àrea i la seva orientació. Per reproduir les observacions electrofisiològiques, vam haver de suposar l'existència d'unes neurones "double-opponent" sense selectivitat a orientació i la falta de connexions laterals entre neurones "single-opponent". A més a més, hem testejat les connexions laterals modelitzades simulant la modulació del centre i voltant. Hem observat que quan l'estímul té un alt contrast, el resultat d'aquestes connexions és inhibitori, però és facilitatori quan el contrast és baix.

Acknowledgements

First, I would like to thank my PhD supervisor *Dr. Xavier Otazu* for his useful advice and comments about the work. I believe that he has done his best to help me in this project. Although we did not always agree, I appreciated so much the time spent discussing about the results, methods and new ideas. If I repeated the PhD, I would choose him again as my supervisor. I hope we will be able to continue collaborating in new projects.

I also would like to express my gratitude to *Dr. C. Alejandro Parraga* and *Dr. Olivier Penacchio*. The former made me aware of the importance of writing well the papers, to make them comprehensible. Moreover, he introduced to me in the psychophysics world, pointing out the importance of being accurate. The latter is a research and personal reference for me. Both together make me to believe that "the simplest, the best".

My sincere thanks to the rest of neurobitters, in particular, *Dr. Arash Akbarinia*, who is also another reference because of his hard working capability, and *Nilai Sal-lent*, who helped me so much conducting the experiments. *Us mereixeu tota la sort a la vida*. Furthermore, I would like to thank *Prof. Dr. Julie Harris* who welcomed me at University of St Andrews and all the *CVC members* for their great support and for doing my life more easy.

Last, but of course not least, I believe that this PhD could not be possible without the support of all both my family (*mama, Javi, papá, Miqui* and *Carlota*) and my in-laws (*Joe, Isa, Maria, Viktor, Anna* and *Moni*). *Moltes gràcies a tots per tot!*

I would like to give a special mention to my love *Bel*. When I started this project, she was my girlfriend and now she is my fiancée, but she is more than that, she is also my best friend. *T'estimo molt*.

Contents

Declaration of Authorship	v
Abstract	x
Catalan abstract	xiv
Acknowledgements	xvii
1 Introduction	1
1.1 What's color?	1
1.2 Is color that important?	1
1.2.1 Is object detection and/or recognition the aim of color vision?	1
1.3 How do we perceive colors?	3
1.4 How is color measured?	5
1.4.1 Could the physical and the perceived color be different?	5
1.5 Computational models	6
1.6 Sections of the dissertation	7
1.7 Summary of published works/studies	7
I Psychophysics	9
2 HDR	13
2.1 Introduction	13
2.1.1 Historical Context	13
2.1.2 Electronic HDR imaging	14
2.1.3 Tone-Mapping Operator	15
2.1.4 "Global" vs "Local" analysis	16
2.2 State-of-the-Art	17
2.2.1 Previous TMO Psychophysics	17
Experiments without a reference HDR scene	17
Experiments with a reference HDR scene	17
Experiments using an HDR monitor	19
2.2.2 Tone-Mapping Operators	19
2.3 Methods	22
2.3.1 Materials	22
2.4 Experiments	25
2.4.1 Experiment 1: Segment Matching	25
Procedure	25
Experimental Design	25
Participants	26
Results	26
2.4.2 Experiment 2: Scene Reproduction	28

	Procedure	28
	Experimental Design	29
	Participants	29
	Results	29
2.5	Discussion	30
2.5.1	Comparison to other Studies	32
2.6	Conclusions	33
2.7	Related Publications	34
3	Color Induction	35
3.1	Optics considerations	35
3.2	Color induction in equiluminant flashed stimuli	36
3.2.1	Introduction	36
3.2.2	Methods	37
	Apparatus	37
	Stimuli	38
	Subjects	41
	Experimental Procedure	42
3.2.3	Ethics approval	42
3.2.4	Data Analysis	42
3.2.5	Results	43
	Experiment U	43
	Experiment S	44
3.2.6	Discussion	46
	Uniform surround (Experiment U)	46
	Striped surround (Experiment S)	48
3.2.7	Computational Model	49
3.2.8	Conclusions	51
3.3	The effect of luminance and brightness differences on color assimilation	51
3.3.1	Introduction	51
	Color contrast	52
	Color assimilation	52
	Brightness induction	53
	Color processing by the human visual system	53
3.3.2	Methods	55
	Apparatus and Stimuli	55
	Subjects	58
	Experimental procedure	59
	Statistical analysis	59
3.3.3	Results	60
	Luminance experiment results	60
	Brightness experiment results	62
3.3.4	Discussion	65
	Psychophysics	65
	Neurophysiology	67
3.3.5	Conclusions	69
3.3.6	Future work	70
3.4	Related publications	71

II Computational Modeling	73
4 A computational model of color processing in V1	77
4.1 Introduction	77
4.1.1 Receptive fields	78
4.1.2 Lateral connections	80
4.1.3 Feedback connections	82
4.1.4 Color processing in the parvocellular pathway of V1	82
4.1.5 Computational models	83
4.2 Methods	84
4.2.1 Layer $4C\beta$	86
Simple cells	87
Complex cells	88
4.2.2 Layer 2/3	89
Simple cells	89
Complex cells	90
4.3 Results	92
4.3.1 Temporal frequency	92
4.3.2 Grating area	92
4.3.3 Spatial frequency	93
4.3.4 Orientation	94
4.3.5 Center-surround modulation	97
4.3.6 Lateral connections between SO cells	97
4.4 Discussion	97
4.5 Conclusions	99
4.6 Future work	101
4.7 Related publications	102
5 General Conclusions	103
A Statistical Analysis of Section 3.3	105
Bibliography	111

List of Figures

1.1	Is color that important?	2
1.2	Rods' and cones' density in the retina	3
1.3	Cones' visual spectra sensitivities	4
1.4	Visual pathway's scheme	5
1.5	Optical and visual illusions	6
2.1	Tone-mapping workflow	14
2.2	Chiaroscuro technique	15
2.3	High dynamic range scenes used in the experiments	23
2.4	Experiment 1 tasks	25
2.5	Experiment 1 results (slope difference)	27
2.6	Experiment 1 results (RMSE)	28
2.7	Experiment 2 results	30
3.1	Color induction examples	36
3.2	Examples of stimuli used in the equiluminant flashed color induction experiments	38
3.3	Spatial configuration of the stimuli used in the equiluminant flashed color induction experiments	40
3.4	Temporal configuration of the stimuli used in the equiluminant flashed color induction experiments	40
3.5	Results of Experiment U	44
3.6	Results of Experiment S	45
3.7	Computational simulation of the equiluminant flashed color induction experiments	50
3.8	Stimuli design in the luminance experiment	57
3.9	Luminance profile of stimuli for the <i>test ring</i> case	58
3.10	Color induction results for luminance experiment	61
3.11	Color induction results for the brightness experiment	63
3.12	Visual summary of the results for the <i>test ring</i> case	70
4.1	Receptive fields of ON- and OFF-neurons	79
4.2	Examples of simple and complex cells response	80
4.3	Simple cells in V1	81
4.4	Firing rate functions	85
4.5	Scheme of the provided architecture	86
4.6	Lateral connections summary	87
4.7	Stimuli used to test the architecture	91
4.8	Study of the drifting grating's temporal frequency	93
4.9	Study of the drifting grating's area	94
4.10	Study of the drifting grating's spatial frequency	95
4.11	Study of the drifting grating's orientation	96
4.12	Center-surround modulation	98

4.13	Results when lateral connections between SO cells are modeled	99
4.14	Electrophysiology recordings for different spatial frequencies	100
4.15	Electrophysiology recordings for different orientations	101

List of Tables

2.1	Summary of TMOs' characteristics	20
2.2	Both L* CIELab and luminances values of the reference table's patches	23
2.3	Photometric assessment of the scene facets	24
2.4	Performance of all TMOs in the Segment Matching experiment	26
2.5	Summary of all statistical analysis from Section 2.4.2	30
2.6	Ranking obtained by averaging the scores given by Case V Thurstone Law in the three different scenes	31
3.1	Summary of the experimental conditions for equiluminant flashed color induction experiments	41
3.2	Summary of the nested ANOVA results	46
3.3	Perceived brightness in the luminance experiment	62
3.4	Perceived brightness in the brightness experiment	64
A.1	Summary of the nested ANOVA results for both luminance and bright- ness experiments	106

List of Abbreviations

ANOVA	AN alysis O f V ariance
cRF	C lassical R eceptive F ield
CV	C ircular V ariance
DO	D ouble- O pponent
HDR	H igh D ynamic R ange
HVS	H uman V isual S ystem
LDR	L ow D ynamic R ange
LGN	L ateral G eniculate N ucleus
LSD	L east S ignificant D ifference
NO	N on- O pponent
O/P	O rthogonal-to- P referred O rientation
RF	R eceptive F ield
RFS	R eceptive F ield S imilarity
RMSE	R oot M ean S quare E rror
SO	S ingle- O pponent
TMO	T one- M apping O perator

Dedicated to my family and friends

Chapter 1

Introduction

1.1 What's color?

The answer to this question is not as simple as one could think. The definition of color depends on the personal background: a physicist would say that color is the spectrum of light that is reflected from a surface; a psychologist would say that it is the light you perceive; an engineer would say that it is a coordinate in a given color space and a neuroscientist would say that it is a visual feature that activates certain mechanisms of the visual system. Hence, we can say that color definition depends on the point of view. Fortunately, in this PhD, we have not tried to elucidate what color is, but we have studied this visual feature from different points of views: from psychology (through psychophysics) to neuroscience (through computational models).

1.2 Is color that important?

In our daily life, color is a helpful feature to describe the objects present in our environment. For example, when we are at a parking looking for our car, we differentiate our car from the others because of its brand and model (its shape), but also because of its color (see Figure 1.1 for a visual example). Nevertheless, in object recognition, color by itself is not as discriminative as shape (Stockman and Brainard, 2010). Therefore, if we describe our car as a combination of brand, model and color we would have a reduced number of candidates, but if we only describe it using the color instead, we would have a huge number of candidates (see Figures 1.1c for a visual example). In that sense, *Computer Vision* algorithms have shown that color descriptors, in combination with others such as shape, achieve excellent results in object detection and recognition (Van de Sande, Gevers, and Snoek, 2010; Khan et al., 2012).

1.2.1 Is object detection and/or recognition the aim of color vision?

Color vision is a striking feature of the *human visual system* (HVS). The Old World Monkeys were the first mammals who developed trichromacy (three different photoreceptors) and, thus, color vision. In particular, in some species the trichromatic color vision is linked to the gender (*e.g.*, female are trichromats but male are dichromats). The fact that we are able to perceive colors is not casual. Nowadays, nobody doubts that it is due to natural selection, but what's the aim of color vision? To this question, several theories arise: the frugivory and folivory theories (Reagan et al., 1998; Lucas et al., 1998; Reagan et al., 2001). The former supports the idea that color vision helps to detect fruits and the latter to detect edible young leaves (Mollon, 1989; Reagan et al., 1998; Lucas et al., 1998; Dominy and Lucas, 2001; Reagan et al.,

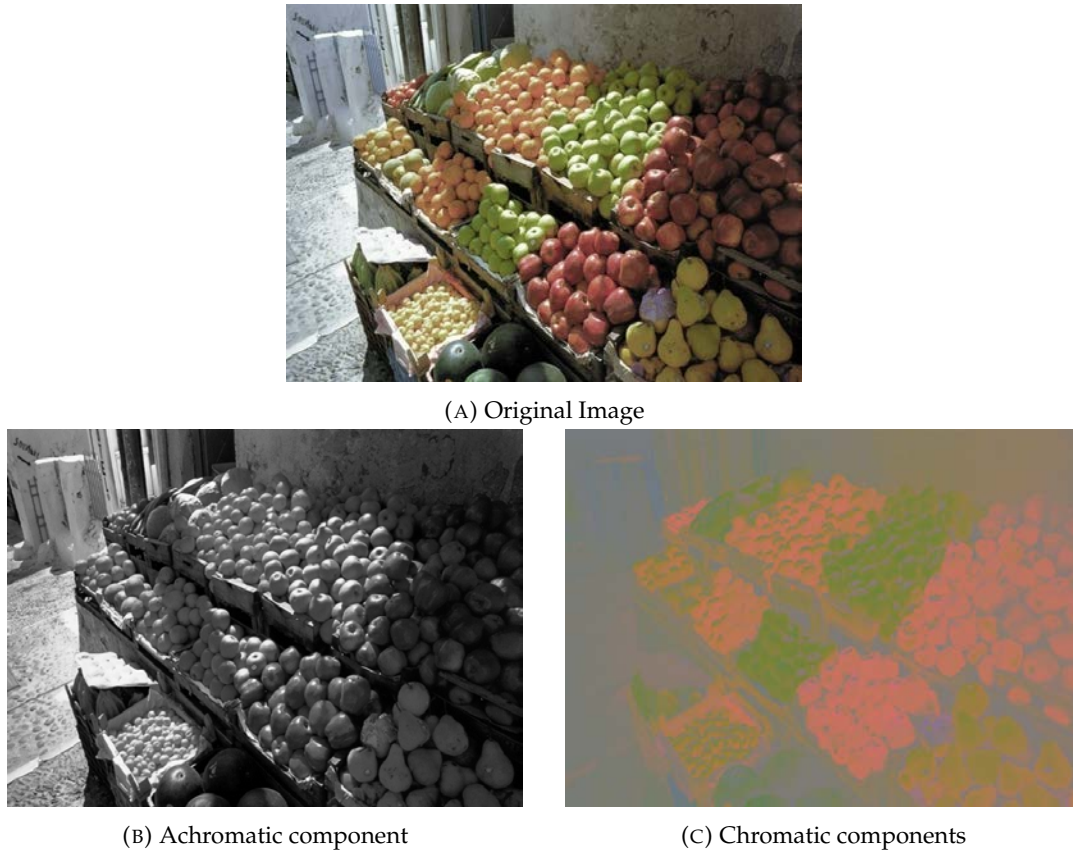


FIGURE 1.1: In the original image we can distinguish perfectly the different fruits (different varieties of apples, oranges, pears, etc.). When we separate the achromatic and the chromatic components, we can observe that fruits are more distinguishable in the achromatic domain than in the chromatic one, although it is not as easy as in the original image. Thus, chromatic components help to discriminate objects but it is not the most discriminatory feature. Figure adapted from (Stockman and Brainard, 2010).

2001; Lucas et al., 2003). Although at a first sight they could be considered opposite, both theories could be complementary and both could explain trichromacy survival (Sumner and Mollon, 2003). On one hand, the authors of frugivory theory did an empirical test: They collected the fruits eaten by three different primate species and several leaves (Reagan et al., 2001). The authors concluded that, for the three studied species, the trichromacy assists fruit detection against the foliage. Also, they concluded that the spectral response of the cones is optimal to this detection task, supporting the frugivory hypothesis, but also that fruit colors have been co-evolved to be well detected by their consumers. On the other hand, the authors of the folivory theory did an observational study of the feeding behaviors in eight primate species during a year (Lucas et al., 2003). The authors observed that trichromats tend to consume more reddish leaves than dichromats but there were not significant differences for red fruits, concluding that trichromats evolved in a context where they had to consume leaves. Moreover, the authors did not observed fidelity to any fruit hue and they pointed out that fruits have a wide range of chromaticities and that red is only one possibility. Thus, it is feasible to conclude that the aim of color vision is to detect (but maybe also to recognize) objects.

1.3 How do we perceive colors?

The light reflected by the objects is projected by the cornea and lens onto the rear surface of the eye: the retina. This light is absorbed by the *rods* and *cones*. The rods are responsible for the achromatic night vision (scotopic and mesopic vision, low light levels), while the cones are responsible for the achromatic and chromatic vision during daytime (photopic vision, high light levels). Cones are concentrated in the fovea while rods are almost absent in it (in particular at the central region of the fovea) (see Figure 1.2). The cone mosaic is composed by: L-, M- and S-cones, which are sensitive to long, medium and short wavelengths of the visible spectra and associated to red, green and blue colors, respectively (see Figure 1.3). For instance, color blindness is caused by a deficient response of one or more of these cones (McIntyre, 2002). The *ganglion cells* present in the retina combine the outputs of rods and cones (cone opponency) and segregate the information in three different pathways: *magno-*, *parvo-*, and *koniocellular*. The magnocellular pathway (parasol cells) is a combination of L- and M-cones, with a strong rod input, thus, it carries the luminance information. The ganglion cells that generate the parvocellular pathway (midget cells) consider the M- and L-cone on-center and M- and L-cone off-center varieties, having very little rod input. Thus, this pathway processes the red-green color information. Finally, the ganglion cells responsible for the koniocellular pathway (small-bistratified and other cells) compare the S-cone on- and off-center to the L- and M-cells. This pathway processes the blue-yellow color information and it does not have rod input (Dacey and Lee, 1984; Callaway, 1998; Sincich and Horton, 2005; Nassi and Callaway, 2009; Callaway, 2014; Kaplan, 2014; Lee, 2014). The output of ganglion cells is transformed to electrical impulses and they are sent to the *Lateral Geniculate Nucleus* (LGN), in the *thalamus*, through the optical nerve (see Figure 1.4).

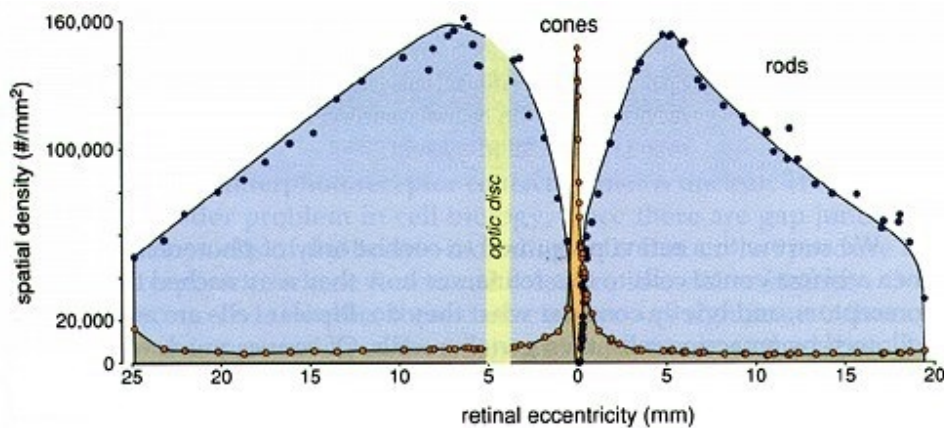


FIGURE 1.2: Rods' and cones' density as a function of eccentricity. Cones are concentrated at the fovea (0 deg), while rods are located out of it (> 10 deg). Figure adapted from (Rodieck, 1988).

There are several chromatic spaces consistent with retinal and LGN physiology, being the most popular the ones defined by MacLeod and Boynton (1979) and Derington, Krauskopf and Lennie (1984). The LGN receives feedback from higher areas but mainly projects to the primary visual cortex (also known as V1, see schematics in Figure 1.4). The latter has three different types of neurons: *single-*, *double-* and *non-opponent* neurons (SO, DO and NO neurons, respectively) (Johnson, Hawken, and Shapley, 2001; Shapley and Hawken, 2002; Johnson, Hawken, and Shapley, 2008; Shapley and Hawken, 2011). SO neurons (or *Color* neurons) respond best to large

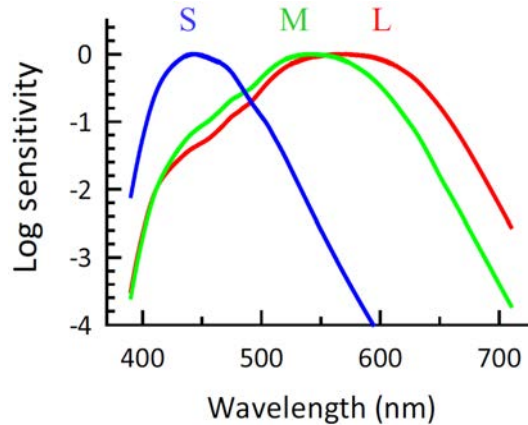


FIGURE 1.3: The three types (S-, M- and L-cones) of cones are sensitive to short, medium and long wavelengths of the visible spectra, respectively. These photoreceptors are responsible for trichromacy, *i.e.*, color vision.

chromatic areas, DO neurons (or *Color-Lum* neurons) respond to both chromatic and luminance variations, *i.e.* edges, and NO neurons (or *Lum* neurons) respond best to luminance variations. Regarding spatial frequency selectivity, Lum and Color-Lum neurons are band-pass (*i.e.*, they respond best to medium spatial frequency stimuli of 2 cpd) and Color neurons are low-pass (they respond optimally to spatial frequencies $< 0.5\text{ cpd}$ and do not respond at all to spatial frequencies $> 2\text{ cpd}$) (Johnson, Hawken, and Shapley, 2001; Johnson, Hawken, and Shapley, 2008; Shapley and Hawken, 2011; Xing et al., 2015; Nunez, Shapley, and Gordon, 2018). Considering orientation selectivity, SO do not have orientation selectivity (*i.e.*, when the stimulus is rotated, they respond equally) and DO and NO can both have and do not have orientation selectivity (Johnson, Hawken, and Shapley, 2008).

Additionally, neurons can also be classified as *simple* and *complex*. Simple cells can be SO, DO and NO cells which receive input from LGN, while complex cells are mainly DO and they usually receive input from simple cells. Simple cells have ON- and OFF-regions and, when they have orientation selectivity, its bandwidth is narrow and they do not respond at all to the orthogonal-to-preferred orientation. In contrast, complex neurons do not segregate ON- and OFF-regions, typically respond to direction of motion and, when they have orientation selectivity, they also have a bandwidth, but they respond to all orientations (Rolls and Deco, 2002; Andoni, Tan, and Priebe, 2014). The role of these different neurons is not fully understood, but it is suggested that DO neurons play an important role in color perception (Nunez, Shapley, and Gordon, 2018).

From V1, the visual information is mainly sent (although some feedback to LGN) to higher visual areas such as V2, V4 and Inferior Temporal cortex (IT) which allows the HVS to perform high visual tasks such as texture analysis, form perception and edge detection (Loffler, 2008; Freeman and Simoncelli, 2011; Landy, 2014). These higher visual areas, in turn, send feedback to V1. We can classify the connections that exist in the HVS according to their origin and their target. In that sense, there are inter- and intra-area connections (*e.g.*, connections from one area to another one and connections within the same area, respectively). In turn, intra-area connections can be differentiated between inter- and intra-layer connections (*i.e.*, connections between different layers of the same area and connections within the same layer). Due

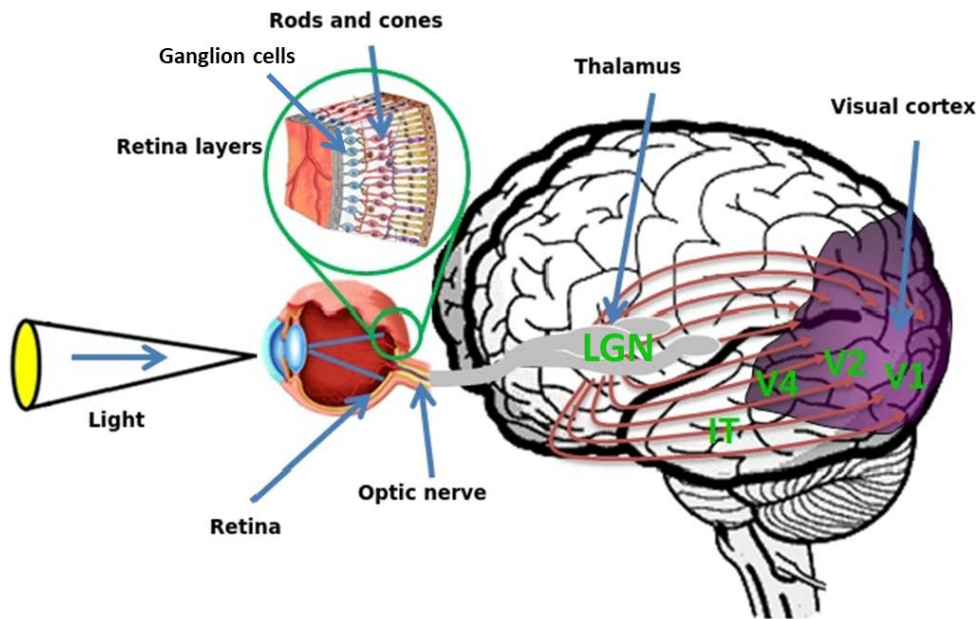


FIGURE 1.4: Schematics of the visual pathway. Only considering the feedforward path, the light is transformed to electrical impulses at the retina and they are sent to the primary visual cortex (V1) through the LGN (in the thalamus). Then, V1 projects the visual information to higher areas such as V2, V4 and IT. Figure adapted from (Akbarinia, 2017).

to the different properties of these connections and the different amount (or the percentage) of SO, DO and NO neurons from one layer to another, V1 shows several laminar differences such as the spontaneous firing rate and the orientation selectivity (Johnson, Hawken, and Shapley, 2001; Johnson, Hawken, and Shapley, 2008). For instance, the higher layers of V1 such as layer 2/3 and layer 4A have a higher orientation selectivity than the lower ones such as layer 4C α and layer 4C β (Ringach, Shapley, and Hawken, 2002; Johnson, Hawken, and Shapley, 2008).

1.4 How is color measured?

One method to measure the physical color is using a spectroradiometer (a device that measures the spectral power distribution of a source). From a psychological point of view, it is possible to use psychophysics to measure the perceived color. Psychophysics is a psychology branch that investigates the relationship between the physical stimuli and the perceptual experience (visual perception in our case). In psychophysics, the experimenters use standard procedures such as cancellation, pairwise comparison and asymmetric matching (among others) to measure the color (or visual) perception.

1.4.1 Could the physical and the perceived color be different?

The answer to this question is "certainly, yes." There are two types of illusions: the optical and the visual illusions. In both of them, the reality and the perception are different. The former can be defined by its physical properties while the latter is a consequence of the HVS processing. Figure 1.5a shows an optical illusion, in this case, the refraction of a drinking straw in a glass of water. The refractive power of

the water makes the straw to appear displaced (the illusion occurs due to the optical properties of the water). Figure 1.5b shows a visual illusion, in this case, the borders seem to tilt but they are horizontally aligned. This visual effect, named *tilt effect*, occurs due to the HVS architecture (Todorovic, 2017). Although tilt effect is one of the most striking visual effects, many others such as *color constancy*, *aftereffects* and *brightness* and *color induction* exist.

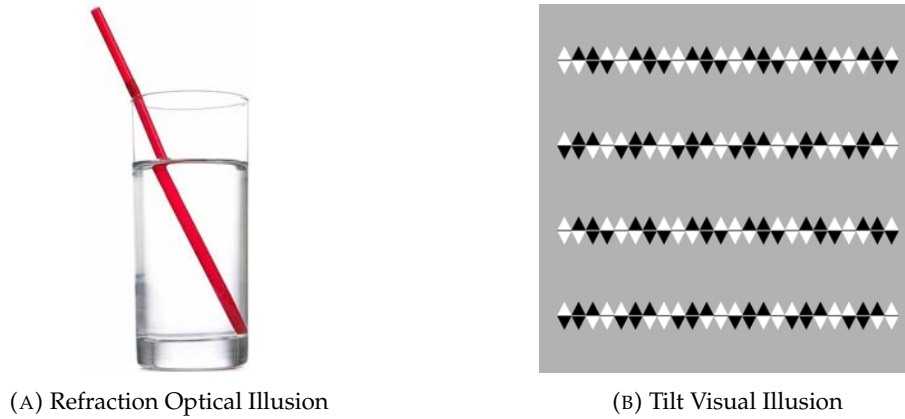


FIGURE 1.5: Examples of both optical and visual illusions. In (A) the drinking straw appears to be displaced due to the refraction power of the water. In (B) the borders seem to tilt (the first and the third clockwise, and the others anti-clockwise). Figures adapted from (Science Photo Library, 2018) and (Kitaoka, 2007), respectively.

Since these visual effects are the result of the neural mechanisms present in the HVS, they are usually used to study the involved mechanisms (Cao and Shevell, 2005; Hurlbert and Wolf, 2004; Gordon and Shapley, 2006; Xing et al., 2015). For example, it is considered that color induction (both color contrast and color assimilation) is the result of the lateral connections present in V1 (Zaidi et al., 1992). Thus, in this thesis we have used the color induction effect for a better understanding of these *lateral connections*.

1.5 Computational models

Computational models are mathematical models that help to study the behavior of complex systems. Since this kind of models need an extensive computational power, they started to emerge in the 90's (when powerful computers, and computer clusters, appeared). We can differentiate two different types of computational models: the phenomenological and the mechanistic. The aim of both types is data prediction, but the mechanistic models mimic the mechanisms of a system associated to a given task to reproduce its results, while the phenomenological reproduce the results independently of the mechanisms. Phenomenological models are very common in *Engineering*, where the aim is to solve a problem, but not to understand the solution. In contrast, mechanistic models allow scientists to make assumptions on the different model components and to point out the possible unobserved properties of these components.

In this thesis we have defined a new mechanistic computational model that simulates the first layers of the parvocellular pathway (possibly the most studied and understood chromatic pathway) in V1. We reproduced several electrophysiological observations of the neurons that comprise these layers.

1.6 Sections of the dissertation

My PhD has been composed by two different main topics and this dissertation is divided according to them:

1. Psychophysics

In this part (Part I), we present the psychophysical experiments that we have conducted. First, to get in touch with the psychophysics' methodology and human perception, we conducted a psychophysical experiment to evaluate different *tone-mapping operators*. The novelty of these experiments is that we placed the real scene next to the monitor. Thus, subjects performed the experiments while they observed the real scene. Second, we conducted experiments to study different properties of the color induction effect. We studied the color induction when flashed stimuli were presented and the effect of both luminance and brightness differences on color assimilation.

2. Computational Modeling

In this part (Part II), we present a new firing rate computational model. This multilayer model is focused on the parvocellular pathway in V1, where the red-green color information is processed. The aim of this architecture is to model the *receptive fields* (RFs) and their lateral connections present in this pathway and to reproduce some electrophysiology recordings from literature.

1.7 Summary of published works/studies

Several publications in the following journals and conferences have arisen from this dissertation.

1. Psychophysics

(a) HDR

- Which tone-mapping operator is the best? A comparative study of tone-mapping perceived quality (Cerda, Parraga, and Otazu, 2014), *European Conference on Visual Perception (ECVP)*, 2015.
- Which tone-mapping operator is the best? A comparative study of the perceptual quality (Cerda-Company, Parraga, and Otazu, 2018), *Journal of the Optical Society of America A*, 2018.

(b) Color induction

- Is luminance a key factor for static and flashed chromatic assimilation? (Cerda-Company and Otazu, 2017b), *European Conference on Visual Perception (ECVP)*, 2017.
- Color induction in equiluminant flashed stimuli (Cerda-Company and Otazu, 2019), *Journal of the Optical Society of America A*, 2019.
- Luminance spatial distribution plays a major role in color assimilation (Cerda-Company et al., 2018b), *European Conference on Visual Perception (ECVP)*, 2018.
- The effect of luminance differences on color assimilation (Cerda-Company et al., 2018c), *Journal of Vision*, 2018.
- Stronger colour induction in migraine (Otazu et al., 2018), *European Conference on Visual Perception (ECVP)*, 2018.

- Colour induction in migraine (Cerde-Company et al., 2018a), *Applied Vision Association (AVA) Christmas Meeting*, 2018.

2. Computational Modeling

- Brightness and colour induction through contextual influences in V1 (Otazu, Penacchio, and Cerde-Company, 2015b), *Scottish Vision Group (SVG)*, 2015.
- A multi-task neurodynamical model of lateral interactions in V1: chromatic induction (Cerde-Company and Otazu, 2016a), *European Conference on Visual Perception (ECPV)*, 2016.
- A new dynamical firing rate model of the parvocellular pathway in V1 (Cerde-Company, Otazu, and Penacchio, 2018), *Barcelona Computational, Cognitive and Systems Neuroscience (BARCCSYN)*, 2018.

3. Miscellaneous (unpublished)

- An excitatory-inhibitory firing rate model accounts for brightness induction, color induction and visual discomfort (Otazu, Penacchio, and Cerde-Company, 2015a), *Barcelona Computational, Cognitive and Systems Neuroscience (BARCCSYN)*, 2015.
- Dynamic colour induction can be reproduced by a neurodynamical model of lateral interactions in V1 (Cerde-Company and Otazu, 2016b), *Barcelona Computational, Cognitive and Systems Neuroscience*, 2016.
- Equiluminant colour induction in flashed and static stimuli (Cerde-Company and Otazu, 2017a), *Scottish Vision Group (SVG)*, 2017.

Part I

Psychophysics

*“There is no truth.
There is only perception”*

Gustave Flaubert

Chapter 2

HDR

Tone-mapping operators (TMOs) are designed to generate perceptually similar low-dynamic range images from high-dynamic range ones (see Figure 2.1). We studied the performance of fifteen TMOs in two psychophysical experiments where observers compared the digitally-generated tone-mapped images to their corresponding physical scenes. All experiments were performed in a controlled environment and the setups were designed to emphasize different image properties: in the first experiment we evaluated the local relationships among intensity-levels, and in the second one we evaluated global visual appearance among physical scenes and tone-mapped images, which were presented side by side. We ranked the TMOs according to how well they reproduced the results obtained in the physical scene. Our results show that ranking position clearly depends on the adopted evaluation criteria, which implies that, in general, these tone-mapping algorithms consider either local or global image attributes but rarely both. Regarding the question of which TMO is the best, *KimKautz* (Kim and Kautz, 2008) and *Krawczyk* (Krawczyk, Myszkowski, and Seidel, 2005) obtained the better results across the different experiments. We conclude that a more thorough and standardized evaluation criteria is needed to study all the characteristics of TMOs, as there is ample room for improvement in future developments.

2.1 Introduction

In almost all naturalistic viewing situations, we are immersed in scenes that could be described as *High Dynamic Range* (HDR), in other words, the intensity difference between the brightest and the darkest patch is much higher than the difference both imaging and capturing devices can faithfully capture. For instance, the energy ratio between sunlight and starlight is approximately about 100,000,000:1 (Ferber and Luka, 2009). If the Human Visual System (HVS) was to linearly represent these extreme differences in its normal daylight operation, it would require a much larger sensitivity range for its retinal sensors (cones) and neural pathways than is achievable within biological limitations. Instead, millions of years of evolution have solved this problem by adapting the sensorial and neural machinery, allowing it to non-linearly convert the large natural intensity range into a much smaller range of about 10,000:1 (Reinhard et al., 2005; Snowden, Thompson, and Troscianko, 2006).

2.1.1 Historical Context

The problem of translating the HDR world into *Low Dynamic Range* (LDR) depictions is very old. Renaissance painters such as da Vinci and Caravaggio tried to solve it by creating an artistic technique called *Chiaroscuro*, which pays attention to strong contrasts in different painted areas, creating very strong effects. This and the need

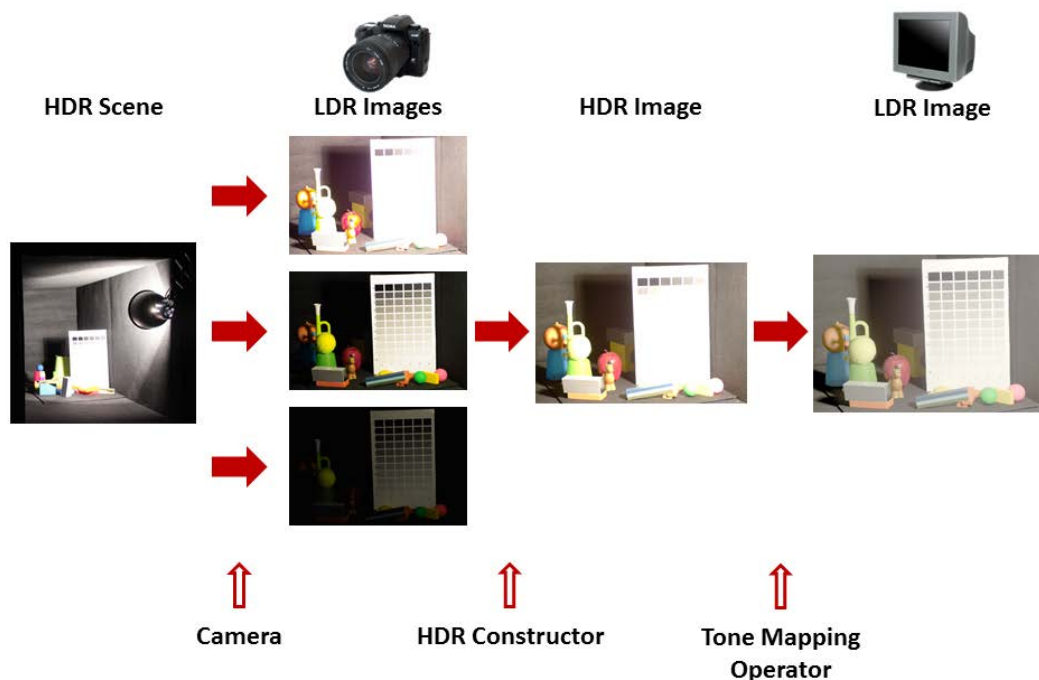


FIGURE 2.1: General workflow of a tone-mapping process. Several LDR images, with different exposure times covering different luminosity ranges of a physical scene, are captured by a camera. From these images a HDR image is obtained, which can be processed by a TMO in order to obtain a new LDR image that can be displayed on a standard LDR monitor.

to overcome the limitations of physical materials (oil paints and substrates) inspired later artists to produce remarkable paintings. Perhaps the most dramatic were created by depicting a single artificial source of light (such as a candle), making the details of the central subject very bright, while other subjects are slightly darker (see Figure 2.2). It can be argued that some of the works by Rembrandt and Constable are no different from today's HDR photography (McCann, 2007; Parraman, 2010; McCann and Rizzi, 2012).

The arrival of photography implied a new set of challenges given the strong limitations of early light-sensitive material (Mees, 1921). Examples of the first characterization of silver halide films as plots of density vs exposure was made by Hurter and Driffield in 1890 (McCann and Rizzi, 2012). In particular, outdoor scenes were very difficult to capture and early photographers experimented with multiple exposures to overcome dynamic range problems. When photographs involved human subjects, these had to remain still during the whole process so that several exposures could be combined into a single image.

2.1.2 Electronic HDR imaging

Analog HDR imaging allowed only limited manipulations (via exposure time, chemical reactions or the combination of several exposures, etc.) but the arrival of electronic digital imaging made possible for long-range interactions of pixels located in different parts of the image. This opened the field to multiple possibilities including mimicking the operation of the HVS and the work of chiaroscuro artists.



FIGURE 2.2: Examples of Caravaggio's chiaroscuro paintings. In **(A)** Salome receives the Head of John the Baptist and in **(B)** The Taking of Christ.

Physiological and psychophysical research has shown that photopic human vision is the result of highly nonlinear processing of the information captured by retinal cones. This processing includes the inhibition of the output of a neuron by the output of surrounding neurons in its field of view (Barlow, 1953), which results in higher sensitivity for edges and spots than for uniform light. Other processing includes the combination of visual information in the retina into a series of post-receptoral chromatically-opponent channels to transmit it to the visual cortex via the optic nerve (Derrington, Krauskopf, and Lennie, 1984). In the cortex, visual information is mostly processed in terms of its spatial frequency and visual orientation (Blakemore and Campbell, 1969). In the 1960's a series of psychophysical experiments with achromatic Mondrians run by Edwin Land demonstrated that patches reflecting light with exactly the same physical properties appear completely different to observers (Land, 1964). This implies that a digital image (where these patches produce exactly the same pixel values) cannot be modified using a pixel-wise transformation to simulate the appearance reported by observers. In other words, the information contained in individual pixels is not enough to mimic human vision. A comprehensive review of these experiments can be found in (Land and McCann, 1971; McCann, 2004; McCann, 2017; McCann, 1999). Other effects to consider are related to how the visual cortex processes local brightness interactions (Otazu, Vanrell, and Parraga, 2008; Otazu, Parraga, and Vanrell, 2010). More detailed experiments have shown the effects of edges in illumination perception by matching the appearance of painted wooden facets to that of a painted test target ("ground truth") (McCann, Parraman, and Rizzi, 2014), a paradigm very similar to ours (see below).

In order to mimic the response of the HVS, electronic imaging systems set out to use information not only from single pixels but from the entire scene. This allowed them a much larger flexibility to calculate appearances and to apply them to electronic displays or prints. Ironically, later HDR algorithms reverted to the old "multiple exposures" and "pixel-wise" processing techniques of analog photography for the same task (see below).

2.1.3 Tone-Mapping Operator

Mapping the HDR of the world into LDR media presents an important challenge for visual representation technologies mainly because most imaging devices (cameras

and monitors) are only able to obtain/display images within a small range of about 100:1 (Reinhard et al., 2005) which can be increased up to 1000:1 for specialized HDR led-based displays (Ruppertsberg et al., 2007). To solve this problem, an assortment of non-linear image processing techniques were defined to display HDR scenes in LDR devices. To construct the HDR image (see Figure 2.1), many LDR images of the same scene are usually taken at different exposure values, capturing a much larger dynamic range. This HDR image is generated by extracting from each LDR image the information corresponding to its region of interest (where it is neither over- or under-exposed) and combining them. Since this new HDR image cannot be displayed on a standard LDR monitor, an algorithm is needed to reduce its dynamic range to match that of the monitor. A common solution is to use a Tone-Mapping Operator (TMO) to reduce the dynamic range while keeping the perceptual characteristics of the original HDR image approximately constant. The performance of these TMOs depends of several factors including lighting and viewing conditions, aesthetic/realistic preferences, local/global assumptions, etc. and are usually evaluated using computational (Aydin et al., 2008; Yeganeh and Wang, 2012) and psychophysical (Drago et al., 2003b; Kuang et al., 2004; Yoshida et al., 2005; Ledda et al., 2005; Ashikhmin and Goyal, 2006; Cadík et al., 2006; Yoshida et al., 2007; Kuang et al., 2007; Kuang, Johnson, and Fairchild, 2007; Akyüz et al., 2007; Cadík et al., 2008) methods.

Although HDR images are able to reproduce a wider range of luminance highlights and shadows than LDR ones, the presence of veiling glare both in the camera and the eye limits the possible range of accurate luminance measurements (McCann and Rizzi, 2012). Since HDR are perceptually closer to the original scene, there must be other reasons than simply obtaining a larger range of luminances for this perceived improvement. It has been hypothesized (McCann and Rizzi, 2012) that the improvement comes from a better preservation of relative spatial information that comes from digital quantization (spatial differences in highlights and shadows are preserved) and TMOs use this to replicate the HVS processing.

In this work we present a new set of experiments and analysis to psychophysically evaluate the performance of 15 state-of-the-art TMOs. This allowed us to rank the TMOs according to how well they represent the original scene as human observers perceive it. Unlike previous studies, all the experiments were performed in a controlled environment and tone-mapped images were presented side by side with the physical scene.

2.1.4 "Global" vs "Local" analysis

At this point we believe it is important to clarify the terminology used throughout this work. The term "Tone" is traditionally used to describe pixel data (as in "Tone Mapping") and was introduced by Mees (Mees, 1921) in 1920 to explain how exposure was related to photographic print density (silver halide response). Indeed "Tone Scale" is the name given to a look-up table that transforms data in an input space to a desired output space.

The term "*Global TMO*", which is also used by several authors (Tumblin and Rushmeier, 1993; Ward, 1994; Reinhard et al., 2002) generally refers to an algorithm that applies the same pixel-wise adjustment to all pixels in the image (although, in fact, it uses the most local information: a single pixel). In contrast, the term "*Local TMO*" generally defines an algorithm that applies a combination of pixel-wise processing and spatial transformations to improve the image. Although confusing we will follow the traditional terminology here, calling Global TMOs to algorithms that

apply pixel-wise processing and Local TMOs to algorithms that apply a combination of pixel-wise and spatial image processing.

We will refer to our psychophysical experiments (see below) as "*Scene Reproduction*" when observers judge images by freely comparing them, and "*Segment Matching*" when they match the luminances of specific points in the scene to those of a reference table in the same scene.

2.2 State-of-the-Art

2.2.1 Previous TMO Psychophysics

Although the idea of using algorithms to match the brightness of real scenes to that of imaging devices is not new (Miller, Y., and D., 1984; Tumblin and Rushmeier, 1993), TMOs did not become popular until the turn of the century, when affordable digital cameras became available (Ferwerda et al., 1996; Ashikhmin, 2002; Durand and Dorsey, 2002; Fattal, Lischinski, and Werman, 2002; Reinhard et al., 2002; Drago et al., 2003a; Krawczyk, Myszkowski, and Seidel, 2005; Li, Sharan, and Adelson, 2005; Reinhard and Devlin, 2005; Kuang, Johnson, and Fairchild, 2007; Mertens, Kautz, and Van Reeth, 2007; Meylan, Alleysson, and Ssstrunk, 2007; Kim and Kautz, 2008; Ferradans et al., 2011; Otazu, 2012). To date, many different psychophysical experiments have been performed and they can be classified as follows:

Experiments without a reference HDR scene

One of the first psychophysical experiments to evaluate TMOs compared the performance of 6 TMOs on 4 different (synthetic and photographic) scenes by asking subjects to make pairwise perceptual evaluations and by rating stimuli with respect to three attributes: apparent image contrast, apparent level of detail, and apparent naturalness (Drago et al., 2003b). The results showed that preferred operators produced detailed images with moderate contrast.

Kuang et al. (2004) performed pairwise comparisons on 8 different TMOs using 10 different scenes and two conditions (color and gray-level) where subjects had to choose the preferred image considering general rendering performance (including tone compression performance, color saturation, natural appearance, image contrast and image sharpness). Their results showed that the gray-scale tone-mapping performances are consistent with those in the overall rendering results, if not the same.

Experiments with a reference HDR scene

Yoshida et al. (2005) conducted a psychophysical experiment based on a direct comparison between the appearance of real-world scenes and TMO images of these scenes displayed on a LDR monitor. In their experiment, they differentiate between global and local operators, and introduced, for the first time, the comparison between tone-mapped image and real scene, selecting two different indoor architectural scenes. Fourteen subjects were asked to give ratings according to several criteria like realism (image naturalness in terms of reproducing the overall appearance of the real world views) and image appearance (brightness, contrast, detail reproduction in dark regions, and in bright ones). They found that none of these image appearance attributes had a strong influence on the perception of naturalness by itself. This work was extended to find out which attributes of image appearance accounted for the differences between tone-mapped images and the real scene (Yoshida et al.,

2007). They observed a clear distinction between global and local operators. However, they concluded again that none of the evaluated image attributes had a strong influence on the perception of naturalness by itself which suggested that naturalness depends on a combination of the other attributes with different weights.

In another work, Ashikhmin and Goyal (2006) performed three different experiments. Subjects ranked different tone-mapped images depending on the task. In the first experiment, the authors asked which image they liked more without having the reference scene. In the second one, the authors asked which image seemed more real without viewing the reference scene and, in the third one, they asked which image was the closest to the real scene viewing the reference scene. They observed that rankings were totally different when subjects could compare the tone-mapped image to the reference scene.

In a subsequent study, Kuang et al. (2007) performed three different experiments they named *preference evaluation*, *image-preference modeling* and *accuracy evaluation*. In the *preference evaluation* experiment, pairwise comparisons between tone-mapped images were performed. Here they used only color images and the aim was to evaluate the general rendering performance by instructing observers to consider perceptual attributes such as overall impression on image contrast, colorfulness, image sharpness, and natural appearance. In contrast, in the *image-preference modeling* experiment, they rated gray-scale images (which were gray-scale versions of the first experiment color images). Here, observers considered perceptual attributes such as highlight details, shadow details, overall contrast, sharpness, colorfulness and appearance of artifacts, comparing the TMOs' visual rendering "to their internal representation of a 'perfect' image in their minds" (Kuang et al., 2007). In the *accuracy evaluation*, both pairwise comparison and rating techniques were used in order to evaluate the perceptual accuracy of the rendering algorithms. The pairwise comparison of TMOs was performed without viewing the real scene and subjects were asked to compare the overall impression on image contrast, colorfulness, image sharpness, and overall natural appearance. An additional rating evaluation was performed using the real scenes set up in the adjoining room as references. Here, subjects had to rate image attributes like highlight contrast, shadow contrast, highlight colorfulness, shadow colorfulness, overall contrast and the overall rendering accuracy comparing to the overall appearance of the real-world scenes. In both experiments, observers did not have immediate access to the real scene and had to rely on their memories (either short- or long-term) to perform the tasks.

To validate the iCAM06 operator (Kuang, Johnson, and Fairchild, 2007), its authors performed two psychophysical experiments similar to the previous ones (Kuang et al., 2007). The first experiment was a pairwise comparison without viewing the reference scene. Observers had to choose the tone-mapped image that they preferred based on overall impression on image quality (considering contrast, colorfulness, image sharpness, and overall natural appearance). In the second experiment, observers were also asked to evaluate overall rendering accuracy by comparing the overall appearance of the rendered images to their corresponding real-world scenes, which were set up in an adjoining room.

While looking for a definition of an overall image quality measure, Cadik et al. (2006) studied the relationships between some image attributes such as brightness, contrast, reproduction of colors and reproduction of details. They performed two psychophysical experiments, using 14 TMOs, in order to propose a scheme of relationships between these attributes, being aware that some special attributes, which were not evaluated (e.g. glare stimulation, visual acuity and artifacts), can influence their relationships. In the first one, 10 subjects were asked to perform ratings using

five criteria: overall image quality and the four basic attributes (brightness, contrast, reproduction of detail and colors). These evaluations were performed using a real scene as a reference (a typical real indoor HDR scene). In the second experiment, subjects did not have access to the real scene and they had to rank image printouts according to the overall image quality and the four basic attributes.

In a new study, Cadík et al. (2008) performed exactly the same type of experiments adding two new scenes, that is, they had a total of three scenes, i.e. a real indoor HDR scene, a HDR outdoor scene and a night urban HDR scene. In the first experiment, subjects were asked to rate overall image quality and the quality of reproduction of five attributes by comparing samples to the real scene. These attributes were the same four basic ones of their previous work and the lack of disturbing image artifacts (which was one of the non-evaluated special attributes). These experiments were set-up in an uncontrolled natural environment, so subjects had to perform the experiments at the same time of the day as the HDR image was acquired. In the second experiment, subjects had no possibility of directly comparing to the real scene and had to rank the image printouts according to the overall image quality, and the quality of basic attributes.

Experiments using an HDR monitor

In 2005, Ledda et al. (2005) performed two different psychophysical experiments comparing 6 different TMOs to linearly mapped HDR scenes displayed on a HDR device. They used 23 different color and gray-scale HDR scenes showing 3 different images per comparison: the HDR and two tone-mapped images. In the first experiment, subjects were asked to select the TMO image more similar to the HDR reference by judging its global appearance. In the second one, they were asked to make their judgment based on reproduction detail.

In a later work, Akyüz et al. (2007) asked subjects to rank six images (1 HDR image, 3 tone-mapped images, 1 objectively good LDR exposure value and 1 subjectively good LDR exposure value) according to their subjective preferences. They found that participants did not systematically prefer tone-mapped HDR images over the best single LDR exposures.

All the previous studies have been focused on subjective comparisons of global and local image appearance attributes such as contrast, colorfulness, sharpness, reproduction artifacts, etc. either within TMOs or against the real scene. While this is no doubt extremely important, we believe a good TMO should output a scene that produces the same visual sensation as the physical scene, in particular the interrelations between objects and their perceived attributes. For instance, no study has been conducted (as far as we know) to evaluate whether objects represented within a TMO image maintain the same perceived visual differences as the real scene. This is the main objective of our work.

2.2.2 Tone-Mapping Operators

As mentioned before, TMOs can be classified according to their processing in *global* and *local*. Global operators perform the same computation in all pixels, regardless of spatial position, which make them more computationally efficient at the cost of losing contrast and image detail. Some examples of global TMO are (Drago et al., 2003a; Ferwerda et al., 1996; Kim and Kautz, 2008; Reinhard and Devlin, 2005). On the other hand, local operators, which take into account surrounding pixels, produce

images with more contrast and higher detail level, but they may show problems with halos around high contrast edges. Local operators are inspired on the local adaptation process present at the early processing stages of the human visual system. Some examples of local operators are (Ashikhmin, 2002; Durand and Dorsey, 2002; Fattal, Lischinski, and Werman, 2002; Krawczyk, Myszkowski, and Seidel, 2005; Kuang, Johnson, and Fairchild, 2007; Li, Sharan, and Adelson, 2005; Meylan, Alleysson, and Süsstrunk, 2007; Otazu, 2012). There are some tone-mapping operators which could be global or local depending on their setup configuration parameters. One example is (Reinhard et al., 2002) and another one is (Ferradans et al., 2011), which is developed in two stages, the first global and the second local. A brief summary of the properties of each tone-mapping operator used in our experiments is given in Table 2.1. The first column shows the names that we will use to refer to each operator throughout this work. The characteristics of each TMO are detailed below:

TABLE 2.1: Summary of used TMOs' characteristics. Second column shows whether the TMO is global (G) or local (L). Third column shows whether it is inspired by the HVS, and following columns show whether it processes luminance and color information.

TMO	Global/Local	HVS	Luminance	Color
<i>Ashikhmin</i>	L	✓	✓	
<i>Drago</i>	G		✓	
<i>Durand</i>	L		✓	✓
<i>Fattal</i>	L		✓	
<i>Ferradans</i>	L	✓	✓	✓
<i>Ferwerda</i>	G	✓	✓	✓
<i>iCAM06</i>	L	✓	✓	✓
<i>KimKautz</i>	G		✓	
<i>Krawczyk</i>	L		✓	
<i>Li</i>	L		✓	
<i>Mertens</i>	-			
<i>Meylan</i>	L	✓	✓	✓
<i>Otazu</i>	L	✓	✓	
<i>Reinhard</i>	G		✓	
<i>Reinhard-Devlin</i>	G		✓	

- *Ashikhmin* (Ashikhmin, 2002). This local TMO is inspired by the processing mechanisms present at the first stages of the HVS. Intensity range is compressed by a local luminance adaptation function and, in a last step, detail information is added.
- *Drago* (Drago et al., 2003a). This global TMO is based on luminance logarithmic compression that, depending on scene content, uses a predetermined logarithmic basis to preserve contrast and details.
- *Durand* (Durand and Dorsey, 2002). This local TMO decomposes the image in two layers: the base and the detail. Large-scale variations of the base layer are encoded, while the magnitudes of the detail layer are preserved.
- *Fattal* (Fattal, Lischinski, and Werman, 2002). This local TMO manipulates the gradient fields of the luminance image. Its idea is to identify high gradients in different scales and attenuate their magnitudes, while maintaining their directions.

- *Ferradans* (Ferradans et al., 2011). This TMO can be executed as global or local because it is divided in two stages. In the first stage, it applies a global method that implements the visual adaptation, trying to mimic human cones' saturation. In the second stage, it enhances local contrast using a variational model inspired by color vision phenomenology. In our work, this operator was run as local.
- *Ferwerda* (Ferwerda et al., 1996). This global TMO is based on computational model of visual adaptation that was adjusted to fit psychophysical results on threshold visibility, color appearance, visual acuity, and sensitivity over the time.
- *iCAM06* (Kuang, Johnson, and Fairchild, 2007). This local TMO is based on the iCAM06 color appearance model, which gives the perceptual attributes of each pixel, like lightness, chromaticity, hue, contrast and sharpness. It includes an inverse model which considers viewing conditions to generate the result.
- *KimKautz* (Kim and Kautz, 2008). This global TMO is based on the assumption that human vision sensitivity is adapted to the average log luminance of the scene and that it follows a Gaussian distribution.
- *Krawczyk* (Krawczyk, Myszkowski, and Seidel, 2005). This local TMO is inspired on the anchoring theory (Gilchrist et al., 1999). It decomposes the image into patches of consistent luminance (frameworks) and calculates, locally, the lightness values.
- *Li* (Li, Sharan, and Adelson, 2005). This local TMO is based on multiscale image decomposition that uses a symmetrical analysis-synthesis filter bank to reconstruct the signal, and applies local gain control to the subbands to reduce the dynamic range.
- *Mertens* (Mertens, Kautz, and Van Reeth, 2007). This technique fuses original LDR images of different exposure values (exposure fusion) to obtain the final "tone-mapped" image, which avoids the generation of an HDR image. Guided by simple quality measures like saturation and contrast, it selects "good" pixels of the sequence and combines them to create the resulting image. Thus, for this method instead of an HDR image we used a stack of LDR images.
- *Meylan* (Meylan, Alleysson, and Ssstrunk, 2007). This local TMO is derived from a model of retinal processing. In a first step, a basic tone-mapping algorithm is applied on the mosaic image captured by the sensors. In a second step, it introduces a variation of the center/surround spatial opponency.
- *Otazu* (Otazu, 2012). This local TMO is based on a multipurpose human color perception algorithm. It decomposes the intensity channel in a multiresolution contrast decomposition and applies a non-linear saturation model of visual cortex neurons.
- *Reinhard* (Reinhard et al., 2002). This TMO can be executed as global or local. It performs a global scaling of the dynamic range followed by a dodging and burning (local) processes. In our work, this operator was run as global which is its default value in the toolbox.
- *Reinhard-Devlin* (Reinhard and Devlin, 2005). This global TMO uses a model of photoreceptors adaptation which can be automatically adjusted to the general light level.

2.3 Methods

In order to compare TMOs, we performed two different experiments called *Segment Matching* and *Scene Reproduction* experiments. The aim of the first experiment was to study the internal relationships among gray-levels in the tone-mapped image and in the real scene (i.e. a segment matching experiment similar to (McCann, Parraman, and Rizzi, 2014)). The aim of the second experiment was to evaluate TMOs according to how similar their results were perceived to be with respect to the real scene. In both cases, we obtained a ranking of the different TMOs. Behind these experiments is the idea that a good TMO is one whose output is perceptually similar to the real scene and, to do that, a good reproduction of the objects' relationships is needed.

2.3.1 Materials

Our experiments were performed in a controlled environment where the only sources of light were a lamp, which illuminated the real scene and a CRT screen. We used a ViSaGe MKII Stimulus Generator and a Mitsubishi Diamond-Pro®2045u CRT monitor side-by-side with a handmade real HDR scene. The monitor was calibrated via a customary Cambridge Research Systems Ltd. software for ViSaGe MKII Stimulus Generator (Rochester, England) and a ColorCal (Minolta sensor) suction-cup colorimeter. Both the monitor and the real scene were setup so that the objects in both scenes subtended approximately the same angle ($18.13 \times 13.81^\circ$) and looked similarly positioned to the observer.

We built three different HDR scenes, each including a gray-level reference table and two solid parallelepipeds (cuboids). The reference table was built by printing a series of 65 gray squares ($2.8 \times 2.2 \text{ cm}$) arranged in a flat 11×6 distribution. The arrangement of rows and columns was labelled A,B,C,...,K for the rows and 1,2,3...,6 for the columns. The lightness of these patches decreased monotonically from the top (patch A1 - #1) to the bottom (patch K5 - #65), as measured by our PR-655 SpectraScan®Spectroradiometer. The printed values were selected so that their CIE L^* (lightness) value was equally spaced, meaning that their distribution was approximately uniform in terms of perceived lightness (see Table 2.2). The cuboids consisted of pieces of wood ($3.6 \times 3.6 \times$ variable length between 9.4 and 10 cm), whose sides (facets) were covered with arbitrary samples of the same printed paper as the reference table. There were two cuboids in each scene (one under direct illumination and the other in the shade). The third column of Table 2.3 shows the patch of the reference table that the cuboid's facet corresponded to, the fourth column indicates its position with respect to the illumination and the last column indicates its luminance (when placed within its scene). Table 2.2 also shows the luminance values for these patches once lit by our light source. The chromaticity of all printed material was CIE $xy = (0.3652, 0.3817)$. The rest of the scenes consisted of many plastic and wooden objects of different colors and shapes (see Figure 2.3).

Two facets of one cuboid and three of the other were always visible from the subjects' location, resulting in 15 different gray facets in total (see Table 2.3). The incandescent lamp (100 W) had its bulb painted blue to simulate D65 illumination and was set up so that the luminance of the brightest object was about the same as the maximum luminance the monitor was capable of producing (about 100 cd/m^2).

We photographed the real scene using a Sigma Foveon SD10 camera placed in the exact same position as the subjects' heads during the psychophysical experiments. The same camera was calibrated for use in other measurements (*Camera Calibration Methods*) and because of this, we have a fairly good idea of the linearity and spectral

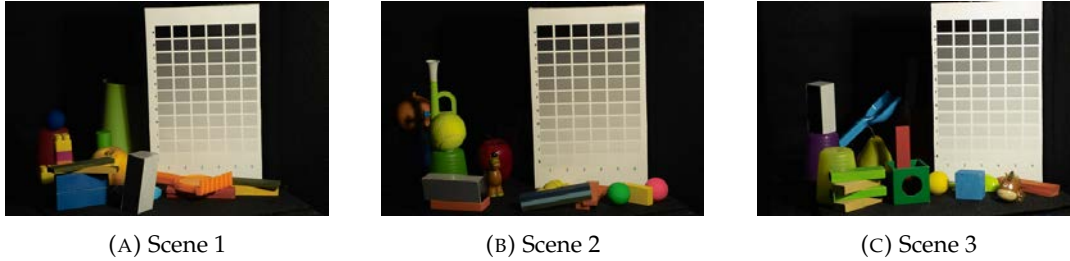


FIGURE 2.3: To show the general appearance of the physical scenes, here we show a single LDR exposure (chosen by simple visual inspection by the authors) from the set of LDR exposures used to create the HDR images. Since they are a single LDR exposure, the cuboids in the dark regions are not completely visible in these pictures.

TABLE 2.2: In this table we show the L^* CIE Lab color space values and the luminance values (cd/m^2) of each patch in the reference table. The lightness values have been measured by our PR-655 SpectraScan®Spectroradiometer under a uniform illumination. In contrast, the luminance values were measured in the scene by the same Spectroradiometer. The lightness of the patches monotonically increases from patch #1 (A1) to patch #65 (K5). Middle gray is universally defined as 18% reflectance on a white surround. In this table, 18% max is patch #34 (F4).

Lightness (L^*) of patches in the reference table						
Coordinate	1	2	3	4	5	6
A	1.50	3.64	5.76	7.88	9.97	12.06
B	14.13	16.18	18.22	20.25	22.26	24.26
C	26.24	28.20	30.15	32.08	34.00	35.90
D	37.78	39.65	41.50	43.33	45.15	46.95
E	48.73	50.49	52.24	53.96	55.67	57.36
F	59.03	60.68	62.31	63.91	65.50	67.07
G	68.61	70.14	71.64	73.11	74.57	76.00
H	77.40	78.78	80.13	81.46	82.76	84.03
I	85.27	86.49	87.67	88.82	89.93	91.01
J	92.05	93.06	94.02	94.94	95.81	96.63
K	97.40	98.11	98.74	99.30	99.73	
Luminance (cd/m^2) of patches in the reference table						
Coordinate	1	2	3	4	5	6
A	0.559	0.565	0.617	0.692	0.853	0.815
B	0.901	0.957	1.007	1.360	1.484	1.622
C	1.575	1.734	1.992	2.218	2.624	2.978
D	3.031	3.243	3.651	4.133	4.634	5.076
E	5.215	5.718	6.439	7.199	7.827	10.39
F	12.95	15.85	16.94	18.69	20.63	21.32
G	22.53	23.67	25.79	28.34	30.40	31.47
H	32.66	34.2	37.69	38.40	42.75	44.63
I	46.28	48.39	52.27	55.57	58.1	60.61
J	61.76	66.17	67.75	69.82	74.71	78.24
K	78.96	84.67	90.37	96.38	104.0	

TABLE 2.3: Photometric assessment of the scene facets used in our matching experiments. Column 3 indicates the corresponding gray patch (same material) from the reference table. Column 4 indicates whether the facet was directly illuminated or in the shade and column 5 shows its luminance from the observer’s point of view.

Luminance values (cd/m^2) of the scene facets				
Scene	Facet	Original Patch	Light/Shade	Luminance (cd/m^2)
1	1	B4	light	0.66
1	2	H4	light	59.22
1	3	F4	light	33.38
1	4	B4	shade	5.34
1	5	F4	shade	7.48
2	6	C4	light	3.44
2	7	H1	light	32.13
2	8	C1	shade	5.93
2	9	J1	shade	12.00
2	10	E4	shade	0.80
3	11	A4	light	1.73
3	12	I1	light	25.93
3	13	J1	light	27.46
3	14	G4	shade	31.58
3	15	B1	shade	9.06

sensitivity of its sensors. The setup was arranged so that the images presented on the monitor looked geometrically the same as the real ones shown beside it. Since the walls were covered in black felt, reflections from all other objects were minimized. The dynamic range of the scenes as measured by multiple exposures using the camera were approximately 10^5 for scene 1 and 10^6 for scenes 2 and 3. The dynamic range of the reference table as measured by the PR-655 was 104.0 - 0.559 cd/m^2 .

Although it has been shown that because of glare, is not possible to achieve an accurate representation of scene luminance distribution from a combination of many LDR images, this technique can still provide a good enough approximation (McCann and Rizzi, 2012). In consequence, a set of 25 photographs were taken at different exposure values (from 15 sec to 1/6000 sec) using the same aperture, focal distance, zoom settings and visual field. Individual images were stored in RAW format and transformed into 16 *bits* sRGB (using the camera manufacturer’s software).

To avoid any bias regarding the operators, all experiments started with a 1 *min* subject adaptation to the ambient light. Most TMO implementations were obtained from the popular HDR Toolbox for MATLAB (Banterle et al., 2011) while others (*Ferradans*, *iCAM06*, *Li*, *Meylan* and *Otazu*, were obtained from their corresponding authors’ web pages). In order to avoid benefiting any of the TMOs, we ran all of them with their default settings. In *Ferradans’* case, we had to chose between two different parameters and we selected the default values specified in their paper ($\rho = 0$ and $\alpha^{-1} = 3$). Other cases required that the TMO’s author was asked to perform the best tone-mapping, but we discarded this option because of its impracticality (we could not ask all authors the same) and besides, this practice impairs the reproducibility of the results.



FIGURE 2.4: In Experiment 1, observers performed two tasks. In *Task 1* (A), observers had to match the brightnesses of the 5 cuboids' facets to the brightnesses of 5 patches in the reference table. In *Task 2* (B), observers had to perform the same task on the TMO image displayed on the calibrated monitor. Red arrows are randomly drawn just for illustrative purposes.

2.4 Experiments

2.4.1 Experiment 1: Segment Matching

Procedure

The Segment Matching experiment consisted on two different tasks:

- *Task 1*. After adaptation, subjects were asked to match, in the real scenes (i.e. with monitor turned off), the brightness of the 5 cuboids' facets to the brightness of the patches in the reference table in each scene (see Figure 2.4a). Although there were no time constraints to perform the tasks, subjects were advised to take no more than 30 seconds per match.
- *Task 2*. Here the real scene was not visible and the observers only saw digital (tone-mapped) versions presented on the monitor. Their task was similar to *Task 1*, except that all matches were conducted entirely between the facets and patches shown on the screen (see Figure 2.4b).

There were three conditions for Experiment 1, corresponding to the three different scenes created (see Figure 2.3). Observers performed 240 matchings in total (5 facets \times 15 different tone-mapped images \times 3 scenes plus 15 matchings in the real scenes). In practice, all matchings were conducted by writing for each facet, the coordinates of the matching reference table patch on a piece of paper. The presentation order of the tone-mapped images was randomized.

Experimental Design

In Experiment 1, the independent variables (IVs) were the cuboid's facets and the reference table patches. The dependent variables (DVs) were the subjects' segment matches in the tone-mapped images (*Task 2*) and the control variable (CV) was the subjects' segment matches in the real scene (*Task 1*). Our null hypothesis was that there was not significant difference between the segments matched in the real scene (CV - *Task 1*) and the matches in the tone-mapped images (DVs - *Task 2*) because the TMOs perfectly reproduce the perceptual relationships among the objects present in the real scene.

Participants

Task 1 was completed by a group of 12 observers with normal or corrected-to-normal vision, recruited from our lab academic/research community. This group (8 males and 4 females) was comprised by people aged between 17 and 54. Nine of them were completely naïve to the aims of the experiment. *Task 2* was completed by 10 of the previous observers (8 males and 2 females).

Results

Figure 2.5 shows a plot of the segments matches obtained in *Task 2* against the segments matches in *Task 1*. We fitted a linear model to the results obtained by each TMO. If a TMO reproduced well the interrelations among the gray facets, the fitting should be very similar to the fitting for the real scene (i.e. points should lay about the diagonal).

We performed two different analyses to evaluate to what extent the local interrelations perceived by the observers in the tone-mapped versions corresponded to those perceived in the real scene. In the first analysis, we studied the slopes of the different fitted linear models w.r.t. the slope obtained in the real scene. The smaller the difference, the better the reproduction of the interrelations (it means that the TMO maintained the relationships among the facets and patches). Figure 2.5 shows the offset between the lines fitted to the TMOs and the line fitted to the real scene. In the second analysis, we studied this displacement by computing the root mean squared error (RMSE) between them.

TABLE 2.4: Performance of all TMOs in the Segment Matching experiment. The second and third columns show the analysis' results and the last the type of the TMO. In both metrics (i.e. slope difference and root mean squared error -RMSE- between the diagonal and the TMO fitted line), the smaller (indicated in bold), the more similar to the real scene, and thus, the better.

TMO	Slope Difference	RMSE	Type
<i>Ashikhmin</i>	0.29	11.19	Local
<i>Drago</i>	0.15	7.02	Global
<i>Durand</i>	0.12	5.01	Local
<i>Fattal</i>	0.02	4.66	Local
<i>Ferradans</i>	0.00	5.12	Local
<i>Ferwerda</i>	0.09	7.09	Global
<i>iCAM06</i>	0.01	0.42	Local
<i>KimKautz</i>	0.09	5.51	Global
<i>Krawczyk</i>	0.09	5.46	Local
<i>Li</i>	0.01	4.02	Local
<i>Mertens</i>	0.15	3.84	-
<i>Meylan</i>	0.16	5.93	Local
<i>Otazu</i>	0.24	5.30	Local
<i>Reinhard</i>	0.15	6.72	Global
<i>Reinhard-Devlin</i>	0.16	6.82	Global

All results are shown in Table 2.4, where *iCAM06* has the smallest distance to the real scene in both analyses. Since its slope difference and RMSE are very small, we can assume that the pixel interrelations in its tone-mapped image perceptually mimic the real scene. Given that *iCAM06* is based on a color appearance model

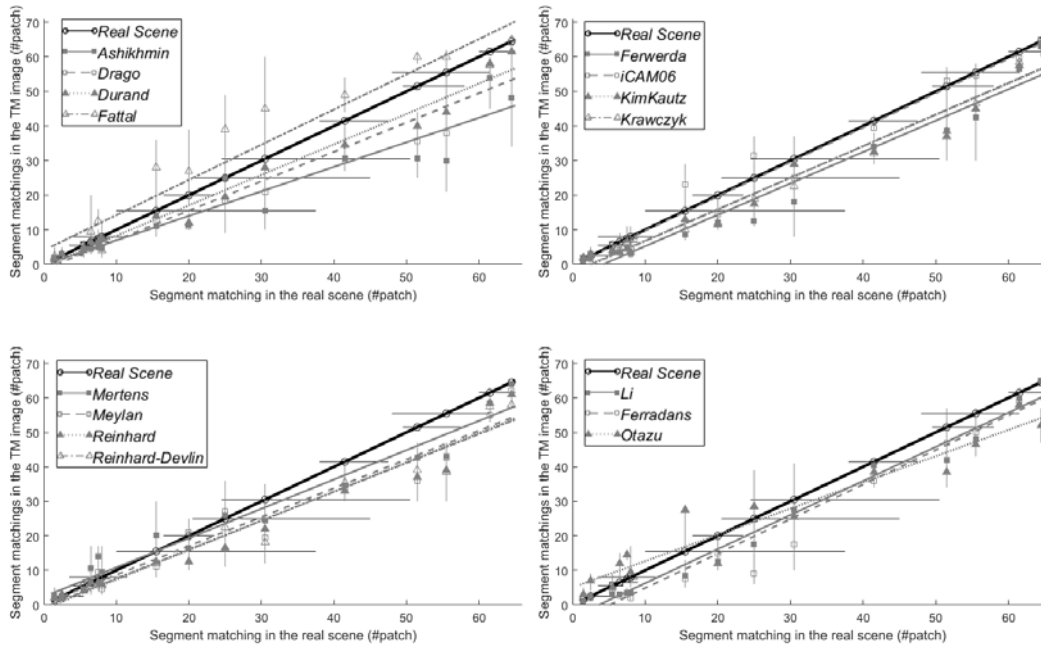


FIGURE 2.5: Results of Experiment 1. Segments matches in the tone-mapped images are plotted against segment matches in the real scene. Markers and lines identify each TMOs. Since not all the data had a normal distribution, the markers show the median of the subjects' observations. Horizontal lines indicate the first and the third quartiles of *Task 1* and vertical lines indicate the first and the third quartiles of *Task 2*. For each operator, we fitted a linear model using the median of the subjects' observations. The figure is divided in four panels for clarity. The real scene is plotted against itself in all panels to provide a fixed reference ($y = x$). In summary, the better the TMO, the closer its fit to the solid black line.

that considers perceptual attributes such as lightness, chromaticity, hue, contrast and sharpness, its results are expected to be in line with observers' perception.

We calculated the Spearman's rank correlation coefficient between the rankings obtained from both Segment Matching analyses (see Table 2.4) and obtained a value of 0.59 ($p < 0.05$). Since both rankings are quite similar, it is worth paying attention to some interesting cases such as *Ferradans*, whose slope is very close to that of the real scene, but the fitted model lays systematically under the real scene's line (i.e. its RMSE is very big). An opposite example is *Mertens* which has a different slope, but its RMSE is the second smallest.

Another interesting observation from Figure 2.5 is that, at the lowest and highest brightness values, the agreement between subjects is higher than at middle values (both horizontal and vertical dispersion lines are smaller). This suggests that the TMOs are more accurate at reproducing both the brightest and the darkest parts of the image. To analyze this effect in more detail, we studied the subjects' results for each facet. In Figure 2.6, the abscissa shows the segments matched in the real scene ordered from darkest to brightest and the ordinate represents the RMSE in the tone-mapped images with respect to the real scene. We defined RMSE as: $RMSE_{scene} = \sqrt{\frac{1}{n} \sum_{vi} (x_i - y_i)^2}$, where x_i is the i -th subject segment matched in the real scene, y_i is the i -th subject segment matched in the tone-mapped image and n is the number of subjects. Again, in almost all TMOs, the RMSE value is smaller for darkest and

brightest facets than for mid-gray facets. Thus, not only the agreement between subjects but also the error ($RMSE_{scene}$) is lower for both brightest and darkest values.

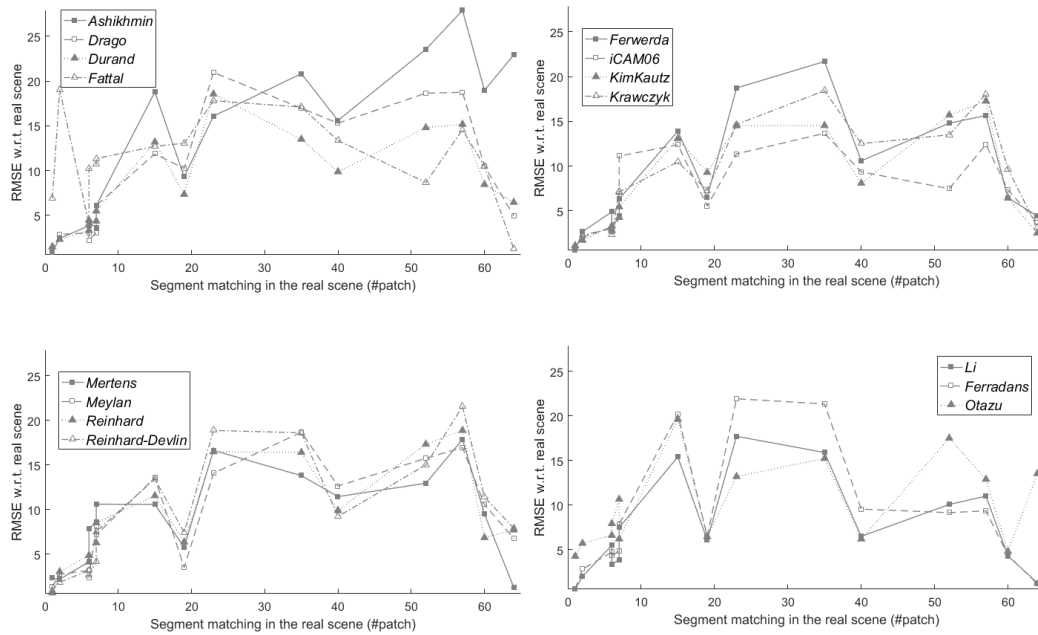


FIGURE 2.6: The RMSE w.r.t. the real scene ($RMSE_{scene}$) is the difference between segments matched in the tone-mapped image and in the real scene. Different types of lines and markers represent different TMOs. Abscissa represents the segments matched in the real scene ordered from darkest to brightest. According to this metric, the smaller the value, the better the TMO.

2.4.2 Experiment 2: Scene Reproduction

Procedure

Experiment 2 consisted of a pairwise comparison of tone-mapped images obtained using different TMOs in the presence of the original scene (side by side). After 1 *min* adaptation in front of the physical scene, a pair of tone-mapped images of the same physical scene was randomly selected and presented sequentially to the observer on the CRT screen besides the real scene. Subjects could press a gamepad button to toggle which image of the tone-mapped pair was presented on the monitor (only one image was displayed at a time). For this task, they were asked to 'select the image that was more similar to the real scene.' As before, there was no time limit but subjects were advised to complete a trial in less than 30 seconds. After an image was chosen, a gray background was shown for two seconds, and a different random pair was selected for the next trial. Every subject performed 105 comparisons per scene taking around 25 minutes in total. There were three experimental conditions, corresponding to the three different physical scenes created (see Figure 2.3). Between conditions, subjects were forced take 5 to 10 minutes breaks outside while the physical scene was replaced.

Experimental Design

In this experiment the IVs were the different TMOs, the DVs were the subjects' evaluations (i.e. the preference matrix), and the CV was the real scene. Our null hypothesis was that there were no differences in the TMOs performances since all of them perceptually reproduce the real scene.

Participants

A group of 10 people with normal or corrected-to-normal vision, 7 males and 3 females recruited from our lab academic and research community, completed this experiment. This group was comprised by people aged between 17 and 54 y.o. Seven of them were naïve to the aims of the experiment.

Results

From the pairwise comparison results, we defined a preference matrix for each subject and each scene. We constructed a directed graph where the nodes were the evaluated TMOs and the arrows pointed from a preferred TMO to a non-preferred TMO, e.g. if the TMO_{*i*} is preferred over the TMO_{*j*} (tone-mapped image from TMO_{*i*} is more similar to the real scene than the one from TMO_{*j*}), we drew an arrow from node_{*i*} to node_{*j*}, for $i \neq j$.

From this graph, we were able to analyse intra-subject consistency coefficient ζ for each scene. The consistency coefficient for each subject and scene is defined by

$$\zeta_{st} = \begin{cases} 1 - \frac{24d_{st}}{n^3 - n}, & \text{if } n \text{ is odd.} \\ 1 - \frac{24d_{st}}{n^3 - 4n}, & \text{if } n \text{ is even.} \end{cases}, \text{ with} \quad (2.1)$$

$$d_{st} = \frac{n(n-1)(2n-1)}{12} - \frac{1}{2} \sum_{i=1}^n a_{ist}^2$$

where s is the scene number ($s \in [1, 3]$), t is the subject number ($t \in [1, m]$), n is the number of evaluated TMOs, and a_i is the number of arrows which leave the node_{*i*}. The maximum ζ value is 1 (perfect consistency within-subject).

The consistency between subjects, i.e. inter-subject agreement, is measured by the Kendall Coefficient of Agreement (Kendall and Babington-Smith, 1940; Ledda et al., 2005). This measure is defined by

$$u_s = \frac{2 \sum_{i \neq j} \binom{p_{ij}}{2}}{\binom{m}{2} \binom{n}{2}} - 1 \quad (2.2)$$

where p_{ij} is the number of times TMO_{*i*} is preferred over TMO_{*j*} and m is the number of subjects. Since the number of subjects is even ($m = 10$), the possible minimum value of u , given by Equation 2.2, is $u = -\frac{1}{m-1}$ and its possible maximum value is $u = 1$.

In order to study if u_s values are significant, we used the chi-squared test (χ^2). The χ_s^2 values are defined by

$$\chi_s^2 = \frac{n(n-1)(1 + u_s(m-1))}{2} \quad (2.3)$$

The number of degrees of freedom of the chi-squared test is given by $\frac{n(n-1)}{2}$.

TABLE 2.5: Summary of all statistical analysis from section 2.4.2. We computed the intra-subject evaluation (consistency coefficient ζ), the inter-subjects evaluation (Kendall Agreement Coefficient u) and calculated chi-squared test to see if u values were significant.

Scene	ζ	u	χ^2	$p, 105 \text{ df}$
1	0.91	0.61	681	< 0.001
2	0.95	0.65	719	< 0.001
3	0.93	0.55	624	< 0.001

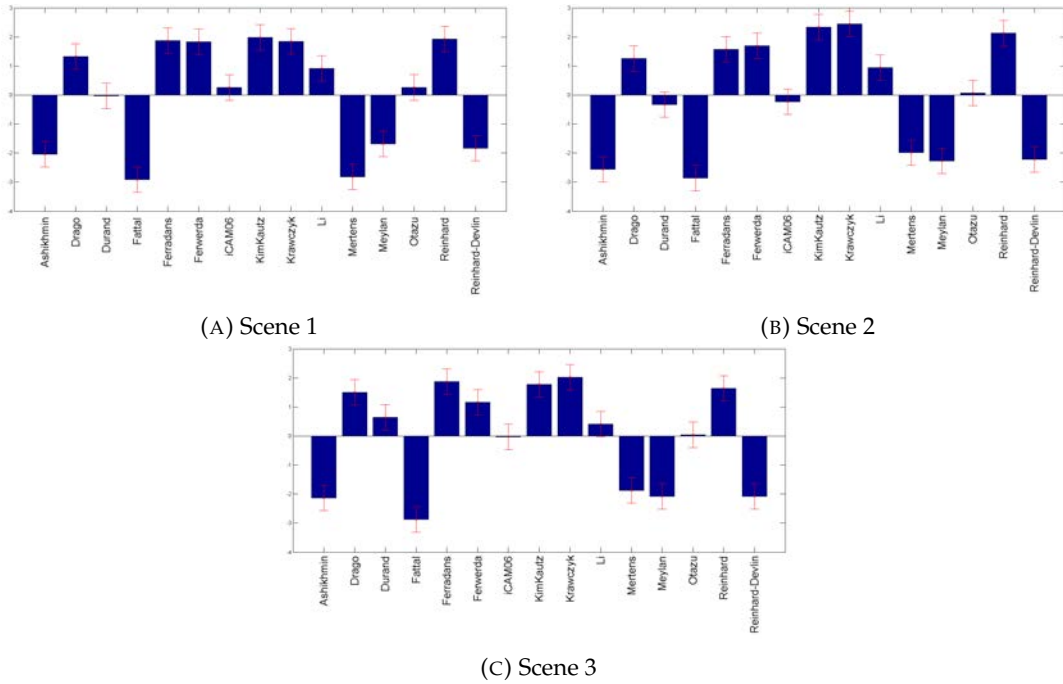


FIGURE 2.7: Case V Thurstone Law's scores for each evaluated TMO for each different scene. Thurstone scores are an arbitrary measure that shows how many times a particular TMO is better than the other ones. Thus, in that case, the higher score, the better TMO. Vertical lines show the 95% confidence limits.

In Table 2.5, we show all statistical measures for each scene, where we can see that intra- and inter-subject consistency values are very high and statistically significant. Then, in Figure 2.7, we show the results of the overall paired comparison evaluations for every scene (obtained from Thurstone's Law of Comparative Judgment, Case V (Montage, 2004)) with 95% confidence limits. Spearman's correlation between these rankings shows that TMOs have similar behaviour across different scenes (their coefficients are equal or higher than 0.90, with $p < 0.05$). We computed the mean value along all the scenes (Table 2.6) and observed that the best ranked TMOs were *KimKautz*, *Krawczyk* and *Reinhard*, which are completely different from the rankings obtained in the previous experiment.

2.5 Discussion

Comparing the results of our two experiments, we observe that in Section 2.4.1 (Segment Matching experiment - see Table 2.4), local TMOs are significantly better than global ones. On the contrary, in Section 2.4.2 (Scene Reproduction experiment - see

TABLE 2.6: Ranking obtained by averaging the scores given by Case V Thurstone Law in the three different scenes. In this ranking, the higher, the more similar to the real scene.

Averaged Thurstone Law's Scores		
TMO	Score	Type
<i>Krawczyk</i>	2.10	Local
<i>KimKautz</i>	2.03	Global
<i>Reinhard</i>	1.90	Global
<i>Ferwerda</i>	1.57	Global
<i>Ferradans</i>	1.48	Local
<i>Drago</i>	1.36	Global
<i>Li</i>	0.75	Local
<i>Otazu</i>	0.13	Local
<i>Durand</i>	0.10	Local
<i>iCAM06</i>	0.00	Local
<i>Meylan</i>	-2.01	Local
<i>Reinhard-Devlin</i>	-2.04	Global
<i>Mertens</i>	-2.22	-
<i>Ashikhmin</i>	-2.25	Local
<i>Fattal</i>	-2.89	Local

Table 2.6), global TMOs are significantly better than local ones. We computed Spearman's correlation coefficient between both experiments rankings and verified that there is no correlation.

An interesting example of this lack of correlation is *iCAM06*. It is clearly at the top of the rankings in the Segment Matching experiment, but it is in the middle position in the Scene Reproduction experiment. This means that it correctly reproduces relationships among gray-levels, but overall features are not maintained. An extreme example is *Fattal*, which is in the fourth position in the Segment Matching rankings, but is the last in the Scene Reproduction ranking. This can be explained because *Fattal* is based on local (or spatial) features, e.g. luminance gradients, but it does not enforce global features (such as global brightness and contrast). In fact, from Table 2.4 (RMSE results) we can conclude that *Fattal* produces a tone-mapped image which is systematically brighter than the real scene. Since *Fattal's* fitted line has almost the same slope as the real scene (see Figure 2.5) removing this offset could improve its performance in the Scene Reproduction experiment.

From the previous results, we infer that overall appearance does not only depend on the correct reproduction of intensity relationships, but it might depend on many other weighted local attributes, such as the reproduction of gray-level and color relationships, contrast, brightness, artifacts, level of detail, etc. This is in agreement with other authors (Yoshida et al., 2005; Yoshida et al., 2007; Cadík et al., 2006; Cadík et al., 2008). Furthermore, our results show that overall attributes should also be considered to correctly reproduce the appearance.

Regarding the question of which is the best TMO, *KimKautz* and *Krawczyk* are very close in all rankings, hence both can be considered equally good.

2.5.1 Comparison to other Studies

In Section 2.4.1 (Segment Matching) we took into account a particular criterion which, up to our knowledge, has never been studied in this kind of TMO ranking experiments. Moreover, we compare our Segment Matching results to the ones obtained by other works that study TMOs applied to gray-level images (given that our analysis has been performed on gray-level facets).

Many works perform overall appearance comparisons, either with (as in our work) or without the real scene. Although Kuang et al. (2004) performed an experiment without a real scene reference, our scene reproduction results agree with theirs in that *Fattal* is the worst ranked operator and *Reinhard* is one of the best ranked. Contrary to our results, Kuang et al. (2004) conclude that *Durand* is better than *Reinhard*. The reason could be that they might have run *Reinhard* in local operator mode, which we did not. Furthermore, they performed a study with gray-scale images and their results showed that *Durand* was better than *Reinhard*, but *iCAM* was worse than *Reinhard*, which is approximately similar to our Segment Matching experiment's results. They differ in *iCAM*'s result, but they used *iCAM* (Fairchild and Johnson, 2000) instead of *iCAM06*, as in our case.

Yoshida et al. (2005; 2007) performed experiments with architectural indoor HDR scenes and they concluded that *Reinhard* and *Drago* were good in terms of naturalness and *Durand* was not ranked as highly as in (Kuang et al., 2004) (in an experiment without the reference scene). Our results agree with Yoshida et al. (2005; 2007). Moreover, Yoshida et al. (2007) showed that global and local operators obtain different results, but global TMO results are more similar among themselves than local TMO. As pointed out in the previous section, this relationship is also present in our study (Tables 2.4 and 2.6).

Ledda et al. (2005) used a HDR display and obtained a ranking according to the overall similarity of TMO images. In this ranking, *iCAM* was the first one, which does not agree with our results. In addition, their ranking shows the following TMO's order: *Reinhard*, *Drago* and *Durand*, which match to our results. These authors also performed experiments in gray-scales obtaining *Reinhard* as the best ranked, which does not agree with our results.

Cadík et al. (2006; 2008) performed a very exhaustive study of perceptual attributes. We agree with some of their results like the good ranking of *Reinhard* (close to the best) and the unnaturalness of *Fattal*. Moreover, we strongly agree with them in that the best overall quality is generally observed in images produced by global TMOs. Nevertheless, we want to point out that there was some conflict between these two studies. In the first one (Cadík et al., 2006), *Durand* was the worst ranked operator, ranked even lower than *Fattal*, but in the second one (Cadík et al., 2008), *Fattal* was the worst ranked and *Durand* was in a middle position. Our results are in line with Cadík et al. (2008).

We do not agree with Kuang et al. (2007) in that *Durand* is always the best ranked operator (with and without a reference scene). Furthermore, in contrast with our results, *Reinhard* is in a middle position of their ranking.

Kuang et al. (2007) suggested, again, that *Durand* was better than *Reinhard* and *iCAM06* was even better than *Durand*. In our results, *Durand* and *iCAM06* are quite close, but *Reinhard* is much better than them. Again, *Reinhard* could have been run in local TMO mode.

In a similar study as Kuang et al. (2004), Ashikhmin and Goyal (2006) concluded that, comparing to the real scene, *Fattal* and *Drago* were two of their overall best performers. We do not agree that *Fattal* is one of the best performers, but we have

to point out that, in their work, they tuned the TMO's parameters, which implies that *Fattal* could be a good TMO when a fine tuning of the parameters is performed. Furthermore, in their work, *Drago* obtained more or less the same results as *Fattal*, but *Reinhard* obtained worse results than them. They do not specify how they run *Reinhard*, but it is possible that they run it in the local mode. They obtained that the trilateral filtering (Choudhury and Tumblin, 2003), which is an improvement of *Durand*, was the worst ranked TMO, so it makes sense that, in our work, *Durand* has obtained worse results than *Drago* and *Reinhard*.

In (Akyüz et al., 2007), the outputs of the most internally sophisticated TMO are statistically worse than the best single LDR exposure. Since a global operator is generally less sophisticated than a local, we could expect that global TMO results are better than local TMO results. Contrary to this theory, *Mertens* (which cannot be considered a sophisticated TMO because it uses single exposure values) is on middle positions in the Segment Matching experiments but it is one of the worst ranked in the Scene Reproduction experiments.

Some authors emphasize the creation and use of particular metrics to compare tone-mapped images. For example, Ferradans et al. (2011) performed an evaluation of several TMOs using the metric of Aydin et al. (2008). Although it is not the purpose of our work, we performed a very preliminary analysis comparing our results to those of Aydin et al. (2008) as shown in (Ferradans et al., 2011). We agree that *Fattal* was the operator with highest total error percentages, but disagree with the general overall TMOs ranking. A detailed analysis comparing numerical metrics and psychophysical results is scheduled for future work.

It is possible to identify several shortcomings in our study that need to be addressed before a more definitive conclusion is achieved. Firstly, we have assumed that the software provided by the Sigma camera manufacturers is accurate enough to convert the scene luminance array to the sRGB digital file used as input to all TMO algorithms. This assumption hides possible inaccuracies because of glare effects, lens aberrations and possible tone/chroma enhancements. In the past, we calibrated this camera and measured the linearity and spectral sensitivity of its sensors for use in daylight settings (*Camera Calibration Methods*) and verified that tone/chroma enhancements are kept to a minimum at least for its raw image settings. For this work we did not employ our own calibration (which is valid within a fairly limited dynamic range) but decided to rely on the manufacturer's algorithm instead. All these limits the reproducibility of our experiments (unless of course the same camera is used). We are also aware that the absence of an accurate radiometric description of our scenes also limits the reproducibility of our experiments. To this end we provide photometric information at least of the patches and facets used in the matching comparisons (see Tables 2.2 and 2.3) and the dynamic range of the both the monitor and the scenes (see Section 2.3.1).

2.6 Conclusions

Our results show that TMO quality rankings strongly depend on the criteria used for the psychophysical evaluation. Not surprisingly, on one hand, local TMOs are better than global TMOs on our Segment Matching experiment because these operators do not consider just a pixel, but also a region of pixels (i.e. spatial information). On the other hand, global TMOs are better than local ones in our Scene Reproduction

experiment. We have found no significant correlation between Segment Matching and Scene Reproduction rankings, showing that observers are using several visual attributes to perform their tasks and some of these attributes are not considered by TMOs. We conclude that TMOs should take into account both local and global characteristics of the image, which implies that there is ample room for improvement in the future development of TMO algorithms. Furthermore, we suggest that an agreed standard criteria should be defined for a proper and fair comparison among them.

Our rankings also show there is no TMO that is clearly better than all the others across our experiments, but *KimKautz* and *Krawczyk* are perhaps the best ranked since they do not underperform in any of the metrics.

As a general conclusion, since none of the tested TMOs satisfies all the testing criteria ("Segment Matching", "Scene Reproduction" and their respective analyses), operators have to be selected depending on each particular task. This is a consequence of the lack of coherent understanding of the goals of a TMO, which is reflected in the wide variety of evaluation methods and results present in the literature. From a scientific point of view, a TMO should aim to perceptually reproduce the real scene instead of modifying image appearance according to aesthetics (for which we already have a wide selection of image tools). Having said so, it is also important to consider that these operators are widely used in digital cameras and mobile phone's cameras and TMO users often prefer aesthetic improvements over accurate scene reproduction.

2.7 Related Publications

- Which tone-mapping operator is the best? A comparative study of the perceptual quality (Cerdeira-Company, Parraga, and Otazu, 2018), *Journal of the Optical Society of America A*, 2018.

Chapter 3

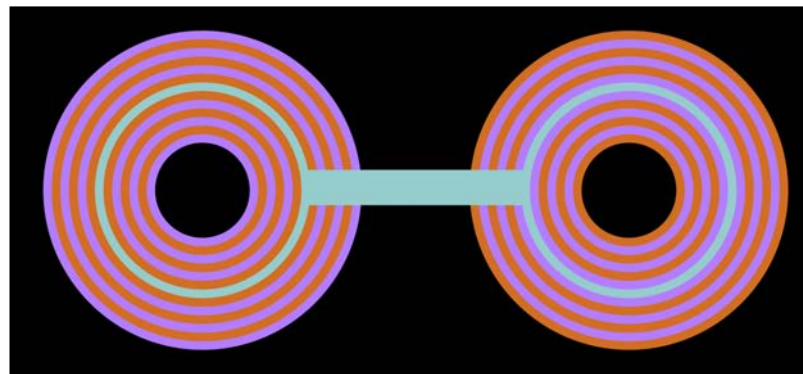
Color Induction

The phenomenon of color induction (which occurs when the perceived color of an object changes according to the colors of the objects around it) has been known and exploited by artists for centuries (Chevreul, 1839; Von Bezold, 1876). There are two types of color induction: *color contrast* and *color assimilation* (see Figure 3.1). Color contrast occurs when the perceived color (the target) shifts *away* from the surrounding color (the inducer) and color assimilation occurs when the perceived color shifts *towards* the inducer. For instance, given a gray object surrounded by green objects, if the first is perceived as reddish (the color complementary to green), we say that color contrast is occurring. On the other hand, if the gray object is perceived as greenish, we say that color assimilation is happening. The type of induction (contrast or assimilation) is usually associated to the spatiochromatic characteristics of the surround. Psychophysical research has shown that uniform surrounds tend to induce color contrast, while striped surrounds tend to induce color assimilation (Monnier and Shevell, 2003; Monnier and Shevell, 2004; Otazu, Parraga, and Vanrell, 2010).

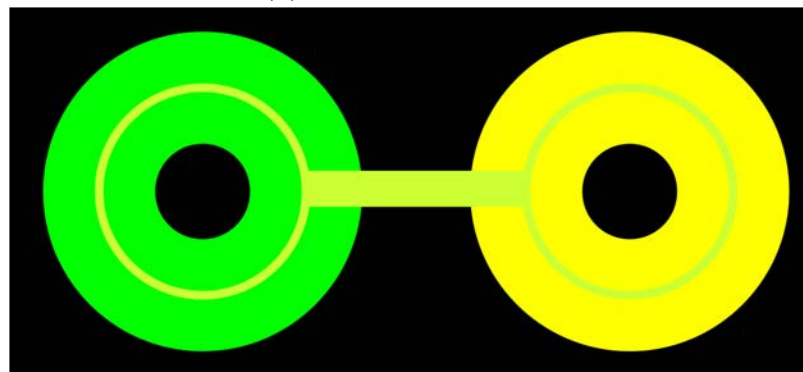
In this chapter, we have studied two different stimuli characteristics that play an important role in color induction: the temporal frequency and both luminance and brightness differences. We have divided it in two main sections according to the studied features. First, we studied the temporal frequency effect on color induction using equiluminant stimuli. Then, we studied both the luminance and brightness differences effect on color assimilation using temporally static stimuli. We focused the second study on color assimilation because it was less explored than color contrast and because the color induction appears and disappears just by increasing the luminance or brightness contrast. At the end of this chapter, we detail the publications that aroused from these studies.

3.1 Optics considerations

There are optical effects that influence visual perception and may account for some of the properties of assimilation. The most often cited are wavelength-independent spread light and wavelength-dependent chromatic aberration. Spread light is a consequence of optical imperfections in the lens which change the light of the test stimulus that reaches the retina (Devinck, Pinna, and Werner, 2014). To calculate the influence of spread light, Smith et al. (2001) used the function derived by Williams et al. (1994) and a method similar to Shevell and Burroughs (1988). They calculated the amount of light that spread into their test stimulus region considering an equiluminant square-wave grating and observed that, as spatial frequency increases, the spread light contribution (to the center of the test stimulus region) increases. In their case they obtained that for stimuli of 4.0 *cpd* and below the spread light contribution was negligible.



(A) Color assimilation effect



(B) Color contrast effect

FIGURE 3.1: Examples of both **(A)** color assimilation and **(B)** color contrast effects. In the top panel the target ring is perceived as greenish (left) and bluish (right), but as the rectangle shows they are both of the same color. The difference between these two stimuli is the order of the inducers (the rings that surround the target one). Thus, in the left stimulus, the target ring is shifted towards the orange, while in the right stimulus it is shifted towards the purple. In the bottom panel the target ring is shifted away from its inducers (green and yellow, respectively) and it is perceived as yellowish and greenish, but again they are of the same color.

Chromatic aberration is also a source of spread light which depends on spectral wavelength and increases with higher spatial frequencies. Smith et al. (2001) found that even for square-gratings of 9 cpd , the effects of chromatic aberration were small, concluding that it does not appear to be a key factor for color assimilation. Similarly, Bradley et al. (1992) concluded that chromatic aberration is more relevant at higher spatial frequencies than at lower ones (Devinck, Pinna, and Werner, 2014).

Although these optical effects could account for part of the color assimilation results, most authors agree that even for high spatial frequencies there are clear neural contributions (Helson, 1963; De Weert and Kruysbergen, 1997; Monnier and Shevell, 2003; Cao and Shevell, 2005; Devinck, Pinna, and Werner, 2014).

3.2 Color induction in equiluminant flashed stimuli

3.2.1 Introduction

In striped surround stimuli, the spatial frequency of the stripes is a key factor to induce color assimilation (Fach and Sharpe, 1986; Smith, Jin, and Pokorny, 2001), with

higher spatial frequencies ($> 2.74 \text{ cpd}$) leading to a stronger assimilation (Cao and Shevell, 2005; Otazu, Parraga, and Vanrell, 2010). Nevertheless, Smith et al. (2001) found that thick ($< 0.7 \text{ cpd}$) stripes can induce color contrast.

Color induction has also been studied using dynamic and flashed stimuli (Anstis, Rogers, and Henry, 1978; Kelly and Martinez-Uriegas, 1993; De Valois, Webster, and De Valois, 1986; Singer and D'Zmura, 1994; Kaneko and Murakami, 2012). In dynamic stimuli, the inducer is modulated along time, being the temporal frequency of the surround modulation an important factor for color induction, *e.g.* stronger induction at low temporal frequencies, falling down beyond 2 – 3 Hz (De Valois, Webster, and De Valois, 1986; Singer and D'Zmura, 1994). In flashed stimuli, the target stimulus is presented during a brief time (a 'blank' frame is usually shown when the target stimulus is not presented) (Kaneko and Murakami, 2012). Some of these studies measured the color induction of afterimages (Anstis, Rogers, and Henry, 1978; Kelly and Martinez-Uriegas, 1993). They showed that color contrast can produce afterimages and, conversely, color afterimages can induce color contrast (Anstis, Rogers, and Henry, 1978). Furthermore, Kelly and Martinez-Uriegas (1993) concluded that isoluminant chromatic stimuli create isoluminant chromatic afterimages.

Recently, Kaneko and Murakami (2012) published an extensive study in color induction using equiluminant flashed color stimuli with uniform surrounds. They measured the color induction at different flash durations (from 10 ms to 640 ms) and observed that color contrast significantly depends on the duration of the flash. They concluded that the shorter the flash duration, the stronger the contrast. Since they used uniform surrounds, only color contrast was reported.

In this study, we extend the one of Kaneko and Murakami (2012), using both uniform and striped surrounds and both static and flashed stimuli (see several static stimuli examples in Figure 3.2). Similarly to other studies (Monnier and Shevell, 2003; Monnier and Shevell, 2004; Otazu, Parraga, and Vanrell, 2010; Cao and Shevell, 2005; Fach and Sharpe, 1986; Smith, Jin, and Pokorny, 2001; Kaneko and Murakami, 2012; Anstis, Rogers, and Henry, 1978; Kelly and Martinez-Uriegas, 1993; De Valois, Webster, and De Valois, 1986; Singer and D'Zmura, 1994), we expect to observe color contrast in uniform surround stimuli and color assimilation in striped surround stimuli. Furthermore, we expect to reproduce the Kaneko and Murakami's results (2012) for flashed uniform surrounds and to analyze whether color induction depends on flash duration for both striped and uniform surrounds. In previous papers (Otazu, Vanrell, and Parraga, 2008; Otazu, Parraga, and Vanrell, 2010; Penacchio, Otazu, and Dempere-Marco, 2013) one author of this paper simultaneously reproduced psychophysical results of both color and brightness induction using a Wavelet model and a neurodynamical model of V1. These models suggest that color contrast and color assimilation could be the result of the same mechanism (lateral connections) (Zaidi et al., 1992; Zaidi, 1999; Penacchio, Otazu, and Dempere-Marco, 2013). Thus, our hypothesis is that uniform and striped surrounds, when flashed, would induce similar temporal color induction effects, but in opposite directions (color contrast and color assimilation, respectively).

3.2.2 Methods

Apparatus

All experiments were conducted in a dark room, on a calibrated 21" SONY GDM-F500R CRT monitor ($1024 \times 768 \text{ px}$, 100Hz) with a viewable image size of 19.8". The display was viewed binocularly and freely (subject's head was not constrained) from

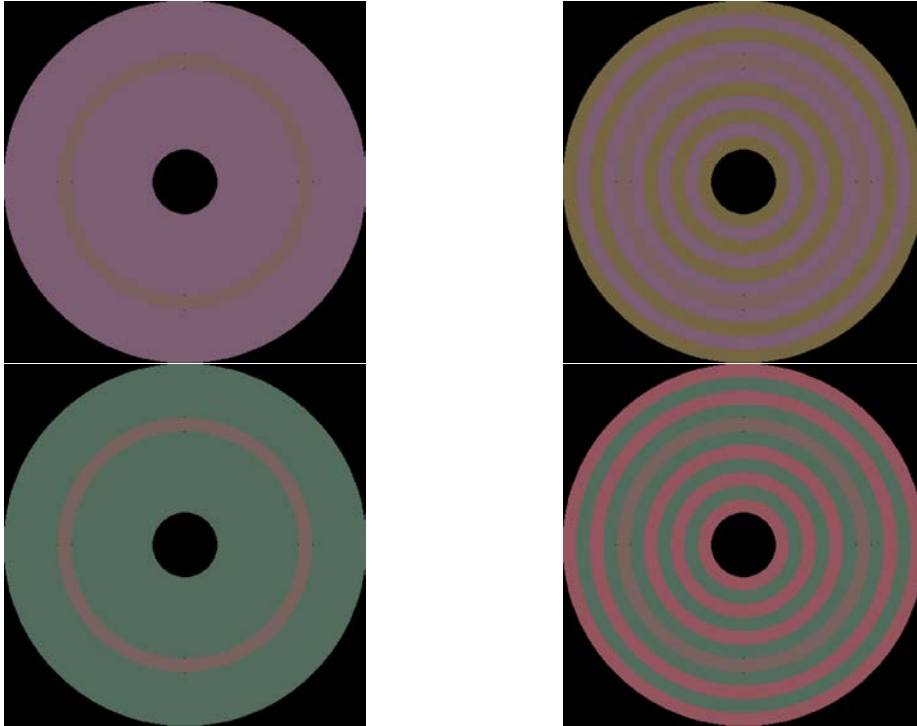


FIGURE 3.2: Examples of some stimuli used in this study (see Table 3.1). In this figure, we can observe that the achromatic ring (surrounded by 8 black dots) is perceived differently depending on the surround chromaticity. This effect is called color induction. For instance, on the top-left panel, the achromatic ring surrounded by a purple inducer is perceived as lime-ish, while the achromatic ring surrounded by a green inducer (bottom-left panel) is perceived as reddish. In this figure, the Spatial Conditions 2 and 3 of the Experiment U (left panels, from top to bottom) and the Spatial Conditions 2 and 3 of the Experiment S (right panels, from top to bottom) are shown.

an approximate distance of 132 *cm*, subtending around 17.3×13.0 *deg* of visual angle for the observer. The monitor was connected to a Wildcat Realizm R500 PCI Express graphics card through a digital video processor (Cambridge Research Systems ViSaGe MKII Stimulus Generator) capable of displaying 14-bit color depths. The monitor was calibrated via a customary software for the stimulus generator (Cambridge Research Systems, Ltd., Rochester, UK) and a ColorCal (Minolta sensor) suction-cup colorimeter.

Stimuli

The software was implemented in Matlab (The MathWorks, Inc., Natick, MA, US), and the video processor was managed using the Cambridge Research Systems custom-made toolbox. We used the same spatial configuration of visual stimuli as Otazu et al. (2010), which was inspired by Monnier and Shevell (2003; 2004). In this study, we added a temporal component, following Kaneko and Murakami (2012) flash duration values.

All stimuli were defined in the MacLeod-Boynton color space (Boynton, 1986), which is based in the Smith and Pokorny cone fundamentals (Smith and Pokorny, 1975). In this opponent space, the *l* axis represents the red-green opponency (*i.e.*,

'L vs M' cone opponency) and the s axis represents the purple-lime opponency (*i.e.*, 'S vs (L+M)' cone opponency), where s is normalized to unity equal-energy white (Boynton, 1986).

Spatial Configuration Several stimuli examples are shown in Figure 3.2 and a schematic of the stimuli's spatial configuration is shown in Figure 3.3. The test frame was composed by two circularly symmetric patterns (*i.e.*, the test and the comparison stimuli) presented side by side and separated by 8.68 deg of visual angle from the observer's point of view. Similarly to Otazu et al. (2010), the stimuli's background was dark and the test ring (in the test stimulus) was achromatic and surrounded by concentric rings (inducers) of spatially alternating colors (the 1st and 2nd inducer, according to the physical distance to the test ring). When these two inducers had the same chromaticity, the surround was a uniform region. The striped surround was built with 11 circular stripes (stripes' spatial frequency was 1.94 cpd) because, as observed in Otazu et al. (2010), they produce more color induction than 5 stripes and are not as thin as 17 stripes. In fact, in the 17 stripes case, observers reported that for the shortest flash they could not detect the test ring. To make the detection of the test ring easier, we drew 8 black dots of 1 pixel size: 4 dots in the inner radius of the test ring and 4 points in the outer radius (at 0, 90, 180 and 270°). The comparison ring, on the right side of the frame, was always surrounded by a uniform achromatic disk approximately metameric to equal-energy white ($l = 0.66$, $s = 0.98$ and $Y = 20 \text{ cd/m}^2$) (Monnier and Shevell, 2004).

All chromaticities were located on the individual subject-calibrated equiluminant planes. The calibration of subjects' equiluminant plane was performed using the Minimally Distinct Border (MDB) (Boynton and Kaiser, 1968; Kaiser, 1971; Wagner and Boynton, 1972; Kaiser et al., 1990; De Valois and De Valois, 1988a; Brill, 2014; Boynton, 1973). Thus, for each subject, all the colors of the stimuli were shown on his/her perceptually equiluminant surface.

Temporal Configuration In Figure 3.4, we show the temporal configuration of the stimuli. Two different frames were defined: the test frame and the blank frame. During the blank frame, the test stimulus was an achromatic disk of the same intensity as the test ring. During the test frame, the test stimulus (either striped or uniform) was flashed while the achromatic test ring was not modified. That is, the achromatic test ring remained constant along the experiment and only the chromatic surrounding rings were flashed. The time duration of our blank frame was 1 s and the flash duration took values from 10 to 320 ms in a dyadic temporal frequency sequence (*i.e.*, 10, 20, 40, 80, 160 and 320 ms, $N_{tc} = 7$, see temporal conditions in Table 3.1). The stimulus sequence (*i.e.*, blank and test frames) was repeated until subjects finished the task.

In addition, we also used static stimuli, which was equivalent to infinite flash duration of the test frame.

All the experimental conditions (both spatial and temporal) are shown in Table 3.1. These inducers' colors were chosen because they are located on the cardinal axes of the MacLeod-Boynton color space (Boynton, 1986), with the achromatic locus at the center.

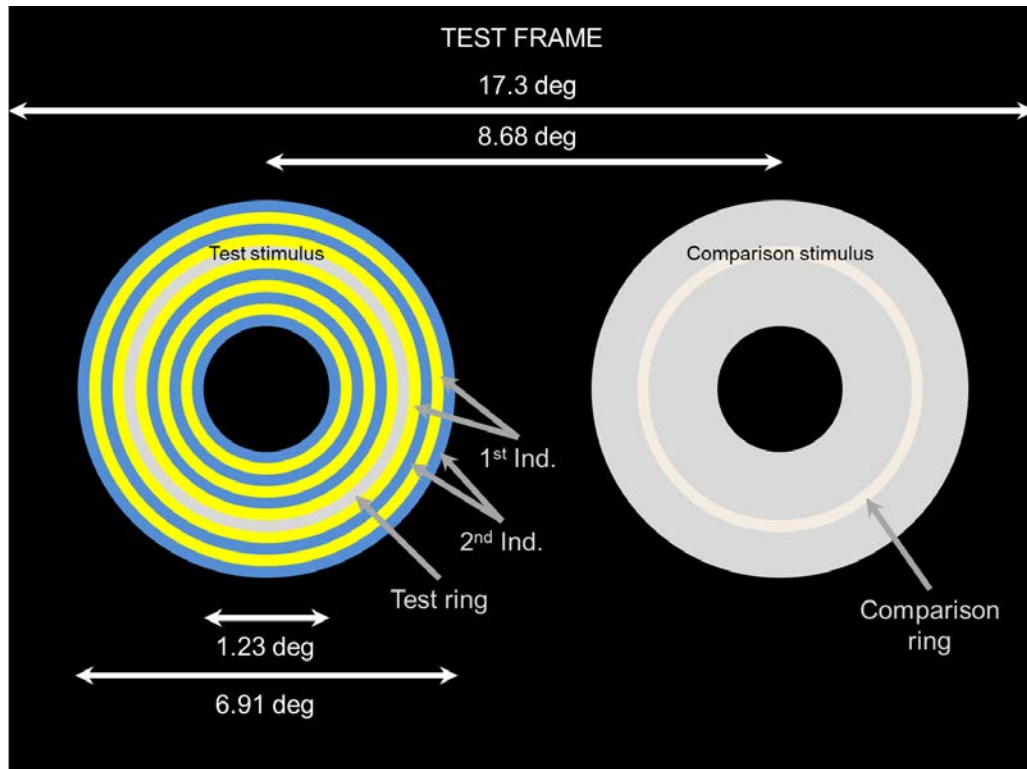


FIGURE 3.3: Spatial configuration of the stimuli. Subjects had to adjust the chromaticity of the comparison ring in order to perceptually match the chromaticity of the test ring. The colors in this figure are illustrative. All experimental conditions are described in Table 3.1.

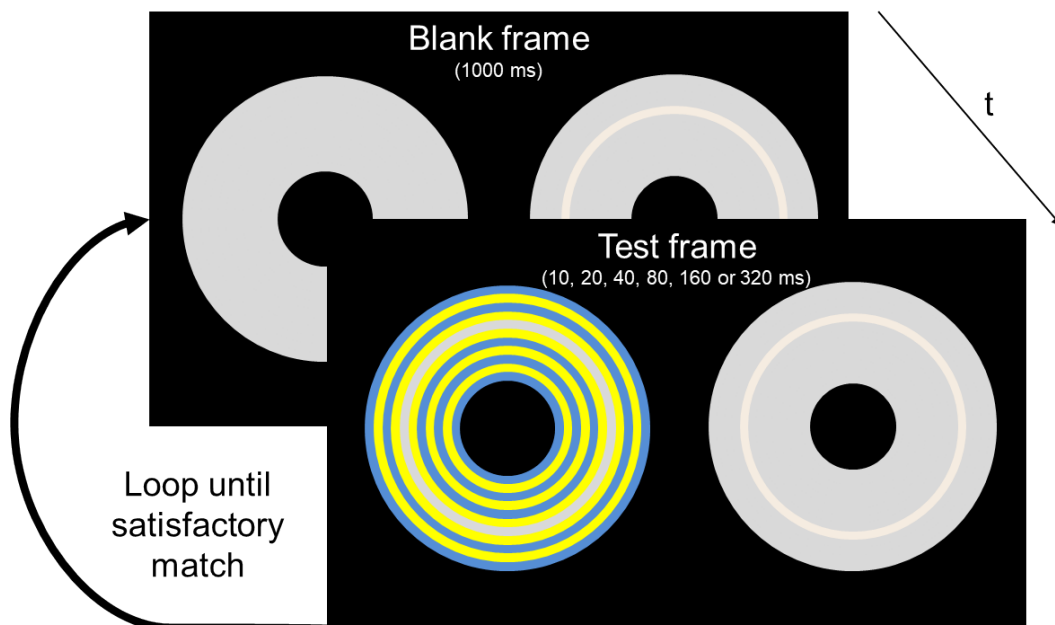


FIGURE 3.4: Temporal configuration of the stimuli. The blank frame was shown during 1 s and the duration of the flash (when the test frame was presented) depended on the temporal condition. All experimental conditions are described in Table 3.1.

TABLE 3.1: Summary of the experimental conditions (both spatial and temporal). In the spatial conditions, we detail the chromaticity sets in MacLeod and Boynton color space. Only l and s chromatic axes are reported because all chromaticities were located on the individual subject-calibrated equiluminant planes ($Y = 20 \text{ cd/m}^2$). In the temporal conditions, we indicate the flash duration in ms . During the flash, the test frame was presented. In particular, in the static condition only the test frame was presented (unlimited duration). The last column indicates the color name of the inducers. When two color names (e.g., red-green) are indicated, it means that the 1st (e.g., red) and the 2nd (e.g., green) inducers are different.

Experiment U (Uniform surround)							
Spatial Conditions							
	Test Ring		1st Inducer		2nd Inducer		Inducer's color
	l	s	l	s	l	s	
1	0.66	0.98	0.69	0.98	0.69	0.98	Red
2	0.66	0.98	0.66	1.38	0.66	1.38	Purple
3	0.66	0.98	0.63	0.98	0.63	0.98	Green
4	0.66	0.98	0.66	0.58	0.66	0.58	Lime
Temporal Conditions (in ms)							
10, 20, 40, 80, 160, 320, static							

Experiment S (Striped surround)							
Spatial Conditions							
	Test Ring		1st Inducer		2nd Inducer		Inducers' color
	l	s	l	s	l	s	
1	0.66	0.98	0.69	0.98	0.63	0.98	Red-green
2	0.66	0.98	0.66	1.38	0.66	0.58	Purple-lime
3	0.66	0.98	0.63	0.98	0.69	0.98	Green-red
4	0.66	0.98	0.66	0.58	0.66	1.38	Lime-purple
Temporal Conditions (in ms)							
10, 20, 40, 80, 160, 320, static							

Subjects

The experiments were done by six observers ($N_{sub} = 6$), four of them from our lab (AA, DB, LR and XO), who were familiar with color spaces, and two others who were not related to the lab (BG and CM). All of them were informed of the aim of the experiments and consented to participate in the experimentation. Five observers were completely naïve (AA, BG, CM, DB and LR), while one of them is one of the authors of the paper (XO). Three of them are male (AA, DB and XO) and the other three are female (BG, CM and LR). The ages were comprised between 22 and 45 years old. All of them had normal or corrected-to-normal vision, tested using the Ishihara (Ishihara, 1972) and the D-15 Farnsworth Dichotomous Test (Farnsworth, 1947). To learn the experimental procedure, all observers did a one day training session before starting the experiments. All the data collected during this training session was discarded.

Experimental Procedure

The subjects' task was to adjust the chromaticity of the comparison ring until they perceived it equal to the test ring. To do the task, they used a Logitech© gamepad and they were instructed to do the match according to the test ring color perceived during the test frame, ignoring the after-effect produced during the blank frame.

We conducted two different experiments (*Experiments U* and *S*) to study how the surround chromaticity and the flash duration influence the color perception. Since color induction strongly depends on the surround type, we divided the experiments according to it. In Experiment U, the test ring had a uniform surround and, in Experiment S, the test ring had a striped surround.

To reduce the available color space to one-dimension, similarly to Kaneko and Murakami (2012), we performed a previous experiment where subjects were able to adjust the chromaticity in a MacLeod-Boynton two-dimensional color space. We observed that in both experiments (Experiment U and S) the observations were approximately on the cardinal axis which includes the test and inducers' chromaticities. Thus, we reduced the available color space to one-dimension, *i.e.*, the observers only changed the comparison ring chromaticity along l or s axis, depending on the experimental spatial condition (*1-D Experiment*).

For each 1-D Experiment (Experiments U and S) we had 28 different experimental conditions (4 different spatial conditions - $N_{sc} = 4$ - and 7 temporal conditions - $N_{tc} = 7$ -, see Table 3.1). Each subject evaluated each experimental condition 10 different times (*i.e.*, 10 different observations, $N_{obs} = 10$). An experimental condition was determined by the combination of a spatial condition and a temporal condition. Each run started with 3 minutes of dark adaptation (Kaneko and Murakami, 2012) and subjects performed 48 different observations (8 different spatial conditions, 3 different temporal conditions, and 2 repetitions). Subjects did not have any time restriction, but they were advised not to take more than 1 minute for each experimental condition. On average, each run took about 30 minutes. Subjects evaluated the static conditions of both experiments on two days apart. In that case, they performed 24 observations in each run (8 different spatial conditions, 1 temporal condition -static- and 3 repetitions, except for the last run, which was 4 repetitions), taking about 15 minutes.

To mitigate a potential memory effect, we defined a pseudo-random order of the temporal conditions in each run, while the spatial conditions were randomized.

3.2.3 Ethics approval

All experiments conducted in this study have been approved by the Ethical Committee of our University (Comissio d'Ètica en l'Experimentacio Animal i Humana de la Universitat Autònoma de Barcelona).

3.2.4 Data Analysis

To estimate the strength of color induction we used a one-dimensional metric (see Equation 3.1) which is sensitive to both color contrast and color assimilation. In Equation 3.1, ΔC_i is the strength of the induction phenomenon along any of the two axes of the MacLeod-Boynton color space ($i = [l, s]$) and C_i^c is the chromaticity of the

comparison ring along the axis considered. Similarly, C_i^t and C_i^s are the chromaticities of the test ring and 1st inducer ring along the same axis respectively.

$$\Delta C_i = \frac{C_i^c - C_i^t}{C_i^s - C_i^t}, \quad (3.1)$$

According to Equation 3.1, when ΔC_i is negative, color contrast is induced since the chromaticity *difference* between the comparison ring and the test ring ($C_i^c - C_i^t$) shifts *away* from that of the 1st inducer ($C_i^c - C_i^t$ has different sign from $C_i^s - C_i^t$). Similarly, when ΔC_i is positive, color assimilation is induced since the chromaticity difference between the comparison ring and the test ring shifts *towards* that of the 1st inducer ($C_i^c - C_i^t$ has the same sign as $C_i^s - C_i^t$).

It is important to note that there is a region below the just noticeable difference (JND) where no color changes are perceived and, therefore, no color induction (neither contrast nor assimilation) is induced. We estimated this region ($\Delta E = 1$) from the CIELab color space, which is an approximately perceptually uniform. Since both inducers were defined on the same color axis, we defined induction in each of the orthogonal axes i separately. This metric does not include the 2nd inducer because only the 1st one determines the type of color induction (color contrast or color assimilation).

For each experimental condition, we averaged all 10 observations of each subject and computed the average and the standard error of means (SEM) of all 6 subjects ($N_{sub} = 6$).

We used a nested ANOVA analysis to observe whether temporal conditions affect to color induction. Once the nested ANOVA indicated that there are significant differences, a Fisher's Least Significant Differences post-hoc analysis (Fisher's LSD) was performed to group the temporal conditions according to the color they induce.

3.2.5 Results

Experiment U

In this experiment, we study the color induced by equiluminant uniform surrounds on an achromatic test ring at different temporal conditions (see Table 3.1). The results (Figure 3.5) show that chromatic contrast is induced in all experimental conditions, except at the 10 *ms* flash in the purple-lime opponent axis. In fact, under these experimental conditions (Spatial Conditions 2 and 4 -purple and lime inducers- flashed during 10 *ms*), observers pointed out that the test frame detection was very difficult.

The statistical analyses show that for Spatial Conditions 1, 3 and 4, maximum color contrast induction is produced by 40 *ms* flash, while in the Spatial Condition 2 there is no peak at 40 *ms*. Furthermore, for all spatial conditions there are no significant differences between the perceived colors at 80 and 160 *ms*. Moreover, the induction produced by a 320 *ms* flash was similar to the induction produced by the static stimulus. All the ANOVA statistics' details are shown in Table 3.2 and the letters below error bars in Figure 3.5 show the temporal conditions that induced statistically similar colors (Fisher's LSD post-hoc analysis' results). The temporal conditions which have the same letter can be considered that induce the same perceptual color.

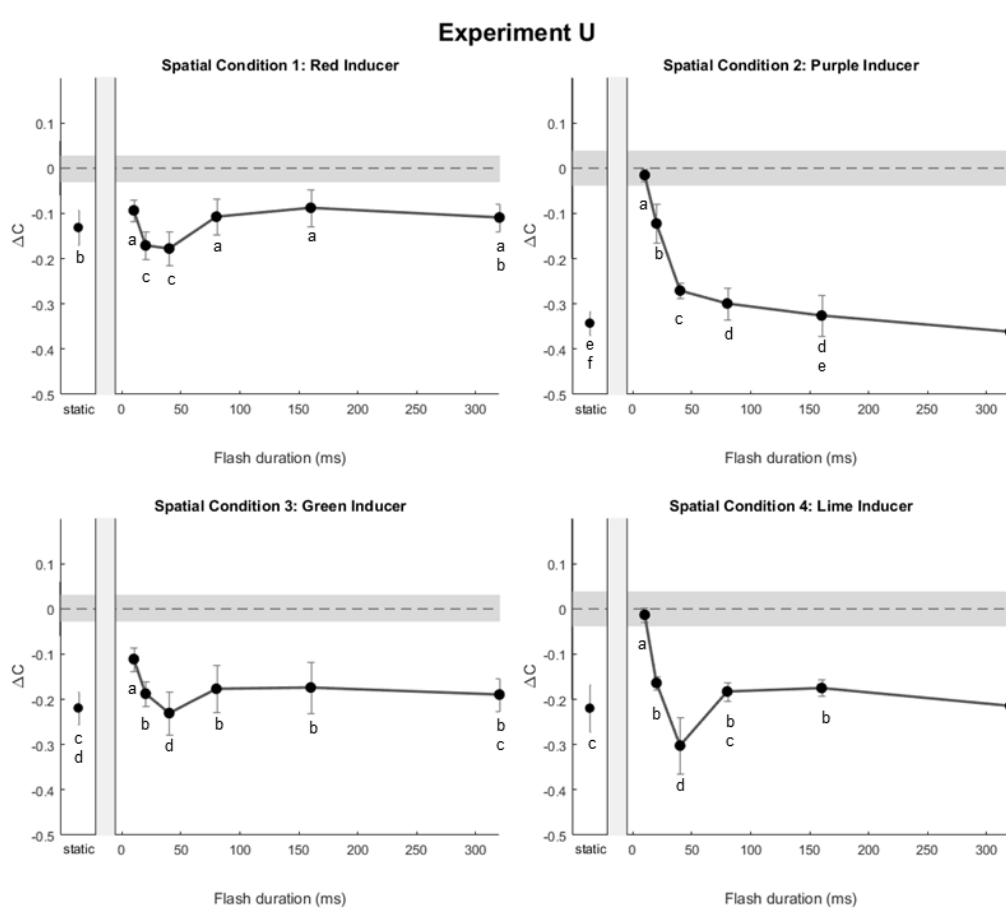


FIGURE 3.5: Results of Experiment U. The averaged (mean of 6 observers) color induction metric (ΔC) is plotted against the flash duration (7 different temporal conditions). Separate plots correspond to the different spatial conditions (see Experiment U in Table 3.1). The gray area is the region where subjects cannot perceive chromatic differences ($\Delta C \in [-JND, JND]$). Error bars indicate ± 1 SEM. An ANOVA analysis of the data (see Table 3.2) shows that there are significant differences in color induction strength for different temporal conditions. Fisher's LSD post-hoc analysis (letters below the error bars), which allows us to measure which temporal conditions are significantly different, stresses that the peak of color induction is always perceived at 40 ms, except for Spatial Condition 2. Furthermore, static stimulation induces the same color as the longest flash duration (320 ms) and the perceived color at 80 and 160 ms does not vary. In all chromatic conditions, chromatic contrast ($\Delta C < 0$) or no induction is induced.

Experiment S

In this experiment, we study the color induced by equiluminant striped surrounds on an achromatic test ring under different temporal conditions (see Experiment S in Table 3.1). In Figure 3.6, we can observe that Spatial Conditions 1 and 4 do not induce any color when the stimuli are flashed. Only one out of 6 subjects observed assimilation in flashed Spatial Condition 1, and 2 out of 6 perceived assimilation in flashed Spatial Condition 4. By contrast, static stimulus of Spatial Condition 1 induces chromatic assimilation ($\Delta C > 0$). In Spatial Conditions 2 and 3 only color contrast ($\Delta C < 0$) is perceived.

Subjects pointed out that, again, they left a gray color for Spatial Conditions 2 and 4 (purple-lime axis) flashed during 10 *ms* because they were not able to see the test frame.

Similarly to Experiment U, ANOVA analysis shows significant differences between the induction produced by flashes of different durations in all spatial conditions (see Experiment S in Table 3.2). We have not observed any grouping or behavioral pattern over all spatial conditions in the Fisher's LSD post-hoc analysis. Since the profile of the results of Figures 3.5 and 3.6 are completely different and the strongest induction in this experiment is not observed at the same flash duration as in the previous one, our initial hypothesis should be rejected.

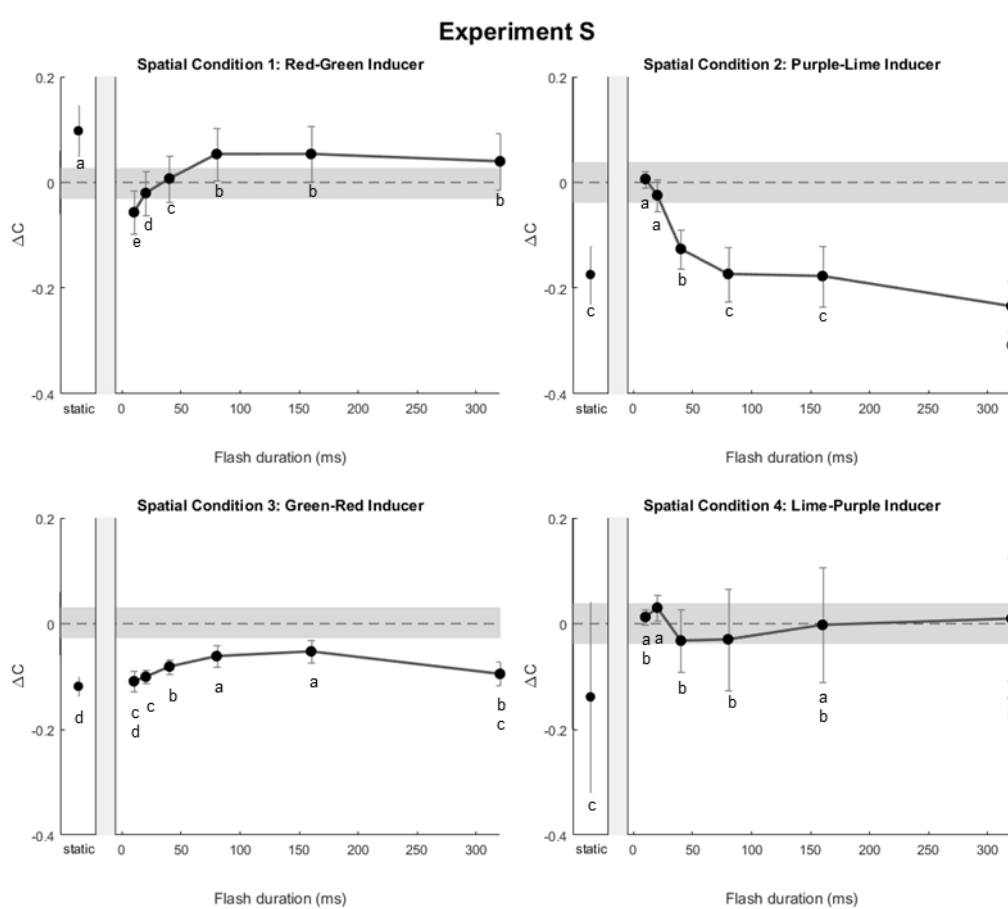


FIGURE 3.6: Results of Experiment S. The averaged (mean of 6 observers) color induction metric (ΔC) is plotted against the flash duration. Separate plots correspond to the different spatial conditions (see Experiment S in Table 3.1). The gray region indicates where induction cannot be perceived ($[-JND, JND]$). Error bars indicate $\pm 1 SEM$. An ANOVA analysis of the data (see Experiment S in Table 3.2) shows that there are significant differences between color induction for different temporal conditions. Like in Experiment U, we do a Fisher's LSD post-hoc analysis (letters below error bars) to know the temporal conditions that induce significantly different colors. In this Experiment, we observe that the static stimuli induction has significant differences with respect to the induction produced by a 320 *ms* flash. No color assimilation has been induced, except by static stimulus in Spatial Condition 1.

TABLE 3.2: Summary of the nested ANOVA results. The first column indicates the experiment (Exp), the second one the spatial condition according to Table 3.1, the third the effect (between groups, within groups and the error), the fourth the degrees of freedom, the fifth the sum of squares (SS), the sixth the mean square (MS) and the last two the F and p values. These results show that, in all spatial conditions, color induction depends on the temporal condition of the stimulus (*i.e.*, the flash duration). The nested ANOVAs have 6 and 378 degrees of freedom, corresponding to $N_{tc} - 1$ and $N_{tc}N_{sub}(N_{obs} - 1)$, respectively.

Exp	Spatial Cond	Source	df	SS	MS	F	p
U	1	Flash Duration	6	0.47	0.08	18.74	<0.001
		Observer(Flash Duration)	35	2.52	0.07	17.18	<0.001
		Error	378	1.59	0.00		
	2	Flash Duration	6	6.05	1.01	160.80	<0.001
		Observer(Flash Duration)	35	2.56	0.07	11.65	<0.001
		Error	378	2.37	0.01		
	3	Flash Duration	6	0.53	0.09	11.95	<0.001
		Observer(Flash Duration)	35	3.68	0.11	14.12	<0.001
		Error	378	2.82	0.01		
	4	Flash Duration	6	2.75	0.46	41.43	<0.001
		Observer(Flash Duration)	35	2.55	0.07	6.58	<0.001
		Error	378	4.18	0.01		
S	1	Flash Duration	6	0.97	0.16	84.26	<0.001
		Observer(Flash Duration)	35	4.66	0.13	69.44	<0.001
		Error	378	0.72	0.00		
	2	Flash Duration	6	2.77	0.46	27.19	<0.001
		Observer(Flash Duration)	35	4.09	0.12	6.88	<0.001
		Error	378	6.41	0.02		
	3	Flash Duration	6	0.22	0.04	20.56	<0.001
		Observer(Flash Duration)	35	0.71	0.02	11.60	<0.001
		Error	378	0.66	0.00		
	4	Flash Duration	6	1.14	0.19	10.87	<0.001
		Observer(Flash Duration)	35	21.50	0.61	35.06	<0.001
		Error	378	6.62	0.02		

3.2.6 Discussion

We have divided the discussion into two parts, according to the two experiments (Experiment U and Experiment S).

Uniform surround (Experiment U)

Our results from uniform surround stimuli (see Figure 3.5) show that static uniform surrounds induce color contrast in all experimental conditions, in line with previous studies (Monnier and Shevell, 2003; Monnier and Shevell, 2004; Gordon and Shapley, 2006; Otazu, Parraga, and Vanrell, 2010; Kaneko and Murakami, 2012). Concretely, Gordon and Shapley (Gordon and Shapley, 2006) used uniform surrounds to study how the luminance and brightness of the test region affect color induction, observing color contrast in all conditions. In accordance to Kirschmann's Third

Law (Kirschmann, 1891), they concluded that brightness, but not luminance, is crucial in the effect on color induction. They found that color contrast is maximal when the stimulus is equibrightness (but not equiluminant) and, as brightness contrast is increased, the color contrast is reduced. In their study, Kaneko and Murakami (2012) also used equiluminant stimuli (using the heterochromatic flicker photometry technique) and they also found color contrast under all conditions. They used flashed stimuli and measured the color contrast induced by color surrounds presented in different temporal conditions. They concluded that the shorter the flash duration, the stronger the color contrast. By contrast, we observe a clear peak of color contrast when stimuli are flashed during 40 ms. Although our study shares several features with Kaneko and Murakami (2012) such as temporal conditions, temporal configuration, equiluminant stimuli and methodology, there are some differences between the current and their study. They measured color induction on a central disk and we measure it on a ring similar to the one used by Monnier and Shevell (2003) and Otazu et al. (2010). Thus, the visual angle of the evaluated feature is different (a disk of 1 deg and a ring width of 15.5 min of visual angle). In addition, they introduced a thin black ring around the central disk, *i.e.*, a border of lower luminance between the central disk and its color surround, which could lead to different results (Xing et al., 2015). Carefully analyzing their raw data, we can observe that in some spatial conditions there is not a clear peak of color contrast at the shortest flash (10 ms), but there is around 20 and 40 ms. Moreover, they showed two subjects (subjects MS and YY) who seemed to obtain similar results to ours: they had a peak of induction during the short flashes (around 20 ms), but not at the shortest (10 ms). Thus, all these reasons could explain the dissimilarity between our and their results.

It is assumed that color induction (both color contrast and assimilation) is the result of neural mechanisms in V1 (Zaidi et al., 1992; Zaidi, 1999; De Weert and Kruijbergen, 1997; Cao and Shevell, 2005) and stimuli on *l* (red and green surrounds) and *s* (purple and lime surrounds) axes are nearly independently processed at the first stages of the HVS, *i.e.*, in the retina, LGN and V1 (Sincich and Horton, 2005). Since stimuli on the *l* axis are processed by the parvocellular pathway and stimuli on *s* axis are processed by the koniocellular pathway (Nassi and Callaway, 2009), we expected to obtain different results using stimuli that independently activate these different visual pathways. In particular, we expected to observe different temporal behaviors for each pathway because parvocellular and koniocellular pathways have different processing speeds (Casagrande et al., 2007; Briggs and Usrey, 2009). From the obtained results (see Figure 3.5), we can see that the color contrast when the inducer is purple (Spatial Condition 2 of Table 3.1) is completely different to that with other color surrounds. This spatial condition induces color contrast, *i.e.*, the achromatic test ring is perceived as lime, when flashed longer than 20 ms. Moreover, it is the only color of the surround with no induction maximum, except at infinite flash duration (*i.e.*, static temporal condition). This stimulus activates the S-OFF channel of koniocellular pathway, which directly projects to layer 4A of V1 (Chatterjee and Callaway, 2003; Callaway, 2014). By contrast, the S-ON channel of the koniocellular, and both parvocellular and magnocellular pathways project to layers 2/3, 4C β , and 4C α of V1, respectively, and all of them converge into layer 2/3 of V1 (Sincich and Horton, 2005). The different processing of S-ON and S-OFF channels of koniocellular pathway could explain the dissimilar psychophysical results (see Figure 3.5) on color contrast when inducers have lime (S-ON on test ring) or purple (S-OFF on test ring) chromaticities. In addition, since all channels of parvocellular pathway (L-ON, L-OFF, M-ON, and M-OFF) are processed in the same layers of V1 (first in layer 4C β , 4B and finally in 2/3), and S-ON channel of koniocellular pathway is mainly

processed in layer 2/3, it could explain this similarity in color induction when inducers have red, green or lime chromaticities (Spatial Conditions 1, 2 and 4).

Striped surround (Experiment S)

Our results from striped surround stimuli (see Figure 3.6) show that, similarly to other authors (Fach and Sharpe, 1986; Smith, Jin, and Pokorny, 2001), striped surrounds can induce color contrast. Only one out of 28 experimental conditions induces color assimilation, namely when the stimulus is static, its 1st inducer is red and the 2nd one is green. In contrast, Monnier and Shevell (2003; 2004) and Otazu et al. (2010) observed that striped surrounds induce color assimilation in all spatial conditions and never found color contrast. Although our study has very similar features to these ones, such as spatial configuration and chromaticities (see Section 3.2.2), they used non-equiluminant stimuli and we have used equiluminant stimuli. Thus, our hypothesis is that this luminance difference could explain the difference between our results and the ones obtained by these authors. Monnier and Shevell (2003; 2004), and Otazu et al. (2010) introduced a luminance difference between the test ring and its surround, and they found chromatic assimilation for striped surrounds. De Weert and Spillmann (1995) found no color induction in equiluminant stimuli, but found color induction when the 1st inducer had lower luminance than the central region. Extending this study, Cao and Shevell (2005) showed that assimilation in the l axis of MacLeod-Boynton color space is found when the inducer luminance is lower than the central region luminance, but not when it is higher, observation that was also reported by De Weert and Spillmann (1995). In the s axis, they showed that color assimilation does not depend on the inducing luminance (*i.e.*, induction was observed when the inducing luminance was either lower or higher than the central region luminance), but depends on the spatial configuration of the inducers (*i.e.*, on both spatial frequency and inducer's spatial separation). Thus, our hypothesis is supported by De Weert and Spillmann (1995) and Cao and Shevell (2005) results. Considering that chromatic assimilation mainly appears when stimulus is not equiluminant, *i.e.*, only when magnocellular pathway is activated, it could suggest that magnocellular pathway could act as a switch-like signaling system activating or deactivating assimilation in both parvocellular and koniocellular pathways in layer 2/3 (where all the pathways converge). In recent neurophysiological and psychophysical studies (Xing et al., 2015; Nunez, Shapley, and Gordon, 2018), the authors concluded that brightness and color interact in V1. In particular, their study supports the hypothesis that the color appearance depends on brightness contrast (Kirschmann, 1891; Gordon and Shapley, 2006; Faul, Ekroll, and Wendt, 2008; Bimler, Paramei, and Izmailov, 2009) because there is a *mutual-inhibition* (*i.e.*, color assimilation) between color-responsive cells and luminance-responsive cells. Furthermore, they proposed that these interactions are driven by double-opponent cells, which respond to both luminance and color differences (Color-Lum neurons) (Johnson, Hawken, and Shapley, 2001; Johnson, Hawken, and Shapley, 2008). The non-opponent neurons, or Lum neurons, are inactive when the stimulus is equiluminant, and single-opponent neurons, or Color neurons, respond to large areas of color and do not respond to luminance differences. These neurophysiological observations, also supports our hypothesis that luminance difference between the test ring and its surround, which activates Lum neurons, could be a key factor to induce color assimilation. In addition, psychophysical studies by Fach and Sharpe (1986), and Smith et al. (2001) concluded that spatial frequency is another crucial factor to induce color assimilation in equiluminant striped stimuli. In particular, they observed

that very thin stripes ($> 9 \text{ cpd}$) induce color assimilation and thick stripes ($< 0.7 \text{ cpd}$) induce color contrast, with a transition point from assimilation to contrast around 4 cpd (Smith, Jin, and Pokorný, 2001). Considering that the spatial frequency of our stimuli is 1.94 cpd , we agree with them: In that range both color contrast and color assimilation could be induced (Fach and Sharpe, 1986; Smith, Jin, and Pokorný, 2001; Cao and Shevell, 2005).

Comparing the results from flashed and static stimuli, we can observe that in almost all spatial conditions (except for Spatial Condition 1), the type of color induction, *e.g.* assimilation or contrast, does not vary between flashed and static stimuli, when the flash is longer than 40 ms .

In both types of surround configurations, *e.g.*, uniform and striped surrounds (see Figures 3.5 and 3.6), we can see that at the shortest flash duration (10 ms) subjects only perceived color induction when the surrounding colors are on the l axis of MacLeod-Boynton color space, but do not perceive any induction when the surround is on the s axis (purple or lime colors). In fact, when subjects finished the experiment they pointed out that under these experimental conditions (purple and lime surround colors flashed for 10 ms) they were not able to see the test frame and, therefore, left an achromatic comparison ring. This consideration goes in line with the physiological observation that the koniocellular pathway is slower than the parvocellular pathway (Casagrande et al., 2007; Briggs and Usrey, 2009), *i.e.*, the purple and lime colors are processed more slowly than the red and green colors.

3.2.7 Computational Model

As pointed out in Section 3.2.1, there are several computational models that reproduce color, or brightness, induction effects (Blakeslee and McCourt, 1977; Blakeslee and McCourt, 1999; Blakeslee and McCourt, 2004; Spitzer and Barkan, 2005; Robinson, Hammon, and de Sa, 2007; Otazu, Vanrell, and Parraga, 2008; Otazu, Parraga, and Vanrell, 2010; Penacchio, Otazu, and Dempere-Marco, 2013). Most of them work on static stimuli and are based on several receptive field properties such as spatial frequency and orientation selectivity. Since the neurodynamical model proposed by Penacchio et al. (2013) is one of the few models that works on temporally dynamic stimuli, we have chosen it to study the temporal evolution of the system when our flashed stimuli are presented. In addition to the spatial frequency and the orientation selectivity of the neurons, it also models their lateral connections, as defined by Li (1998). This computational model was designed to reproduce brightness induction effects using both static and dynamic stimuli, therefore it only considers the luminance channel. Since the spatial configurations that we defined only activate one pathway (parvo- or koniocellular pathway), we applied the model to the activated chromatic channel for the sake of simplicity (Otazu, Parraga, and Vanrell, 2010). To be more biologically plausible, we used a Gabor decomposition instead of the Wavelet one that the authors used in their work, and we analyzed the temporal evolution of the output's firing rate activity. This Gabor decomposition models the receptive fields of V1 (Daugman, 1985) neurons and the response of the model is determined by both the input flashed stimulus, as a sequence of frames (*i.e.*, images), and the interactions between the different neuronal populations. This architecture models the excitatory and inhibitory neurons and their membrane potentials, which are transformed to firing rate activity using sigmoid-like positive non-linear and non-decreasing functions (Penacchio, Otazu, and Dempere-Marco, 2013). Since this model does not consider any difference between parvo-, konio-, and magnocellular

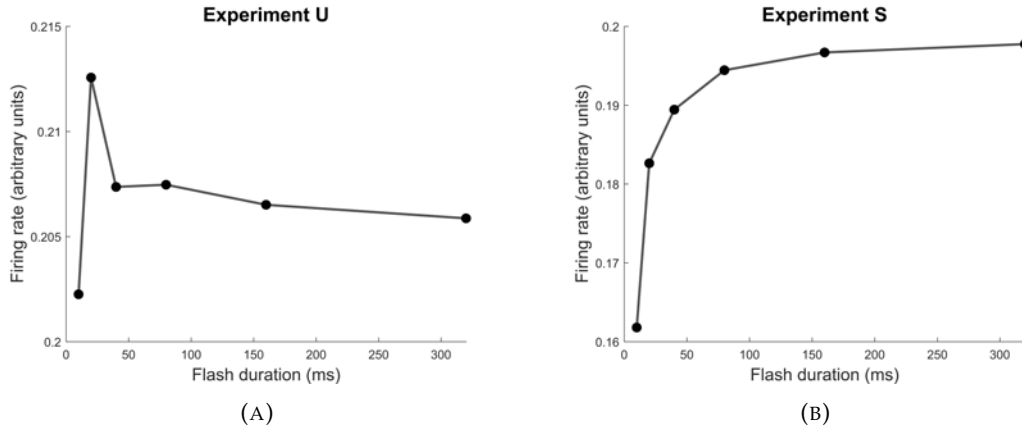


FIGURE 3.7: Computational simulation of the psychophysical experiments presented in this study using the computational model defined by Penacchio et al. (2013). We have chosen this model because it allows us to use dynamic (or flashed) stimuli. Both panels show the mean firing rate activity (in arbitrary units) of the computational model for the different temporal conditions defined in our experiments (see Section 3.2.2 for more details). In (A) we show the results for Experiment U (uniform surround) and in (B) the results for Experiment S (striped surround). We can observe that the uniform surround (left panel) produces a peak of activity for short flashes (at 20 ms), while striped surround does not produce any peak. This observation goes in line with our experimental data which show an induction's peak for short flashes (around 40 ms in Spatial Conditions 1, 3 and 4) when uniform surrounds are presented, but do not when striped surrounds are shown.

pathways, given an experiment (*e.g.*, Experiments U or S), we obtained the same results for the different spatial conditions. In Figures 3.7a and 3.7b, we show the qualitative results of the model. Here, the y axis is the mean firing rate activity (at the spatial frequency associated to the ring size) when the test frame is presented. We can observe that the profiles in Figures 3.7a and 3.7b are different. In Figure 3.7a (Experiment U), the mean firing rate activity for short flashes is higher than the mean activity for long flashes. In contrast, in Figure 3.7b (Experiment S) we cannot observe any peak of activity. These observations go in line with some of our psychophysical results: An induction peak is observed at 40 ms for uniform surrounds (Experiment U) and no induction peak is observed for striped surrounds (Experiment S).

As stated before, the Spatial Conditions 1, 3 and 4 of the Experiment U (the ones that show an induction peak at 40 ms) are processed by the layers $4C\beta$ and $2/3$ in V1. The results of the computational model suggest that it reproduces the lateral connections present in these layers. In contrast, it does not reproduce the results of Spatial Condition 2 (processed by layer $4A$). Thus, the architecture does not correctly model the lateral connections in this layer. In contrast, in the results' analysis of Experiment S, we cannot observe any grouping pattern over the different spatial conditions. Therefore, it is difficult to link these computational model results to the ones obtained in the Experiment S. We can only note that, in both psychophysical and computational results, we cannot observe a peak of either induction or activity.

3.2.8 Conclusions

Taking into account that we only observed color contrast (except for red-green inducer in static striped stimuli) for the two different types of surround (uniform and striped) and that temporal behavior of color induction depends on visual pathways (see Figures 3.5 and 3.6), we can conclude:

- The strongest color contrast is induced by a uniform surround stimulus flashed for 40 *ms*.
- Purple inducer (which induces a lime chromaticity and, thus, activates the S-OFF channel in layer 4A) induces a temporal response that is completely different to the temporal response induced by other inducers such as red, green and lime (which activates other channels in layer 2/3).
- Striped equiluminant stimuli do not induce color assimilation (except for red-green inducers).
- The test frame cannot be perceived during flashes shorter than 20 *ms* when the colors of the surrounding are on the *s* axis of the MacLeod-Boynton color space.
- Our initial hypothesis, *i.e.*, flashed uniform and striped surrounds would induce opposite colors but with a similar temporal behavior, should be rejected.

Considering previous studies, we can also conclude that luminance could be a key factor to induce color assimilation. In particular, assimilation only appears in non-equiluminant stimuli, or in equiluminant striped stimuli with a very high spatial frequency. This could suggest that color contrast and color assimilation effects are the result of different mechanisms or, at least, the result of the same mechanism which needs an interaction with the magnocellular pathway (the luminance channel) to induce color assimilation. In this study we do not analyze which interaction is responsible for color assimilation. Nevertheless, other authors concluded that mutual-inhibition (when Lum cells inhibit Color and Color-Lum neurons) has an important role in color perception (Xing et al., 2015). Our results could support this idea.

3.3 The effect of luminance and brightness differences on color assimilation

In the previous section, we concluded that luminance differences could be a key factor to induce color assimilation. Thus, in this section, we have studied the effect of both luminance and brightness differences on color assimilation.

3.3.1 Introduction

The effects of achromatic contrast (either luminance or brightness contrast) on color induction have received relatively less attention from the scientific community. Luminance is the photometric measure of luminous intensity per unit area of light travelling in a given direction and is usually measured by photometric devices. Brightness is the perception elicited by the luminance of a visual target, which is not necessarily proportional to luminance. Below we review the color induction literature, discriminating between both concepts.

Color contrast

Color contrast has been reported under a wide range of spatiochromatic conditions: *unconstrained*, when there are luminance and/or brightness and color differences between the target and the inducer (Monnier and Shevell, 2003; Monnier and Shevell, 2004; Gordon and Shapley, 2006; Otazu, Parraga, and Vanrell, 2010); *equiluminant*, when there are no luminance differences between the target and the inducer (Gordon and Shapley, 2006; Kaneko and Murakami, 2012); and *equibrightness*, when there are no brightness differences between the target and the inducer (Gordon and Shapley, 2006; Faul, Ekroll, and Wendt, 2008; Bimler, Paramei, and Izmailov, 2009). In general, researchers have found that color contrast does occur under all these conditions with various degrees of strength, which depends mostly on luminance or brightness differences (Gordon and Shapley, 2006). Several psychophysical studies (Gordon and Shapley, 2006; Faul, Ekroll, and Wendt, 2008; Bimler, Paramei, and Izmailov, 2009) indicate that color induction follows Kirschmann's Third Law (Kirschmann, 1891), which says that color contrast is highest when the stimulus is equibrightness (but not equiluminant) and, as brightness contrast is either increased or decreased, color contrast is reduced.

Color assimilation

Although color assimilation is more common than color contrast in daily life (De Valois and De Valois, 1988b) it has been less studied. As color contrast, assimilation has been studied under several spatiochromatic conditions such as unconstrained (Van Tuijl and De Weert, 1979; Ejima et al., 1984; Watanabe and Sato, 1989; De Weert and Spillmann, 1995; Pinna, Brelstaff, and Spillmann, 2001; Monnier and Shevell, 2003; Monnier and Shevell, 2004; Devinck et al., 2005; Cao and Shevell, 2005; Otazu, Parraga, and Vanrell, 2010), and equiluminant (Fach and Sharpe, 1986; Watanabe and Sato, 1989; De Weert and Spillmann, 1995; Pinna, Brelstaff, and Spillmann, 2001; Devinck et al., 2005; Cerda-Company and Otazu, 2017b; Cerda-Company and Otazu, 2019). It has also been studied using several patterns such as the pincushion (Schachar, 1976) and watercolor (Pinna, 1987) illusions and those of Van Tuijl (1975) and Ehrenstein (1941). Using the pincushion illusion, De Weert and Spillmann (1995) used red and green stripes on different chromatic backgrounds and measured the color induction on the background when it was either higher, lower or the same as the luminance of the inducers. Although they did not report the details of their results, they concluded that color assimilation is induced when the luminance of the target's surface is higher than that of the inducers, but not when it is lower. Moreover, they reported that no color change is induced by equiluminant stimuli. In line with this work, Pinna et al. (2001) and Devinck et al. (2005) studied, among other features, the effect of luminance contrast between the two inducers on the strength of the watercolor effect. They concluded that, when the two inducers are nearly equiluminant, color spreading is still present but weak, suggesting that the watercolor effect is the result of a luminance-dependent mechanism (Devinck et al., 2005; Devinck et al., 2006). Using concentric rings, Cao and Shevell (2005) found that assimilation occurred along the l axis of the MacLeod-Boynton color space (Boynton, 1986) when the inducer's luminance was lower than that of the target, but not when it was higher. In the s axis, they found that color assimilation occurs when the inducer's luminance is either lower or higher than that of the target, but its strength depends on the spatial configuration of the inducers (*i.e.*, on both spatial frequency and spatial separation). In the same line, several researchers (Fach and

Sharpe, 1986; Smith, Jin, and Pokorny, 2001) studied the role of the spatial frequency in color assimilation using equiluminant stimuli. They observed that by making stripes increasingly thicker, it is possible to make the transition from assimilation to contrast (Smith, Jin, and Pokorny, 2001). Other researchers (Monnier and Shevell, 2003; Monnier and Shevell, 2004; Otazu, Parraga, and Vanrell, 2010) found similar effects using unconstrained stimuli and observed that thinner stripes induce stronger color assimilation (Otazu, Parraga, and Vanrell, 2010). In summary, there seems to be two major stimuli characteristics that induce color assimilation: spatial frequency content and luminance differences.

Brightness induction

Achromatic inducers change the perceived brightness of the achromatic target region (brightness induction), an effect that has been widely studied for different stimuli (White, 1979; McCourt, 1982; Blakeslee and McCourt, 1977; Blakeslee and McCourt, 2004; Kingdom, 2011). Using a similar paradigm to ours (see below), Hong and Shevell (2004) concluded that the luminance of both the 1st and the 2nd inducers contribute to brightness induction, suggesting that luminance differences between the target region and its surrounds (*i.e.*, the context) are important. Moreover, other studies reported an asymmetry between "brightness" and "darkness", pointing out that the strength of the effect depends on whether the target region is surrounded by bright or dark inducers (Beck, 1966; Festinger, Coren, and Rivers, 1970; Hamada, 1984; De Weert and Spillmann, 1995).

Color processing by the human visual system

The initial stages of visual information processing by the human visual system (HVS) are by far the most understood. Light is absorbed by rods and cones in the retina. Cones operate in well-lit (photopic) conditions and can be classified in three classes: L, M and S which are sensitive to long, middle and short wavelengths (LWS, MWS and SWS) of the visible electromagnetic spectra respectively. Visual information is segregated by ganglion cells into three nearly independent (Livingstone and Hubel, 1988; Sincich and Horton, 2005) pathways called magno-, parvo- and koniocellular and sent to a structure in the thalamus called Lateral Geniculate Nucleus (LGN). The magnocellular pathway carries mainly low-spatial resolution and spatially opponent luminance (LWS + MWS) information, while the other two carry spatiochromatically opponent information (the parvocellular pathway carries high-spatial resolution luminance alongside LWS versus MWS opponent signals and the koniocellular pathway carries SWS versus LWS+MWS opponent signals) (Derrington, Krauskopf, and Lennie, 1984; Nassi and Callaway, 2009). There are several chromatic spaces consistent with retinal and LGN physiology, the most popular being the ones by MacLeod and Boynton (MacLeod and Boynton, 1979) and Derrington, Krauskopf, and Lennie (Derrington, Krauskopf, and Lennie, 1984). The LGN receives feedback from higher areas but projects mainly to cortical area V1, which has three different types of neurons: single- (SO), double- (DO) and non-opponent (NO) neurons (Johnson, Hawken, and Shapley, 2001; Shapley and Hawken, 2002; Johnson, Hawken, and Shapley, 2008; Shapley and Hawken, 2011). SO neurons (or Color neurons) respond best to large chromatic areas; DO neurons (or Color-Lum neurons) respond to both chromatic and luminance variations and NO neurons (or Lum neurons) respond best to luminance variations. Considering spatial frequency selectivity, Lum and Color-Lum neurons are band-pass (*i.e.*, they respond best at

medium spatial frequency stimuli of 2 cpd) and Color neurons are low-pass (they respond optimally to spatial frequencies $< 0.5\text{ cpd}$ and do not respond at all to spatial frequencies $> 2\text{ cpd}$) (Johnson, Hawken, and Shapley, 2001; Johnson, Hawken, and Shapley, 2008; Shapley and Hawken, 2011; Xing et al., 2015; Nunez, Shapley, and Gordon, 2018). Although to fully silence Lum neurons is difficult, equiluminant stimuli of medium to high spatial frequency only produce weak responses in them. In fact, equiluminant stimuli of high spatial frequency ($> 3\text{ cpd}$) also suppresses parvocellular responses (Derrington, Krauskopf, and Lennie, 1984; Granger and Heurtley, 1973; Skottun, 2013).

The neural mechanisms behind color induction are not completely understood. Some explanations rely on retinal mechanisms (Kamermans, Kraaij, and Spekreijse, 1998; VanLeeuwen et al., 2007; Sabbah et al., 2013) while others rely on low-level (Xing et al., 2015; Nunez, Shapley, and Gordon, 2018) or higher cortical mechanisms or combinations of both (Gegenfurtner, 2003; Horiuchi et al., 2014). There are also important interactions between brightness and color that might produce changes in color appearance. For example, increases in the variance of surround colors cause color objects to appear desaturated (they appear more vivid and richly colored against low-contrast gray surrounds than against high contrast multicolored surrounds) (Brown and MacLeod, 1997). The same occurs for increases in surround brightness contrast (Faul, Ekroll, and Wendt, 2008; Bimler, Paramei, and Izmailov, 2009). These effects have been explained by inhibition in cortical V1 circuits generated by local brightness contrast at the boundary between the target and the surround (Xing et al., 2015). In consequence, an important contribution to color induction (both color contrast and color assimilation) is likely to come from these neural mechanisms in V1 (Zaidi et al., 1992; Rossi, Rittenhouse, and Paradiso, 1996; De Weert and Kruysbergen, 1997; Zaidi, 1999; Shapley and Hawken, 2002; Cao and Shevell, 2005), with DO neurons playing a major role in color appearance (Nunez, Shapley, and Gordon, 2018).

In addition to not having a comprehensive explanation for the phenomenon, there are few observations on how achromatic information interacts with the chromatic channels to produce color induction. In previous work, Monnier and Shevell (2003; 2004) reported color assimilation with a luminance difference of $+5\text{ cd/m}^2$ between the target and inducers. Given that using similar but equiluminant stimuli we did not (Cerdea-Company and Otazu, 2017b; Cerdeza-Company and Otazu, 2019) (see previous Section), we wanted to test whether a transition from color contrast (or no induction) to color assimilation occurs just by increasing or decreasing the luminance of the target with respect to its inducers (De Weert and Spillmann, 1995; Monnier and Shevell, 2003; Monnier and Shevell, 2004; Cao and Shevell, 2005; Otazu, Parraga, and Vanrell, 2010; Cerdeza-Company and Otazu, 2017b; Cerdeza-Company and Otazu, 2019). Then, to understand the role of the different *elements* of a patterned stimulus (*i.e.*, 1st and 2nd inducers), we separately varied their luminance (*luminance experiment*). Finally, to study whether color assimilation is due to luminance or brightness differences, we reran the luminance experiment but varying the brightness of the elements instead (*brightness experiment*). To this end, we present two new psychophysical studies where we systematically measured the contribution of both luminance and brightness differences on color induction. First, for each *varied element*, we measured the colors induced in five different luminance conditions: (1) when the target's luminance was much lower than the

inducers' luminance ($\Delta Y = -10 \text{ cd/m}^2$); (2) when the target's luminance was noticeably lower than the inducer's ($\Delta Y = -5 \text{ cd/m}^2$); (3) when the stimuli were equiluminant ($\Delta Y = 0 \text{ cd/m}^2$); (4) when the target's luminance was noticeably higher ($\Delta Y = +5 \text{ cd/m}^2$), and (5) when it was much higher ($\Delta Y = +10 \text{ cd/m}^2$). Then, we defined similar brightness conditions: (1) when the target's luminance (and, thus, its brightness) was much lower than the inducers' brightness ($\Delta B = -10 \text{ cd/m}^2$); (2) when the target's luminance was noticeably lower than the inducer's brightness ($\Delta B = -5 \text{ cd/m}^2$); (3) when the stimuli were equibrightness ($\Delta B = 0 \text{ cd/m}^2$); (4) when the target's luminance was noticeably higher ($\Delta B = +5 \text{ cd/m}^2$), and (5) when it was much higher ($\Delta B = +10 \text{ cd/m}^2$). As the luminance and brightness differences were increased or decreased, we expected to observe significant differences in the strength of color induction since in the equiluminant condition, responses come mostly from Color and Color-Lum neurons, and in the unconstrained conditions all neurons respond (Xing et al., 2015; Nunez, Shapley, and Gordon, 2018). We also expected to observe differences when the luminance was varied in either the target ring or in any of the inducers, since the elements that affect the color induction could be determined by the distance of the neural lateral connections (Zaidi et al., 1992). Finally, if color assimilation is due to luminance differences, we expected to observe color assimilation in the equibrightness condition (where small luminance differences are present).

3.3.2 Methods

Apparatus and Stimuli

We used the same apparatus as in the previous study (see Section 3.2.2).

Two different circularly symmetric patterns (test and comparison stimuli) were simultaneously presented to the observers side by side on the CRT monitor (similarly to the test frame of the previous study; see Figure 3.8). The test stimulus (presented on the left side) was composed by 11 concentric rings of the same width (equivalent to 15.5 arcmin of visual angle), which included the *test ring*. The test ring was always achromatic ($l = 0.66$ and $s = 0.98$) and its luminance, as well as the luminance of the concentric rings, depended on the evaluated luminance condition. We defined five different luminance conditions depending on the luminance of the test ring relatively to the other rings (see Figure 3.9 for the *test ring* case): $\Delta Y = [-10, -5, 0, +5, +10] \text{ cd/m}^2$. The inducer stimuli consisted of two types of rings, called the 1st and the 2nd inducer according to their physical distance to the test ring. These inducer rings always had opponent chromaticities (e.g. when the 1st inducer was red, the 2nd one was green and vice versa). We varied separately the luminance of the different elements present in a patterned stimulus, that is: the *test ring*, *1st inducer* and *2nd inducer*. Additionally, we varied the luminance of *both inducers* in an opposite way (e.g., when the 1st inducer was brighter, the 2nd one was dimmer than the test ring). When we varied the luminance of an element of the patterned stimulus all the other elements (the *unvaried elements*) were equiluminant with respect to an achromatic reference equal to 20 cd/m^2 . For instance, in the *test ring* case, we varied the luminance of the test ring and we kept constant the inducers' luminance and, in the *both inducers* case, we varied the luminance of both inducers, and we kept unvaried the luminance of the test ring. Therefore, for each *varied element*, we had five different luminance conditions. See further equiluminance details in the Section entitled "Equiluminance point measure". Thus, in two luminance conditions the test ring was brighter than its surround, in two it was darker and in one

had the same luminance. We also defined four chromatic conditions according to the 1st and 2nd inducer's chromaticities: red-green, green-red, purple-lime and lime-purple. These were: red ($l = 0.69, s = 0.98$); green ($l = 0.63, s = 0.98$); purple ($l = 0.66, s = 1.38$); and lime ($l = 0.66, s = 0.58$). The colorimetric properties of the inducer's rings were selected to represent orthogonal axes in the MacLeod-Boynton color space (Boynton, 1986) with the achromatic locus at the centre. To facilitate the correct identification of the test ring by the subjects, in all conditions, we placed small pairs of dots in four different positions (see Figure 3.8).

The comparison stimulus (presented on the right side) was the same across all conditions (see Figure 3.8). It consisted of a uniform achromatic disk ($l = 0.66, s = 0.98, Y = 20 \text{ cd/m}^2$) containing the *comparison ring*. Both the test and comparison rings had the same physical dimensions and their respective surrounds (the inducer and the comparison surrounds) had exactly the same size. The rest of the screen was set to its minimum possible value (dark background). Subjects were asked to modify the chromaticity and luminance of the comparison ring to match that of the test ring using the gamepad to navigate on the MacLeod-Boynton color space. We chose to define all chromaticities in the MacLeod and Boynton color space (Boynton, 1986), because it is a commonly used opponent color space (red-green, purple-lime, and bright-dark), based on the Smith and Pokorny (1975) cone fundamentals.

All stimuli were implemented in Matlab (The MathWorks, Inc., Natick, MA, US), and the video processor was controlled via a Cambridge Research System custom-made toolbox.

To evaluate whether color assimilation is due to either luminance or brightness differences, we used exactly the same stimuli as described before, but the unvaried elements were equibrightness instead of equiluminant (see further details in the Section entitled "Equibrightness point measure"). Therefore, we also have five different brightness conditions ($\Delta B = [-10, -5, 0, +5, +10] \text{ cd/m}^2$). The unvaried elements were equibrightness with respect to an achromatic reference of 20 cd/m^2 and the varied element had a brightness equal to the defined luminance difference. For instance, in the 1st inducer case, we varied the luminances of the 1st inducer according to the subject-equibrightness calibration. Thus, the 1st inducer in the brightness condition $\Delta B = -10 \text{ cd/m}^2$ had the same brightness as an achromatic light of 10 cd/m^2 (10 cd/m^2 less than the reference value of 20 cd/m^2).

Equiluminance point measure Equiluminant (or isoluminant) color stimuli are defined as containing variations only in chromaticity. It is commonly used to separate magno- and parvocellular responses in psychophysical experiments, since they are processed by physiologically distinct channels from the retina to the visual cortex. Equiluminant stimuli have been reported as having special perceptual properties. For example, artists use these properties to make a painting to appear unstable (or "jittery") and to cause motion illusions (isoluminant chromatic motion). An equiluminant display consists of an array of stimuli of different colors whose luminances have been selected to maximize these effects. Since the effects are a consequence of the physiology, the *equiluminant point* varies slightly from one observer to the next. In this work, we generated equiluminant stimuli by finding the colorimetric input that generates equiluminance in each of the subjects. Before starting the experiment described above, subjects participated in an equiluminant-point measure procedure, which lasted 3 hours and was performed in 3 different days. We measured individual equiluminant points using the Minimally Distinct Border method (MDB) (Boynton, 1973; Boynton and Kaiser, 1968; Brill, 2014; Kaiser, 1971; Kaiser et al., 1990; Wagner and Boynton, 1972). The stimuli consisted on two juxtaposed

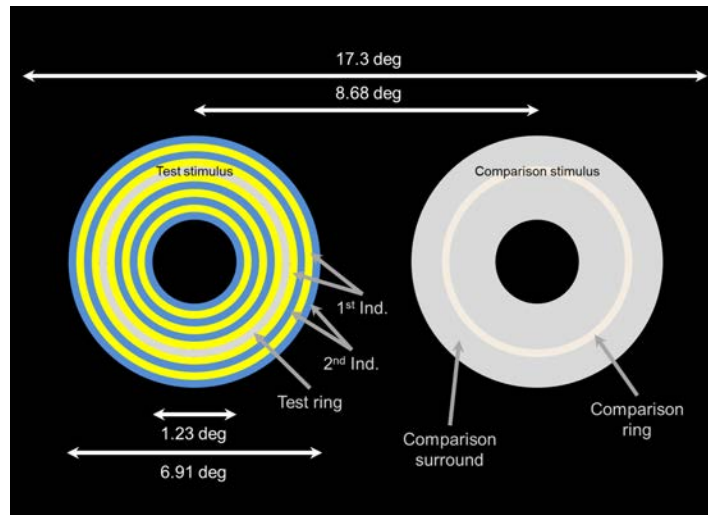


FIGURE 3.8: Stimuli design. The 1st and 2nd inducers consisted of pairs of rings of opposing chromaticities such as red-green or purple-lime. The test ring was always achromatic ($l = 0.66$ and $s = 0.98$) and, as well as the 1st and 2nd inducers, could have 5 different luminance values (luminance conditions): $Y = [10, 15, 20, 25, 30] \text{ cd/m}^2$. When all the elements (test ring, 1st and 2nd inducers) had a luminance of $Y = 20 \text{ cd/m}^2$, the stimulus was equiluminant. Instead, when all the elements had a brightness equal to a luminance of $\Delta Y = 20 \text{ cd/m}^2$, the stimulus was equibrightness. Although it is difficult to see in this figure because of their size, 8 black dots of 1 pixel size were drawn around test ring for easier detection: 4 dots in the inner radius of the ring and 4 points in the outer radius (at 0, 90, 180 and 270°). Subjects had to match the color of the comparison ring to that of the test ring. Colors in this figure might not be the same as the experiment since they were created for illustrative purposes.

semicircular disks presented in the same apparatus as the experiment. One of the disks was achromatic ($l = 0.66$ and $s = 0.98$) and the other had one of the colors defined in the experiment's chromatic conditions (*i.e.*, red, green, purple or lime) plus an achromatic condition, for control. We set the luminance of the achromatic disk at the defined luminance conditions ($Y = [10, 15, 20, 25, 30] \text{ cd/m}^2$) and asked subjects to adjust the luminance of the colored disk until "the border between the colored and the achromatic disks was minimal", *i.e.* when only chromatic but not luminance differences are perceived. Ideally, there would be no border between the two disks (in fact, it happened in the control condition) but in our case, at least a chromatic border was always perceived. At the end of the whole procedure, we obtained an average (from 8 measures) of the luminance necessary to match each of the four colors to the achromatic disk (according to the defined luminance conditions) for each subject. These luminance values were used to construct the inducer rings of the test stimulus in the luminance experiment (see left panel of Figure 3.8).

Equibrightness point measure As stated before, brightness and luminance are similar concepts, but not the same one. Often, when luminance differences are present, there are also brightness differences, but previous studies showed that when a stimulus is equiluminant it is not necessarily equibrightness (Boynton and Kaiser, 1968; Kaiser, 1971; Wagner and Boynton, 1972; Roufs, 1978). Therefore, for each subject we measured their luminance values that makes the stimuli equibrightness.

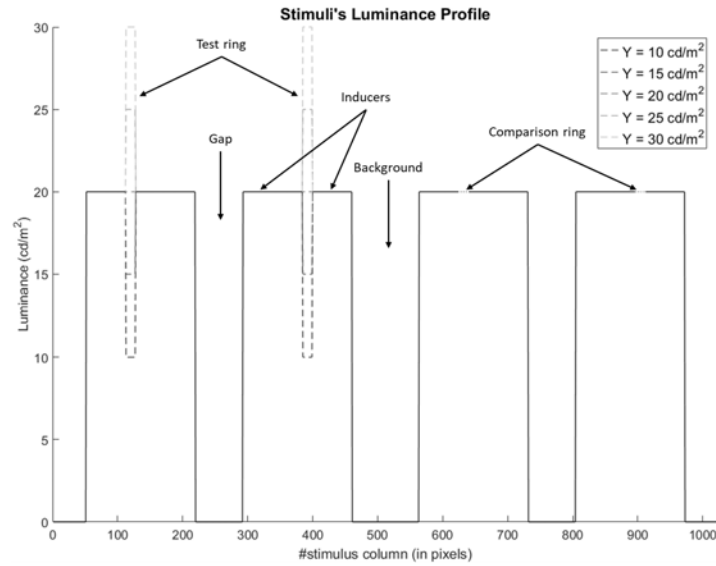


FIGURE 3.9: *Test ring* case: luminance profile of stimuli. This profile was calculated using the central row of Figure 3.8. We used a dark background, in this case, inducers formed an equiluminant surround, and the luminance of the comparison ring was adjustable (dotted line). We defined 5 different luminance conditions for the test ring (dashed lines), in two of them the test ring's luminance was below that of the inducers' luminance ($Y = 10$ and 15 cd/m^2), in two it was above ($Y = 25$ and 30 cd/m^2), and in one it was equiluminant ($Y = 20 \text{ cd/m}^2$). For simplicity's sake, the small black dots that marked the test ring were removed from this figure (they would be placed in both sides of the test ring).

The stimuli consisted in two semicircular disks presented in the same apparatus as the experiment but, in contrast to MDB, separated by a small gap of 30.5 arcmin . Similarly to the MDB, one of the semicircular disks was achromatic (the reference one) and the other one had a chromaticity of the colors defined in the experiment's chromatic conditions (*i.e.*, red, green, purple or lime) plus an achromatic control condition. We set the luminance of the achromatic disk at the defined luminance conditions ($Y = [10, 15, 20, 25, 30] \text{ cd/m}^2$) and asked subjects to adjust the luminance of the colored disk until "the radiance of the colored disk appear as bright as the reference one" (Roufs, 1978). Since this data had a higher intra-subject variability (standard deviation) than the equiluminance point measure, we doubled the number of matches to calibrate the subject-equibrightness point. Then, we obtained an average (from 16 measures) of the luminance necessary to match each of the four colors to the achromatic disk (according to the defined brightness conditions) for each subject. These luminance values were used to construct the inducer rings of the test stimulus in the brightness experiment.

Subjects

Thirteen subjects recruited from our academic community participated in the experiment. Five of them were familiar with color spaces (DB, MM, NS, XC and XO) and eight of them were not (AC, AT, CG, CS, DC, DG, IR and MF). All of them signed the consent form to participate in the experiment, where the aim of the study was described. Ten of them were completely naïve (AC, AT, CG, CS, DB, DC, DG, IR, MF and MM) while the others were not (NS, XC and XO). The age range was between

18 and 46 years old. Ten of them were male (AC, AT, CG, DB, DC, DG, IR, MM, XC and XO) and three of them female (CS, MF and NS). All subjects had normal or corrected-to-normal vision, and they scored as normals in the Ishihara's test (Ishihara, 1972) and the D-15 Farnsworth Dichotomous Test (Farnsworth, 1947). Not all subjects participated in both experiments. Ten of them (AC, CG, CS, DB, DC, MF, MM, NS, XC and XO) participated in the *test ring* case for luminance experiment, eight of them (AC, CS, DC, DG, MF, NS, XC and XO) participated when the inducers' luminance were varied, nine participated in the *test ring* case for the brightness experiment (AC, AT, CS, DC, IR, MF, NS, XC and XO) and seven participated when the inducers' brightness were varied (AC, CS, DC, MF, NS, XC and XO). Thus, a total of seven subjects (AC, CS, DC, MF, NS, XC and XO) did both experiments. Since the experiments were conducted during one year, several people abandoned them due to time constraints. The experiments were approved by our university's ethic committee (Comissio d'Etica en l'Experimentacio Animal i Humana -CEEAH- de l'Universitat Autonoma de Barcelona).

Experimental procedure

Subjects adjusted the color of the comparison ring until "it was perceived the same as the test ring" (asymmetric matching task). To do this, subjects could adjust the chromaticity and the luminance of the comparison ring navigating in the MacLeod-Boynton color space using the gamepad buttons.

For each varied element, the procedure consisted of a training session (discarded) and 5 experimental *sessions* lasting about 40 minutes each. Each of the sessions consisted of three parts: a 3 *min* dark adaptation and 2 *trials* containing 20 matching *runs* each. Individual trials included all possible random combinations of the chromatic and luminance *conditions* of the 1st and 2nd inducer rings [*red – green, green – red, lime – purple, purple – lime*] \times [10, 15, 20, 25, 30] *cd/m²*, totalling 20 runs each. In a single day, a subject would come to the laboratory and spend about 80 minutes (80 runs) in two sessions (between sessions, subjects took 10 *min* break). After 5 sessions, the subject would have ideally finished 10 trials (for one varied element), totaling 200 runs (matches).

Statistical analysis

To test whether luminance and brightness conditions induce different chromaticities, we performed a statistical analysis of the results obtained in our experiment. Our independent variables (IVs) consisted of: chromatic condition, luminance (or brightness) condition, subject id and trial. Our dependent variables (DVs) were the chromaticities induced in the *l* and *s* color space directions (in the metric units defined by Equation 3.1). Our null hypothesis was that all luminance (or brightness) conditions induced the same strength of chromatic induction. We did a nested ANOVA analysis (subject id nested in luminance condition) for each chromatic condition to analyze the induction differences at different luminance and brightness conditions.

When the ANOVA analysis showed significant differences, we did a Fisher's LSD post-hoc analysis to study which luminance (or brightness) conditions induce different chromaticities.

3.3.3 Results

To estimate the strength of color induction we used the metric 3.1 defined in the previous study (see Section 3.2.4). Figures 3.10 and 3.11 show the contribution of luminance and brightness to color induction. The colors indicate the varied element and, in Figure 3.10, the x axis represents the luminance difference ($\Delta Y = Y^t - Y^s$) between the test ring and its surround (5 luminance conditions). Negative values indicate that the test ring was darker than its surround, positive values indicate the opposite and zero difference indicates the equiluminant condition. Similarly, in Figure 3.11 the x axis represents the brightness differences ($\Delta B = b(Y^t) - b(Y^s)$, where $b(Y)$ is the brightness of the luminance Y) between the test ring and its surround (5 brightness conditions). The y axis represents color induction as defined by Equation 3.1 for each luminance (or brightness) and chromatic condition, averaged across subjects with their corresponding standard errors of means (*SEM*). Outlier points were detected using the interquartile range measure (Disraeli, 1996) and were removed from the analysis. Each panel in Figures 3.10 and 3.11 detail a chromatic condition (20 runs in total for each varied element). The gray region shows the JND region, where no chromatic difference is perceived.

Luminance experiment results

Notice that the results depend on both luminance and chromatic conditions (see Figure 3.10). For instance, along the l axis (top panels: red-green and green-red chromatic conditions), results are not symmetric. When the 1st inducer was red (top-left panel), weak color assimilation (positive ΔC_l) was often induced. Conversely, in the top right panel (when the 1st inducer ring was green), color contrast (negative ΔC_l) was always induced when the test stimulus was darker than its surround, and even for the equiluminant condition.

Regarding the s axis, the results of the two chromatic conditions (bottom panels) are quite similar, as if a ‘mirroring’ of the two chromatic conditions (purple-lime and lime-purple) occurs. Here, color assimilation (positive ΔC_s) was induced in almost all cases when the stimuli were unconstrained (not equiluminant) and we varied the luminance of the test or 1st inducer rings. When the 1st inducer was purple (bottom left panel), the assimilation was stronger when the test ring was darker than its surround. Similarly, when the 1st inducer was lime, assimilation was stronger when the test ring was lighter than its surround.

The color induction effect on the test ring also depends on the varied element. When the 2nd inducer is varied, the color induction distribution is almost flat in all panels, pointing out that the luminance of this inducer by itself does not play a role in the color induction effect. In almost all panels (except for the bottom-left panel), the results for the 1st and *both inducers* cases are very similar, suggesting that only the luminance of the 1st inducer plays a role in color induction. Top panels (l axis) show that color induction does not depend much on the varied element (the different color lines overlap). In bottom panels, we can observe that the strength of the effect decreases as the varied luminance is spatially further from the test ring. For the *test ring* case, the effect is stronger than for the 1st inducer case and it is stronger than for the 2nd inducer case.

Since subjects were allowed to manipulate both chromaticity and luminance, we can also analyze whether there was any luminance effect in the matches. Table 3.3 shows the averaged luminance differences and their *SEMs* as defined in the Macleod-Boynton space between the match (*i.e.*, the comparison ring after each trial)

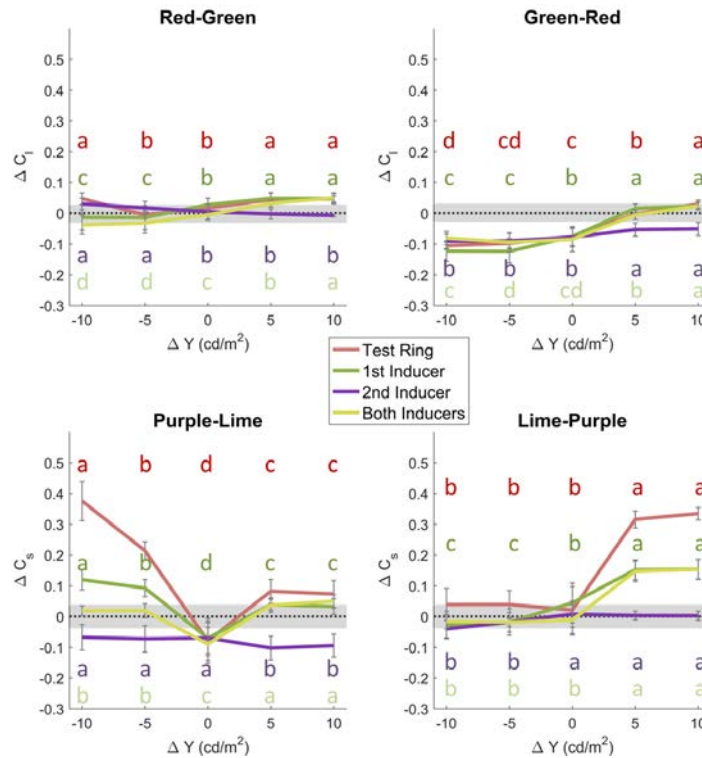


FIGURE 3.10: Color induction for the 20 combinations (runs) of luminance and chromatic conditions. The colors indicate the varied element, abscissas show different luminance conditions and panels show different chromatic conditions. The gray region shows the Just Noticeable Difference (JND) region, where no chromatic difference is perceived. The ordinates show color induction as defined by Equation 3.1: when $\Delta C > JND$ color assimilation is induced, and when $\Delta C < -JND$ color contrast is induced; and the error bars indicate ± 1 SEM. We observe that the results are very different for the l and s color opponent axes. In particular, assimilation is stronger along the s axis. Moreover, no color assimilation is induced by an equiluminant stimulus. The letters above or below the error bars show the results of Fisher's LSD post-hoc analysis, *i.e.*, they indicate whether the differences in our color induction's measures are significant or not: measures that have the same letter cannot be considered different and measures with different letters can.

and the comparison surround (ΔY_{comp}). The first column shows the luminance differences between the test ring and its surround (luminance conditions) and the second one indicates the varied element. We observe that, for the *test ring* element, the values produced by the subjects are quite close to those of the first column (save some weak brightness induction effects) and they do not vary for the different chromatic conditions. These results show that brightness induction does not depend on the chromaticity of the inducers and, thus, it does not depend on the chromatic induction. In general, rings that induce color contrast, induce similar brightness as rings that induce color assimilation. For instance, in the *test ring* case, red-green inducers at $\Delta Y = -10$ induce color assimilation and a brightness induction of $\Delta Y_{comp} = -11.6 cd/m^2$, while green-red inducers at the same luminance condition induce color contrast and the same brightness induction.

Another interesting observation is that this brightness induction is not symmetric when either the 1st or the 2nd inducers are varied. Much stronger brightness

induction is induced for dark test rings ($\Delta Y < 0$) than for bright ones ($\Delta Y > 0$). Furthermore, when both inducers are simultaneously varied in an opposite way, the test ring is always perceived darker than its physical value ($Y = 20 \text{ cd/m}^2$), independently of the 1st inducer's polarity (only negative brightness values are reported).

TABLE 3.3: Luminance differences obtained for the comparison ring in different luminance conditions. The values in the table are the mean and the standard error of means (*SEM*) of the luminance difference between the comparison ring and the comparison surround, calculated for all subjects. When test ring luminance was varied, the values of ΔY_{comp} are similar to those of ΔY , confirming that a small brightness contrast is induced by the inducer rings. Since these brightness contrasts are very similar for different chromatic conditions, the results suggest that luminance is independent of the chromaticity of the inducer (inducers of the same luminance but different chromaticity induce similar brightness).

		ΔY_{comp}			
ΔY	Varied element	Red-Green	Green-Red	Purple-Lime	Lime-Purple
-10	Test	-11.6 ± 0.20	-11.6 ± 0.25	-10.7 ± 0.28	-11.2 ± 0.21
	1 st inducer	-4.55 ± 0.21	-4.1 ± 0.29	-3.8 ± 0.35	-4.5 ± 0.28
	2 nd inducer	-4.5 ± 0.25	-4.9 ± 0.45	-5.1 ± 0.36	-4.0 ± 0.27
	Both inducers	-2.7 ± 0.29	-2.0 ± 0.40	-2.1 ± 0.42	-2.2 ± 0.32
-5	Test	-6.5 ± 0.26	-6.7 ± 0.24	-5.9 ± 0.21	-6.3 ± 0.31
	1 st inducer	-2.8 ± 0.26	-2.5 ± 0.28	-2.4 ± 0.25	-2.34 ± 0.24
	2 nd inducer	-2.9 ± 0.25	-3.4 ± 0.38	-3.4 ± 0.37	-2.6 ± 0.25
	Both inducers	-1.9 ± 0.27	-1.4 ± 0.28	-1.4 ± 0.25	-1.3 ± 0.29
0	Test	-0.9 ± 0.28	-1.0 ± 0.36	0.1 ± 0.12	-0.1 ± 0.11
	1 st inducer	-0.8 ± 0.41	-0.4 ± 0.29	0.1 ± 0.15	-0.1 ± 0.08
	2 nd inducer	-0.9 ± 0.36	-1.0 ± 0.38	0.0 ± 0.09	0.0 ± 0.16
	Both inducers	-0.6 ± 0.34	-0.9 ± 0.32	-0.1 ± 0.08	0.1 ± 0.07
+5	Test	4.9 ± 0.55	4.6 ± 0.53	6.6 ± 0.41	5.8 ± 0.28
	1 st inducer	0.26 ± 0.18	0.1 ± 0.58	0.8 ± 0.48	1.1 ± 0.43
	2 nd inducer	0.3 ± 0.31	0.4 ± 0.13	0.2 ± 0.12	0.5 ± 0.38
	Both inducers	-0.4 ± 0.42	-1.8 ± 0.38	-1.1 ± 0.39	-0.8 ± 0.53
+10	Test	10.5 ± 0.33	11.2 ± 0.66	12.8 ± 0.60	11.9 ± 0.46
	1 st inducer	1.5 ± 0.39	1.4 ± 0.50	2.1 ± 0.55	1.5 ± 0.50
	2 nd inducer	0.7 ± 0.40	1.1 ± 0.36	0.5 ± 0.21	0.7 ± 0.38
	Both inducers	-0.6 ± 0.50	-1.4 ± 0.57	-0.9 ± 0.60	-0.9 ± 0.60

Brightness experiment results

In the subsequent experiment, the results (see Figure 3.11) also show that color induction depends on both the brightness and the chromatic condition. We can observe that the results along the l axis (top panels) are not symmetric. For instance, when the 1st inducer is red, there are several conditions that induce color assimilation, while when the 1st inducer is green, there is no condition that induce color assimilation. Interestingly, when the test ring is darker than its greenish surround (top-right panel), color contrast always occurs.

In the s axis (bottom panels), unconstrained conditions tend to induce color assimilation (except for $\Delta B = -5 \text{ cd/m}^2$). Similar effects are observed when varied

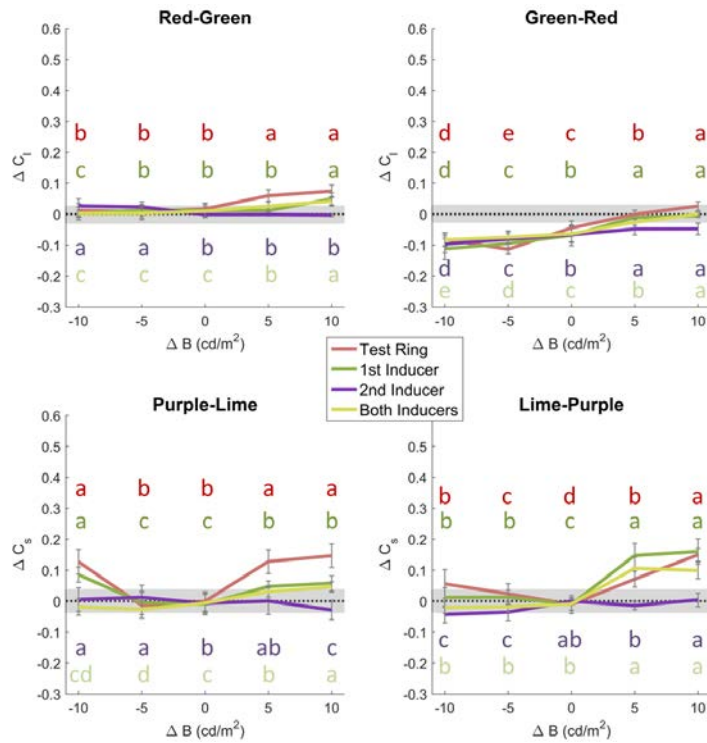


FIGURE 3.11: Color induction for the 20 combinations (runs) of brightness and chromatic conditions. Similarly to Figure 3.10, the colors indicate the varied element, abscissas show different brightness conditions and panels show different chromatic conditions. The gray region shows the Just Noticeable Difference (JND) region, where no chromatic difference is perceived. The ordinates show color induction as defined by Equation 3.1: when $\Delta C > JND$ color assimilation is induced, and when $\Delta C < -JND$ color contrast is induced; and the error bars indicate $\pm 1 SEM$. We observe that the results are very different for the l and s color opponent axes. In particular, assimilation is stronger along the s axis. Moreover, no color assimilation is induced at equibrightness conditions. The letters above or below the error bars show the results of Fisher’s LSD post-hoc analysis, *i.e.*, they indicate whether the differences in our color induction’s measures are significant or not: measures that have the same letter cannot be considered different and measures with different letters can.

the test ring and the 1st inducer brightness. In the purple-lime condition the effect is weaker in the 1st inducer case, but in the lime-purple the effect is almost the same one (in fact, in condition $\Delta B = +5$ the effect is even stronger than that of the *test ring* case).

Comparing both luminance and brightness results (see Figures 3.10 and 3.11), we can observe that they are very similar. In fact, regarding the l axis, the results are almost the same ones: Red-green induces a weak color assimilation in several unconstrained conditions and green-red never induces color assimilation. Along the s axis, the behavior is not as different: Unconstrained conditions induce color assimilation (except for $\Delta B = -5$) and in the equi-conditions (equiluminance and equibrightness) no color assimilation is induced. The major difference is the strength of the color assimilation on the s axis. For the *test ring* element, the strength of the effect is about the half in the brightness conditions with respect to the luminance ones.

TABLE 3.4: Luminance differences obtained for the comparison ring in different brightness conditions. The values in the table are the mean and the standard error of means (*SEM*) of the luminance difference between the comparison ring and the comparison surround, calculated for all subjects. Similarly to Table 3.3, the small brightness contrasts do not depend on the chromatic condition (*i.e.*, on the inducers' chromaticity).

		ΔY_{comp}			
ΔB	Varied element	Red-Green	Green-Red	Purple-Lime	Lime-Purple
-10	Test	-10.6 ± 0.25	-10.8 ± 0.27	-10.7 ± 0.22	-11.4 ± 0.19
	1 st inducer	-3.5 ± 0.32	-3.5 ± 0.39	-3.0 ± 0.36	-4.1 ± 0.10
	2 nd inducer	-3.5 ± 0.29	-3.8 ± 0.39	-4.9 ± 0.27	-3.4 ± 0.39
	Both inducers	-2.1 ± 0.19	-2.2 ± 0.57	-1.2 ± 0.50	-2.8 ± 0.35
-5	Test	-5.3 ± 0.38	-5.3 ± 0.48	-6.0 ± 0.48	-5.5 ± 0.41
	1 st inducer	-0.9 ± 0.79	-1.9 ± 0.41	-0.9 ± 0.67	-2.3 ± 0.32
	2 nd inducer	-1.5 ± 0.48	-1.9 ± 0.71	-2.8 ± 0.38	-1.5 ± 0.56
	Both inducers	-0.3 ± 0.77	-1.1 ± 0.49	0.2 ± 0.40	-1.6 ± 0.36
0	Test	0.6 ± 0.52	0.1 ± 0.06	-0.1 ± 0.38	0.3 ± 0.37
	1 st inducer	0.4 ± 0.57	0.4 ± 0.51	-0.2 ± 0.51	0.1 ± 0.02
	2 nd inducer	-0.1 ± 0.44	0.2 ± 0.53	-0.1 ± 0.61	-0.6 ± 0.32
	Both inducers	0.5 ± 0.62	0.4 ± 0.53	-0.1 ± 0.56	0.3 ± 0.22
+5	Test	6.6 ± 0.70	7.1 ± 0.64	7.3 ± 0.34	5.5 ± 0.58
	1 st inducer	1.0 ± 0.55	1.4 ± 0.54	0.8 ± 0.55	2.4 ± 0.66
	2 nd inducer	1.1 ± 0.44	1.0 ± 0.53	2.6 ± 0.58	-0.1 ± 0.23
	Both inducers	0.0 ± 0.40	-0.1 ± 0.55	-0.7 ± 0.59	0.7 ± 0.52
+10	Test	12.4 ± 0.73	13.3 ± 0.79	13.8 ± 0.45	11.5 ± 0.59
	1 st inducer	2.4 ± 0.73	2.2 ± 0.68	2.1 ± 0.66	2.8 ± 0.70
	2 nd inducer	1.4 ± 0.48	1.6 ± 0.62	2.0 ± 0.49	0.6 ± 0.48
	Both inducers	-0.1 ± 0.40	-0.3 ± 0.49	-0.8 ± 0.62	-0.1 ± 0.66

Similarly to luminance results, Figure 3.11 shows that, in brightness conditions, the effect also depends on the varied element. The further the varied element from the test ring, the weaker is the effect on it. In particular, we can observe that the brightness of the second inducer, as its luminance, does not play any role in color induction and, when both inducers are varied, the results do not differ much to the ones for the 1st inducer case.

The similarity between equiluminance and equibrightness (at least along the *s* axis) is surprising because equiluminance and equibrightness calibrations are substantially different (*i.e.*, in equiluminance condition, there are brightness differences and in equibrightness there are luminance differences), but none of equi-conditions induce color assimilation. If the results differed, we could throw some light to whether luminance or brightness drives the color assimilation effect. Since the effect is only reported in unconstrained conditions (where both luminance and brightness are altered), the results do not show enough evidence of which measure (the physical or the perceptual) mediates in the color assimilation effect. But, considering that color induction is much stronger when the surround forms an equiluminant surface (and not equibrightness), these results could suggest that the luminance differences in the equibrightness conditions are not big enough to induce color assimilation.

Regarding the brightness results of both experiments (see Tables 3.3 and 3.4), we

can observe that they are very similar, even at the equi-conditions. In fact, similarly to luminance experiment, in Table 3.4 we can observe that the different chromatic conditions do not induce different brightness (results are very similar along the different columns). In contrast, *SEMs* values are quite different: They are higher in the brightness conditions than in luminance, *i.e.*, the agreement between observers in the brightness component is lower in the brightness conditions than in luminance ones.

The statistical analyses showed that, in all chromatic conditions, the null hypothesis should be rejected. Therefore, significant differences in color induction exist at different luminance conditions (see Table A.1 in Appendix for the ANOVA details). The letters in Figures 3.10 and 3.11 relate which luminance (or brightness) conditions produce statistically similar results (Fisher's LSD post-hoc analysis; same letter implies no statistical difference).

3.3.4 Discussion

Some of the results described above are consistent with previous work and some are novel. In this section we will try to interpret them in terms of previous psychophysical results and the neural correlate of color perception.

Psychophysics

Chromatic and brightness induction have been studied using many psychophysical paradigms (*e.g.*, matching, cancellation tasks, etc.) that generally rely in sharp-edge patterns presented on a computer screen (White, 1979; Pinna, Brelstaff, and Spillmann, 2001; Devinck et al., 2006; Monnier and Shevell, 2003; Otazu, Parraga, and Vanrell, 2010). In our case, the stimuli are composed by concentric rings with sharp edges that contain energy within a broad range of spatial frequencies (see Figure 3.8). The general case of the Fourier decomposition for a square-wave is (Weisstein, 2018):

$$f(x) = \frac{4}{\pi} \sum_{n=1,3,5,\dots}^{\infty} \frac{1}{n} \sin \frac{n\pi x}{L} \quad (3.2)$$

where L is the period of the square-wave, and n are odd integers. The dominant term of the decomposition ($n = 1$) has the same spatial frequency as the original square-wave and its closest term in the series has a frequency 3 times higher than that (all Fourier components have greater spatial frequencies than that of the square-wave). The relative contributions of the extra terms are $1/3$, $1/5$, $1/7$, etc. To produce the square-wave, all sinusoidal terms become zero at the edges. Although we did not assess the contribution of the $n > 1$ terms, we assumed it to be small since most cortical neurons respond weakly to spatial frequencies outside a one-octave range (De Valois, Albrecht, and Thorell, 1982). Following this, and in order to compare our results to those of the literature, we used concentric rings of fixed spatial frequency (1.94 cpd) whose dominant sinusoidal Fourier component also had this spatial frequency. From this point forward we will refer to the square-wave spatial frequency and the dominant Fourier component indistinctly.

Equiluminant stimuli are widely used to study color induction (De Weert and Spillmann, 1995; Fach and Sharpe, 1986; Smith, Jin, and Pokorny, 2001; Gordon and Shapley, 2006; Kaneko and Murakami, 2012; Xing et al., 2015) but, as mentioned in Section 3.3.1, color assimilation is not as comprehensively studied as color contrast. Some studies used striped equiluminant stimuli, but they mainly focused on the effects of spatial frequencies (Fach and Sharpe, 1986; Smith, Jin, and Pokorny, 2001)

or the spatial configuration of the inducers (Cao and Shevell, 2005), concluding that, for equiluminant stimuli, the spatial frequency distribution is a key factor in color assimilation. In particular, they observed that very thin stripes (9 cpd) induce color assimilation and thick stripes induce color contrast (0.7 cpd), with a transition point from assimilation to contrast near 4 cpd (Smith, Jin, and Pokorny, 2001). Regardless of this, at equiluminance, our stimuli, which are composed by stripes of 1.94 cpd , can induce color contrast (green-red chromatic condition) or generate no induction at all (red-green, purple-lime and lime-purple chromatic conditions). These effects of luminance distribution on color induction have been only sparsely studied. De Weert and Spillmann (1995) did a preliminary psychophysical experiment pointing out that the luminance of a spatial distribution could affect color assimilation, but they did not provide any quantitative support to their results. They measured color induction on a colored background, which had a lower spatial frequency (0.59 cpd) than our test ring and their inducers had red and green chromaticities. As in our *test ring* case, the luminance of the inducers did not vary, but the luminance of the background (the target) was varied. The authors concluded that no color induction (neither contrast nor assimilation) is induced at equiluminance and that the backgrounds should have higher luminance than its inducers to induce color assimilation. For similar chromatic conditions (see red-green and green-red chromatic conditions in Figure 3.10 at equiluminance) we observed: no color induction when the 1st inducer is red and the 2nd is green, and color contrast when the 1st is green and the 2nd is red. Apart from equiluminance, they measured color induction at two different luminance conditions ($\Delta Y = [-2.7, +4.7]\text{ cd/m}^2$) finding color assimilation in both chromatic conditions when the background's luminance was higher ($\Delta Y = +4.7$) than the inducers' luminance. We did not measure color induction in exactly the same luminance conditions, but at similar ones. We agree that color assimilation is not induced in either of the red-green or green-red chromatic conditions at low luminance ($\Delta Y = -5\text{ cd/m}^2$ in our case) and it is induced in red-green at high luminance ($\Delta Y = +5\text{ cd/m}^2$), but we have never found color assimilation when the chromatic condition was green-red. Moreover, we found color assimilation in red-green making the test ring even darker than their low luminance condition. In a subsequent study, Cao and Shevell (2005) also measured color assimilation in two different luminance conditions ($\Delta Y = [-1.33, +2]\text{ cd/m}^2$) and eight chromatic conditions, covering a range. As De Weert and Spillmann, they concluded that in the l direction, the luminance of the inducer has to be lower than the targets' luminance to induce color assimilation and they observed that in the s direction color assimilation does not depend on the luminance difference, but on the spatial configuration of the inducers (spatial frequency and spatial separation). In their work, they did not use equiluminant stimuli (they did not compare against equiluminance) but compared against different luminance conditions. Conversely, we observed that in the presence of a luminance difference, color assimilation is induced in the s direction with a strength that depends on this difference. This could be explained by the spatial frequency content of the stimulus given that both, De Weert and Spillmann (1995) and Cao and Shevell (2005) used stimuli of higher spatial frequency than we did. Regarding the stimulus configuration, we measured color induction in similar conditions as Monnier and Shevell (2003; 2004) did (see purple-lime and lime-purple chromatic conditions at $\Delta L = +5\text{ cd/m}^2$), and we reproduced their results. They observed stronger induction than us, but with higher spatial frequency stimuli (3.3 cpd) and more saturated colors (purple chromaticity $l, s = [0.66, 2.0]$ and lime chromaticity $l, s = [0.66, 0.16]$) (Monnier and Shevell, 2003; Monnier and Shevell, 2004). As Otazu et al. (2010) reported in a similar study, the higher the spatial frequency of the

striped stimuli, the stronger the color induction.

The effect of luminance on color assimilation has been studied using a variety of patterns (Van Tuijl and De Weert, 1979; Ejima et al., 1984; Watanabe and Sato, 1989; Bressan, 1995; Pinna, Brelstaff, and Spillmann, 2001; Devinck et al., 2005; Devinck et al., 2006). For example, the Watercolor effect (Pinna, 1987) is usually studied on a white background because its color assimilation is stronger on that background than on either gray or black (Pinna, Brelstaff, and Spillmann, 2001). As we observed in our results, the strength of color assimilation is not the same when the target region is either brighter or darker than the inducers. In their case, not only the luminance of the target region, but also the luminance contrast of both inducers is important: when both inducers are equiluminant, color assimilation is only weakly induced (Pinna, Brelstaff, and Spillmann, 2001; Devinck et al., 2005). Interestingly, some authors found that the strength of the effect also depends on the chromaticity of the inducers (Schober and Munker, 1967), pointing out that when the inducer was yellow, color assimilation was weaker (Fach and Sharpe, 1986; Devinck et al., 2005). We also found that color assimilation depends on the chromaticity of the inducers, but our weakest effect occurred when the inducer was green, not yellow (for that chromaticity, color assimilation never occurred). Fach and Sharpe (1986) explored the effects of spatial frequency on color induction using equiluminant square-wave gratings whose bars varied from 2 to 20 *arcmin*. They measured color induction for 10 and 20 *arcmin* bars, but unfortunately they did not explore spatial frequencies similar to ours (15.5 *arcmin*). For red-green and blue-yellow equiluminant gratings, they reported color contrast (or no color induction), but never color assimilation. Similarly to them, at equiluminance we only observed color contrast or no color induction.

Neurophysiology

It is well established in the literature that the type of neuron responding in V1 largely depends on stimulus properties such as spatial frequency or chromatic and luminance spatial distribution (Johnson, Hawken, and Shapley, 2001; Johnson, Hawken, and Shapley, 2008; Shapley and Hawken, 2011; Xing et al., 2015; Nunez, Shapley, and Gordon, 2018). In terms of their responses, SO cells are non-orientation selective, being activated mostly by uniform color stimuli while DO cells are orientation selective and responsive to both color and luminance patterns. NO cells are mostly responsive to luminance patterns (Johnson, Hawken, and Shapley, 2008). Since our test stimuli were composed of colored concentric rings of medium spatial frequency (1.94 *cpd*), it is safe to assume that both types of color-responsive neurons (SO and DO) were always activated. In fact, DO neurons might have been close to their maximum sensitivity, which is at 2 *cpd* (Johnson, Hawken, and Shapley, 2001; Johnson, Hawken, and Shapley, 2008). At equiluminance ($\Delta Y = 0$), NO neurons are weakly responsive (Skottun, 2013), but by increasing the luminance contrast these neurons become responsive (Johnson, Hawken, and Shapley, 2001; Johnson, Hawken, and Shapley, 2008). Thus, by presenting several luminance conditions, our stimuli is likely to activate different numbers of NO neurons in V1, varying the strength of the inhibition (mutual-inhibition) on both SO and DO neurons. According to the mutual-inhibition hypothesis (Xing et al., 2015; Nunez, Shapley, and Gordon, 2018), as luminance contrast is increased, color response is inhibited. In terms of color induction, this means that (1) color contrast is greatest at equiluminance when color

response is maximal (mutual-inhibition is minimal) (Xing et al., 2015; Nunez, Shapley, and Gordon, 2018), and (2) color assimilation increases with luminance contrast, *i.e.* when mutual-inhibition is greatest, color response is reduced.

Although we have used equiluminant stimuli with striped instead of uniform surrounds (Xing et al., 2015), we observed (see purple-lime and lime-purple chromatic conditions in Figures 3.10 and 3.11) that color assimilation is stronger as luminance contrast is increased. This seems to support the mutual-inhibition hypothesis, which might be related to the "probably inhibitory" (Zaidi, 1999) lateral connections between neurons that are the principal ingredient for color induction. Considering that our results could only be explained by an interaction between the chromatic and the luminance channels, they do not support models where color induction occurs earlier than V1 (Kamerans, Kraaij, and Spekreijse, 1998; VanLeeuwen et al., 2007; Sabbah et al., 2013). In the same way, we cannot rule out models where color induction occurs at higher levels (Gegenfurtner, 2003; Horiuchi et al., 2014).

Our color induction results are completely different depending on whether the stimuli are defined in the l or the s directions of MacLeod-Boynton color space, suggesting that mutual-inhibition mechanisms are different at different pathways or at different layers of V1. When the stimuli are defined in the l direction (red-green and green-red chromatic conditions), the parvocellular pathway is activated, and when they are in the s direction (purple-lime and lime-purple chromatic conditions), the koniocellular pathway is activated (Nassi and Callaway, 2009). From a feedforward point of view, the parvocellular pathway is first processed in layer $4C\beta$ and then in layer 2/3 (Sincich and Horton, 2005); the koniocellular pathway projects its S-ON channel to layer 2/3 and its S-OFF channel to layer 4A (Chatterjee and Callaway, 2003; Callaway, 2014; Kaplan, 2014); and the magnocellular pathway first projects to layer $4C\alpha$ and then to layer 2/3 (Sincich and Horton, 2005; Kaplan, 2014). Although this is highly speculative and there is no neurophysiological evidence, the dissimilarity of color induction regarding the l and s directions could be due to the different circuitry and composition of the V1 layers (there are different amounts of SO, DO and NO neurons in the different layers) (Johnson, Hawken, and Shapley, 2001; Johnson, Hawken, and Shapley, 2008). Another possibility is that color induction in the l direction is different from that in the s direction because of some 'pre'-processing at layer $4C\beta$.

In any case, it is surprising to find dissimilarities between the red-green and green-red chromatic conditions since both of them are processed by the same layers (assumably) in a similar fashion (Solomon and Lennie, 2007). A plausible reason for this asymmetry might be ecological, since it has been suggested that tropical fruits have co-evolved with the trichromatic color vision of Old World monkeys to facilitate their detection over a background of green leaves (Mollon, 1989; Reagan et al., 1998). In this framework, it makes sense for the HVS to want to enhance their visual targets (via chromatic contrast) when placed against such chromatic backgrounds. This could also explain why we did not observe any instance of chromatic assimilation when the 1st inducer was green.

The 'mirroring' effect observed in the purple-lime and lime-purple chromatic conditions (bottom panels in Figure 3.10) could be produced by mutual-inhibition, or inhibition itself. Looking at the results in more detail, we find that for the purple-lime chromatic condition (bottom-left panel), assimilation is stronger when the test ring is darker than when it is brighter (negative values of ΔL), and the opposite is true for the lime-purple chromatic condition (assimilation is stronger when the test ring is brighter than when it is darker, positive values of ΔL). For a given dark

purple-lime stimulus ($\Delta L < 0$ in bottom-left panel in Figure 3.10), the test ring activates the S-OFF and the Lum-OFF post-receptor channels (konio- and magnocellular pathways, respectively) because the gray test ring excites less the S-cones than the surrounding purple and also has a lower luminance than the 1st inducer. Conversely, for a bright purple-lime stimulus ($\Delta L > 0$ in bottom-left panel in Figure 3.10), the test ring activates the S-OFF and the Lum-ON post-receptor channels (the chromatic information does not change, but luminance does). A possible explanation of this stronger assimilation when the S- and the Lum-OFF channels are activated is that channels of the same polarity inhibit more each other than channels of opposite polarity do. The same might occur in the lime-purple chromatic condition: it activates the S-ON channel while the low luminance condition ($\Delta L < 0$ in bottom-right panel in Figure 3.10) activates the Lum-OFF channel. The latter leads to a weaker inhibition and, thus, to a much weaker (or no) chromatic assimilation than the higher luminance condition ($\Delta L > 0$, which activates the Lum-ON channel).

We also considered the influence of non-neural (optical) effects in our results. Since our stimuli had relatively low spatial frequency (1.94 *cpd*), we could consider that the effects of spread light in our results (see Section 3.1) are much lower than the variability of our observers and therefore negligible.

3.3.5 Conclusions

We performed two psychophysical experiments based on the well-known color induction paradigm of Monnier and Shevell (in concrete, their color assimilation results) (2003; 2004). Our paradigm was similar to theirs, except that we varied both the luminance and brightness difference between the target ring (where the induction was measured) and its surround. We obtained similar results for the same luminance condition they tested ($\Delta Y = +5$, being the test ring the varied element), and observed that for other conditions, color assimilation depends on the luminance contrast of the inducer. This suggests that the magno-, parvo- and koniocellular pathways cannot be considered as having independent processing mechanisms, or at least they have a significant interaction in V1. In particular, our results show that luminance influences color induction, but not the opposite (different chromatic conditions result in similar brightness induction). Moreover, at either equiluminance or equibrightness, color assimilation is not induced.

We were not able to find a simple and global explanation for our results based on linear combinations of chromatic and luminance signals from the visual pathways. Indeed color assimilation depends on both luminance contrast and chromatic condition (see a visual summary of our test ring results in Figure 3.12). Remarkably, in the red-green and green-red chromatic conditions, subjects always see the test ring as "reddish" or "gray" regardless of the spatiochromatic configuration of the inducers or luminance conditions. Also, color assimilation for the red-green and purple-lime color pairs is completely different and luminance contrast seems to play a more important role in the koniocellular than in the parvocellular pathway.

Although our results are significant, they need to be taken with caution since we did not explore other stimuli configurations such as different spatial frequencies or patterns, other color pairs, etc. We did not intent to explore all possible combinations but to concentrate on luminance differences which allowed us to test a single unexplored aspect of color assimilation.

In summary, our results support the hypothesis that mutual-inhibition between V1 neurons plays a major role in color appearance (Xing et al., 2015; Nunez, Shapley, and Gordon, 2018), or at least in color induction. Furthermore, since our results

		Luminance Conditions				
Chromatic Conditions		<i>assim</i> 	<i>no</i>	<i>no</i>	<i>assim</i> 	<i>assim</i>
		<i>contr</i> 	<i>contr</i> 	<i>contr</i> 	<i>no</i>	<i>no</i>
		<i>assim</i> 	<i>assim</i> 	<i>contr</i> 	<i>assim</i> 	<i>assim</i>
		<i>no</i>	<i>no</i>	<i>no</i>	<i>assim</i> 	<i>assim</i>

FIGURE 3.12: *Test ring* case: Visual summary of the results. The columns correspond to the 5 different luminance conditions. In that case, we fixed the luminance of the inducers at 20 cd/m^2 (grey disks) and we evaluated 5 different luminance conditions of the test ring $\Delta Y = [-10, -5, 0, +5, +10] \text{ cd/m}^2$ (black, dark gray, gray, light gray and white rings respectively). The rows correspond to the 4 different chromatic conditions (red-green, green-red, purple-lime and lime-purple). The colors of the concentric rings and their spatial configuration only have an illustrative purpose (we used 11 rings in our experiment instead of 5). The colored dots in the figure indicate the match performed by the subjects, the number of dots indicates the strength of the color induction, and the abbreviations above them indicate the type of color induction effect, *e.g.*, assimilation, contrast or no effect. We observed that (1) color assimilation at equiluminance do not occur, (2) color assimilation is never induced in the second row -in other words, subjects only see the test ring as "reddish" or "gray" regardless of the spatiochromatic configuration of the red/green inducers or luminance conditions-, (3) a 'mirroring' effect occurs between the third and the fourth rows, (4) color assimilation depends on both luminance contrast and chromatic condition. These results support the hypothesis that mutual-inhibition between color and luminance neurons plays a major role in color induction.

strongly depend on the studied chromatic condition, they suggest that this mutual-inhibition mechanism is different for the parvo- and koniocellular pathways, with a 'mirroring' effect occurring between the two koniocellular (S-ON and S-OFF) channels.

3.3.6 Future work

We observed that the luminance difference between the target ring and its surround plays a major role in color assimilation. In particular, when the inducers composed an equiluminant surround. Thus, it would be interesting to study different chromatic conditions defined not only on the cardinal axes of the MacLeod-Boynton color space, but also on the diagonals of this color space, where both parvo- and

koniocellular pathways are activated. The mutual-inhibition hypothesis was formulated considering the interaction between the luminance (magnocellular pathway neurons) and the chromatic channels (either parvo- or koniocellular pathway neurons) (Xing et al., 2015). It would be interesting to study whether activating both parvo- and koniocellular neurons, despite of being all Color or Color-Lum neurons, and not activating the magnocellular pathway (using equiluminant stimuli) the color assimilation occurs. If so, it could suggest that this inhibitory mechanism is not related to a luminance-chromatic interaction but it is an inhibitory mechanism without pathway, or neuron type, selectivity. Moreover, it would be interesting to use the stimuli defined here to study the temporal frequency effect on color assimilation (repeat the previous study but using stimuli that induce color assimilation).

A new computational model of color induction capable of reproducing these results should be implemented. Color induction models such as CIWaM (Otazu, Pargara, and Vanrell, 2010), ODOG (Blakeslee and McCourt, 1999), etc. (Spitzer and Barkan, 2005) are likely to fail to reproduce these results because they assume independent chromatic and luminance channels (*i.e.*, parvo- and konio-, and magnocellular pathways). Thus, a further biologically plausible computational model should include some mutual-inhibition mechanism or at least, some kind of luminance-chromatic interaction.

Probably, the most striking future work that can arise from this study is the idea of color induction in natural environment. In this study we have found that, contrary to the other chromatic conditions, a green inducer never induces color assimilation. Not surprisingly, the green color can be related to the color of the foliage. In fact, the color of the foliage would be in the quadrant between the green and the lime colors in the MacLeod-Boynton color space. From our point of view, it would be very interesting to elucidate whether the color induction effect is a desired effect rather than a side-effect. Up to now, it is assumed that color induction is a side-effect of the neural processing, but it would be interesting to study these color induction effects (both color contrast and color assimilation) in a natural environment. To do so, first, a calibrated dataset of natural images with fruits in their context should be acquired. Then, the color induction should be measured in these images and several properties of the images should be modified to vary the color induction effect. Then, in a subsequent experiment, using a natural task such as fruit detection, we should measure the task performance against the color induction effect, observing whether color contrast or color assimilation helps to do the task. Our hypothesis is that, according to the results of this study, color contrast would be maximal or color assimilation minimal in the natural images (fruits surrounded by greenish context) and that color contrast would improve the fruit detection task, while color assimilation would not.

3.4 Related publications

- Is luminance a key factor for static and flashed chromatic assimilation? (Cerdeña-Company and Otazu, 2017b), *European Conference on Visual Perception (ECVP)*, 2017.
- Color induction in equiluminant flashed stimuli (Cerdeña-Company and Otazu, 2019), *Journal of the Optical Society of America A*, 2019.
- Luminance spatial distribution plays a major role in color assimilation (Cerdeña-Company et al., 2018b), *European Conference on Visual Perception (ECVP)*, 2018.

- The effect of luminance differences on color assimilation (Cerdeña-Company et al., 2018c), *Journal of Vision*, 2018.
- Stronger colour induction in migraine (Otazu et al., 2018), *European Conference on Visual Perception (EVP)*, 2018.
- Colour induction in migraine (Cerdeña-Company et al., 2018a), *Applied Vision Association (AVA) Christmas Meeting*, 2018.

Part II

Computational Modeling

“How do I know that a table still exists if I go out of the room and can’t see it? What does it mean to say that things we can’t see, such as electrons or quarks—the particles that are said to make up the proton and neutron—exist? One could have a model in which the table disappears when I leave the room and reappears in the same position when I come back, but that would be awkward, and what if something happened when I was out, like the ceiling falling in? How, under the table-disappears-when-I-leave-the-room model, could I account for the fact that the next time I enter, the table reappears broken, under the debris of the ceiling? The model in which the table stays put is much simpler and agrees with observation. That is all one can ask.”

Steven Hawking

Chapter 4

A computational model of color processing in V1

4.1 Introduction

The brain is probably the most important organ of the animals because it exerts the control over the other organs. The brain collects the information from sense organs and processes it to determine the actions to take (Carew, 2000). Therefore, the brain has a key-role in animal perception, motor control, arousal, homeostasis, motivation, learning and memory (Ramon y Cajal, 1894; Chiel and Beer, 1997; Dougherty, 1997; Singh, 2006). Since it is involved in a wide range of functionalities, it is probably the most complex organ in the vertebrate's animals and its detailed circuitry is still a mystery. Nevertheless, lots of efforts have been done for a better understanding of the mechanisms that compose this circuitry.

As stated, the brain processes a huge amount of information from all the sense organs. In this thesis, we have focused on one perception sense, in particular, in mammal vision. More concretely, in the humans' color vision.

In humans, light is absorbed by rods and cones in the retina, the outputs of which are combined by the retinal ganglion cells and segregated into three different pathways: the magno-, parvo- and koniocellular pathways. The magnocellular pathway carries luminance information (obtained by the combination of L- and M-cones and rods output), the parvocellular pathway carries the red-green chromatic information (combination of L- and M-cones) and the koniocellular pathway carries the blue-yellow chromatic information (combination of L-, M- and S-cones). All this information is sent to the Lateral Geniculate Nucleus (LGN) in the thalamus through the optical nerve and then to the primary visual cortex (V1), where the three pathways start to interact (Xing et al., 2015; Nunez, Shapley, and Gordon, 2018).

In the early stages of the HVS (up to V1), the neurons extract low-level features thank to their *receptive fields* (RFs), the region in which a stimulus changes the response of a neuron (Hubel and Wiesel, 1959). It is worth to note that the term "receptive field" is sometimes confusing. Authors often say RF to refer to both the *classical RF* (cRF) and the *extra-classical* (also known as non-classical or surround) RF (extra-cRF). The extra-cRF is the region that surrounds the cRF and where stimulus does not cause a neuronal response when presented alone, but it could alter the neuronal response when the cRF is also activated (in general the extra-cRF suppresses the neuronal response) (Blakemore and Tobin, 1972; Levitt and Lund, 1997; Solomon, Peirce, and Lennie, 2004). Nevertheless, this extra-cRF could act also as facilitatory, for low-contrast stimuli. In fact, it has been proposed that the extra-cRF is composed by a *near-surround* and a *far-surround*. The former can be either facilitatory or inhibitory depending on the stimulus contrast and the latter is always inhibitory. Moreover, some authors proposed that the near-surround is mediated by horizontal (lateral)

connections and far surround by inter-area feedback connections (Ichida et al., 2007; Shushruth et al., 2009; Angelucci and Shushruth, 2014). Thus, one can consider that there are at least three main ingredients (see below) in the HVS processing: the RFs, the lateral connections and the feedback connections. From here and so on, we will refer to the cRF and the RF indistinctly.

4.1.1 Receptive fields

Neurons can be classified according to their RF properties (or selectivities). Simple cells' RFs are composed by an antagonistic center and surround. Depending on the light's polarity they respond to, simple cells are classified as ON and OFF: ON-neurons respond (fire) to increments of light and OFF-neurons respond to decrements of light. On one hand, an ON-center/OFF-surround neuron is activated when an increment of light is presented to the center of the RF. In contrast, when the increment of light is presented to the OFF-surround alone, the neuron remains inactive (see left-panel in Figure 4.1). On the other hand, an OFF-center/ON-surround neuron is activated when the increment of light is presented to the surround (see right-panel in Figure 4.1). That means that both the center and the surround are antagonistic and excitatory. Nevertheless, usually it is considered that the center is excitatory and the surround is inhibitory (Solomon and Lennie, 2007). Complex cells respond to both polarities of light instead (see Figure 4.2) and, thus, they are considered as a hierarchical scheme (a pool) of simple cells (Hubel and Wiesel, 1962; Van Kleef, Cloherty, and Ibbotson, 2010). The classification of simple and complex cells is not as straight because different criteria such as presence and degree of ON- and OFF- subregions' overlap, spontaneous activity level, response amplitude, length summation, responses to patterns of random dots, responses to moving light and dark bars and reverse correlation can be used (Mechler and Ringach, 2002; Martinez and Alonso, 2003). Thus, a simple cell could be considered complex and vice versa depending on the adopted criteria.

To study the RFs' properties, researchers usually use drifting gratings. Changing the properties of the drifting grating such as spatial and temporal frequency and orientation, they are able to identify the cell type and, thus, to study its properties. For instance, simple cells have oscillatory response (they fire when the polarity of the grating matches its preference) and complex cells have unmodulated responses (see bottom-panel in Figure 4.2) (Van Kleef, Cloherty, and Ibbotson, 2010). Moreover, uniform stimuli are presented to measure the spontaneous firing rate (Johnson, Hawken, and Shapley, 2001; Ringach, Shapley, and Hawken, 2002; Johnson, Hawken, and Shapley, 2008) and white noise is also presented to map the RFs, usually using the reverse correlation technique (Ringach and Shapley, 2004; Yeh et al., 2009). Neuroscientists have been able to map several RFs such as the ones of single-opponent (SO) and double-opponent (DO) cells (Thorell, de Valois, and Albrecht, 1984; Lennie, Krauskopf, and Sclar, 1990; Johnson, Hawken, and Shapley, 2001; Johnson, Hawken, and Shapley, 2004; Solomon, Peirce, and Lennie, 2004; Solomon and Lennie, 2007; Johnson, Hawken, and Shapley, 2008). Single-opponent RFs are divided in: type I and type II. Both receive nearly equal but opposite input from L- and M- cones (Johnson, Hawken, and Shapley, 2004; Shapley, Hawken, and Johnson, 2014) and, while type II has a circularly symmetric center and surround, type I has a circular but larger surround instead (see Figure 4.3). Therefore, none of these RFs are orientation selective (Ringach, Shapley, and Hawken, 2002). Their main difference is that type I is found in the parvocellular pathway in LGN and also responds to luminance stimuli (see left-panels in Figure 4.3) and type II is found in the parvocellular pathway

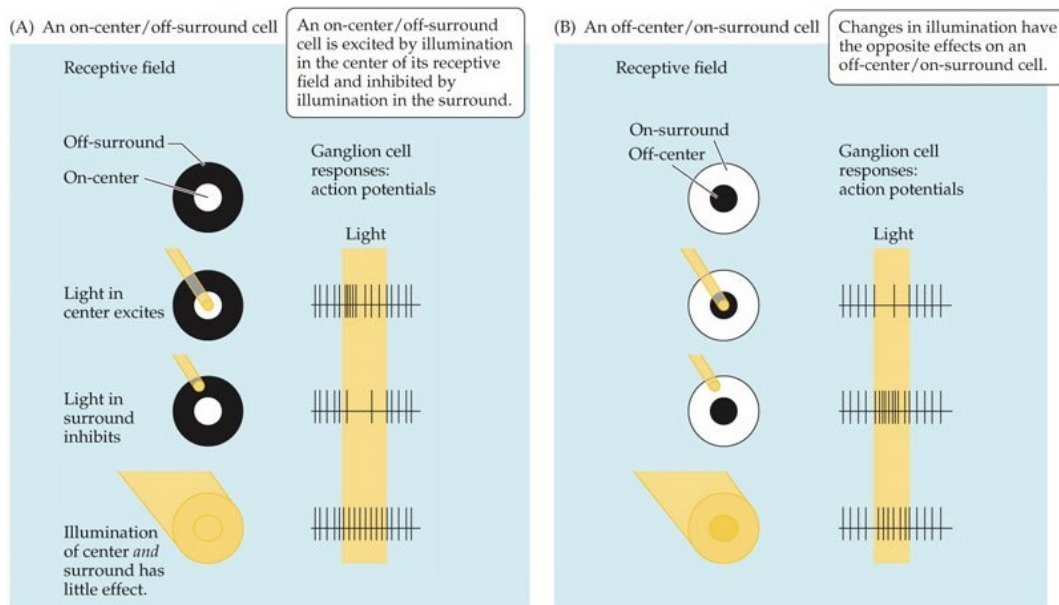


FIGURE 4.1: Receptive fields of ON- and OFF-neurons. **(A)** An ON-center/OFF-surround neuron becomes active when an increment of light is presented to the center of the RF, while it remains inactive when the light is presented on the surround. **(B)** An OFF-center/ON-surround neuron becomes active when the increment of light is presented on the surround, while it remains inactive (does not respond to) when the light is presented to the center. Figure adapted from (Watson and Breedlove, 2015).

in V1 and does not respond to luminance stimuli (Wiesel and Hubel, 1966; Shapley and Hawken, 2002; Johnson, Hawken, and Shapley, 2008; Shapley, Hawken, and Johnson, 2014).

Only one type of double-opponent RF has been mapped: orientation-selective DO cell (Johnson, Hawken, and Shapley, 2004). This neuron receive input from L- and M- cones and, due to its double-opponency, it is selective to both luminance and chromatic oriented edges (see bottom-panel in Figure 4.3) (Johnson, Hawken, and Shapley, 2004). Moreover, several properties of DO cells have been observed and cannot be related to this type of RF, that is, a DO neuron without orientation selectivity (see Figure 4E in (Johnson, Hawken, and Shapley, 2008)). The authors hypothesized that it is plausible to consider the existence of a RF (named hypothetical RF) such the one depicted in Figure 4.3 (Shapley and Hawken, 2002; Conway and Livingstone, 2006; Johnson, Hawken, and Shapley, 2008). This neuron would be responsive to both luminance and chromatic edges and would not have orientation selectivity. In contrast to SO cells, DO cells are much more diverse in its color properties because of the wide range of weights of cone inputs (Johnson, Hawken, and Shapley, 2004).

Regarding temporal properties, simple cell's RFs can change their size, spatial frequency selectivity (Bredfeldt and Ringach, 2002; Malone, Kumar, and Ringach, 2007), orientation selectivity (Mazer et al., 2002), response (De Valois et al., 2000) and polarity along time (DeAngelis, Ohzawa, and Freeman, 1993a; DeAngelis, Ohzawa, and Freeman, 1993b; DeAngelis, Ohzawa, and Freeman, 1995; DeAngelis and Anzai, 2014).

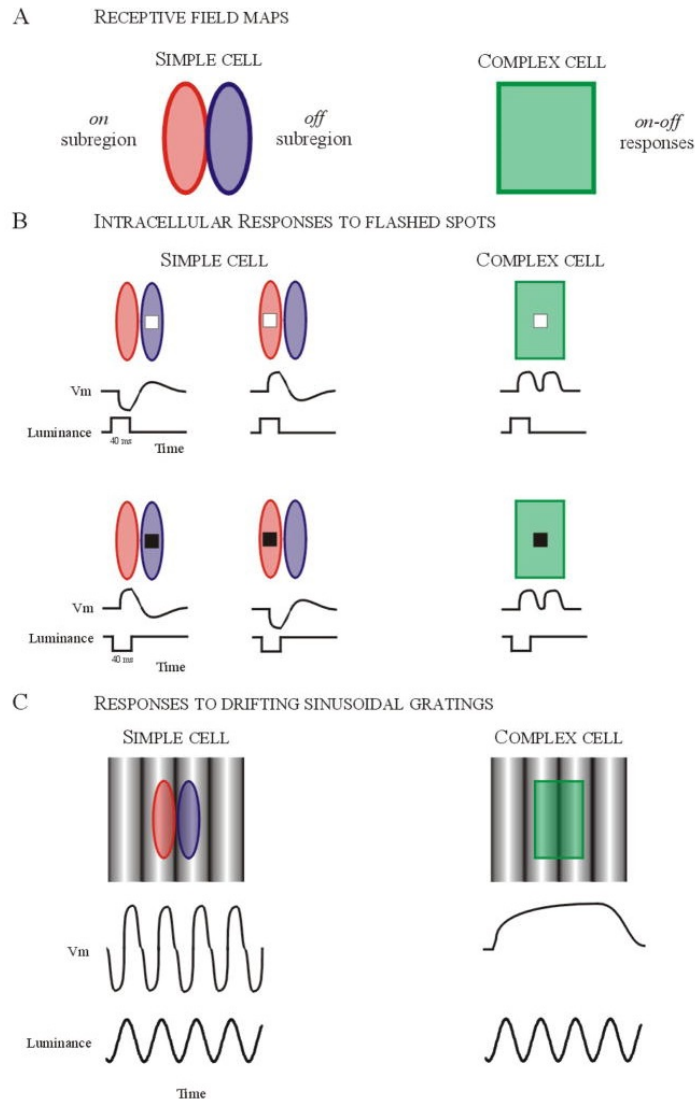


FIGURE 4.2: Due to their different RFs, simple and complex cells respond differently to the same stimulus. In (A) the RFs of a double-opponent simple cell (left) and a complex cell (right) are shown. In contrast to simple cells, complex cells respond to both increments and decrements of light. In the double-opponent RF, the red color indicates the excitatory area and the blue one indicates the inhibitory area. In (B) the response (v_m) of the cells to a ON (white patch) and OFF (black patch) light spots. Notice that complex cell has the same response to both luminance increment (ON light) and luminance decrement (OFF light). In (C) the response of both cells to drifting gratings. Because of simple cell fires when both grating's and preference's polarities match, its response is oscillatory. In contrast, since complex cells respond to both ON and OFF luminances, its response is unmodulated. Figure extracted from (Martinez and Alonso, 2003).

4.1.2 Lateral connections

Because of lateral (also known as horizontal) and feedback connections, when a stimulus is also presented outside the cRF, a cell activity may change. Due to these lateral connections, different neuronal populations in the same layer interact. Since it is considered that there is a close link between both the physiology and anatomy

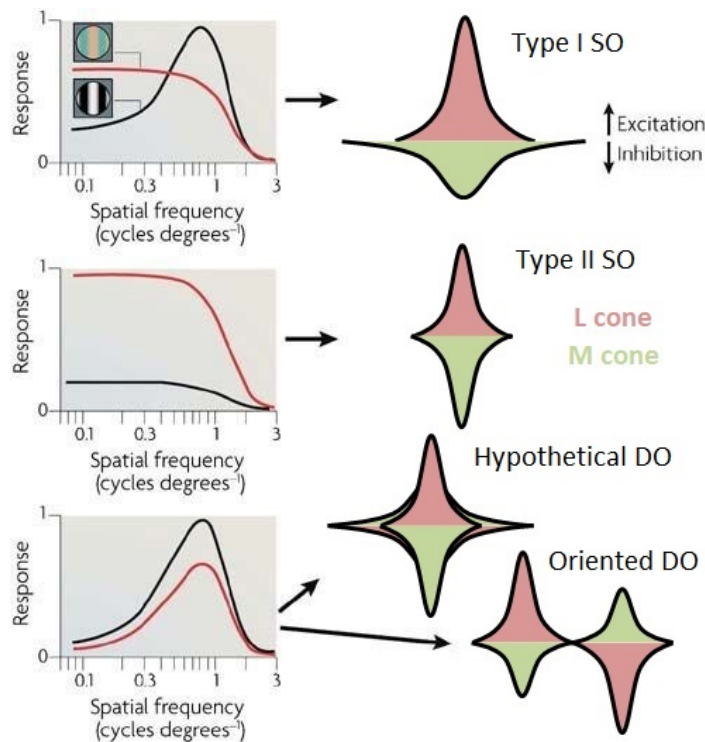


FIGURE 4.3: The different types of simple cells' receptive field. On the right, the spatial and chromatic structure of the receptive fields and, on the left, their spatial frequency selectivity when either luminance (black line) or chromatic (red line) stimuli are presented. Two types of single-opponent RFs are proposed: type I and type II. Type I neurons respond to large chromatic areas and to luminance edges. Type II neurons also respond to large chromatic areas, but have a weak response to luminance stimuli. Since both types of single-opponent RFs are circular, they do not have orientation selectivity. Moreover, two types of double-opponent RFs are proposed: oriented DO and the hypothetical (or concentric) DO. Both RFs respond to both luminance and chromatic edges, but the former has orientation selectivity and the latter does not. Although the hypothetical DO receptive field has not been mapped, several observations (like non-oriented DO cells) point out to its existence (Conway and Livingstone, 2006; Johnson, Hawken, and Shapley, 2008). Figure adapted from (Solomon and Lennie, 2007) and (Johnson, Hawken, and Shapley, 2008).

of these connections and the visual behavior in certain psychophysical tasks (Field, Golden, and Hayes, 2014), psychophysical experiments can shed some light on the performance of these connections (Tolhurst and Barfield, 1978; Sagi and Hochstein, 1985; Field, Hayes, and Hess, 1993; Field, Golden, and Hayes, 2014).

The interaction between neighboring neurons through lateral connections depends on the retinotopical position of the neurons (their physical distance), their spatial frequency and their orientation selectivity. Lateral connections can be excitatory-excitatory (excitatory neighbors activates the excitatory cell) and excitatory-inhibitory (excitatory neighbors activates the inhibitory cell) (Li, 1998; Penacchio, Otazu, and Dempere-Marco, 2013).

These type of connections compose the near-surround of the extra-cRF, playing an important role in the center-surround modulation (Ichida et al., 2007; Shushruth et al., 2009; Angelucci and Shushruth, 2014), and they are able to change the cells'

RF (Xing et al., 2005; Yeh et al., 2009). Thus, it is not surprising that they are an important factor in visual perception and that several effects such as brightness and chromatic induction are the result of the lateral connections present in V1 (Zaidi et al., 1992; Stemmler, Usher, and Niebur, 1995; Stettler et al., 2002; Penacchio, Otazu, and Dempere-Marco, 2013).

4.1.3 Feedback connections

The HVS is a complex network composed by a huge amount of feedforward and feedback connections (Garcia-Marin, Kelly, and Hawken, 2017). Feedback processing has been observed in all stages of the HVS such as retina, LGN, V1 and higher visual areas (Verweij, Kamermans, and Spekreijse, 1996; Kamermans and Spekreijse, 1999; Kolb, 2005; Briggs and Usrey, 2008; Briggs and Usrey, 2014). This feedback can connect one area to another, *e.g.*, corticogeniculate (from V1 to LGN) feedback, or layers or neurons of the same area, *e.g.*, from horizontal cells to cones or from layer $4C\beta$ to layer 6 in V1. As stated before, the neuronal activity is modulated by the RFs, the lateral connections and the feedback connections. In fact, it is believed that feedforward connections such as the ones from retina to LGN drive the activity, while feedback connections modulate it (Sherman and Guillery, 1998; Briggs and Usrey, 2014).

Although feedback functionality is still a mystery, several authors observed that the corticogeniculate feedback sharpens the tuning of LGN receptive fields and modulates the transmission of sensory information between the thalamus and the cortex (Briggs and Usrey, 2008; Briggs and Usrey, 2014). Moreover, feedback connections (which compose the far-surround in the extra-cRF) participate actively in the center-surround modulation (Ichida et al., 2007; Shushruth et al., 2009; Angelucci and Shushruth, 2014; Briggs and Usrey, 2014) and it is suggested to help in figure-background discrimination (feedback from higher visual areas to lower ones amplifies and focuses the neurons' activity of those areas) (Hupe et al., 1998).

4.1.4 Color processing in the parvocellular pathway of V1

The primary visual cortex is composed by several layers, *i.e.*, layers 1, 2/3, 4A, 4B, 4C α , 4C β , 5 and 6. The red-green color information (parvocellular pathway) arrives to V1 in layer 4C β . This layer is formed by simple SO and DO cells and complex cells, it lacks orientation selectivity (Blasdel and Fitzpatrick, 1984; Ringach, Shapley, and Hawken, 2002; Johnson, Hawken, and Shapley, 2008) and there are not large intracortical connections (lateral connections) (Binzegger, Douglas, and Martin, 2004; Chisum and Fitzpatrick, 2004; Hirsch and Martinez, 2006; Binzegger, Douglas, and Martin, 2009; Callaway, 2014). In particular, the simple SO cells that exist in V1 are of type II (circularly symmetric center-surrounds of the same size and almost well-balanced) (Johnson, Hawken, and Shapley, 2004). Then, the information is sent to layer 4B and 2/3. Especially interesting is layer 2/3 because it is the output of V1 to higher visual areas such as V2. The studies of this layer structure are quite controversial because cytochrome oxidase (CO) blobs have been observed in it (Wong-Riley, 1979; Horton and Hubel, 1981). Many studies pointed out that CO blobs contain color information and are the input of the V2 thin stripe and that interblobs contain form information and are the input of pale stripe in V2 (Lu and Rose, 2007), see review in (Sincich and Horton, 2005), but other studies did not find a correlation between the functional properties and CO blobs and interblobs (Levitt, Kiper, and Movshon, 1994; Leventhal et al., 1995; Gegenfurtner, Kiper, and Fenstemaker, 1996;

Friedman, Zhou, and von der Heydt, 2003). Anyway, similarly to layer $4C\beta$, layer 2/3 is composed by SO and DO simple cells and complex cells. The main difference is that layer 2/3 cells have orientation selectivity (Ringach, Shapley, and Hawken, 2002; Johnson, Hawken, and Shapley, 2008) and that horizontal connections in layer 2/3 link preferentially neurons of similar orientation preference (Malach et al., 1993). Thus, layer $4C\beta$ non-oriented neurons serve as input of layer 2/3 oriented ones.

4.1.5 Computational models

Theoretical and computational models can improve our understanding on the HVS. Since their aim is to reproduce what (and/or how) the system does (and/or is), when a model works, it could suggest the components and how they are assembled in the biological architecture. In fact, these models do not necessarily reveal how the HVS works, but they suggest how the HVS could work. Such models are especially interesting when they fail, because they show when the system may not work (Field, Golden, and Hayes, 2014). Thus, theoretical and computational models help to predict the answer to unresolved questions.

For example, several theoretical and computational models have shown that complex cells can be modeled as a pool of simple cells (Hubel and Wiesel, 1962; Van Kleef, Cloherty, and Ibbotson, 2010), see review in (Martinez and Alonso, 2003). These models do not ensure that complex cells work as the authors modeled, but it is a strong suggestion because the modeled architecture reproduces some of their behaviors. Several architectures that link visual functions and physiology have been proposed (Li, 1998; Li, 1999; Courtney, Finkel, and Bachsbaum, 1995; Serre et al., 2007; Otazu, Parraga, and Vanrell, 2010; Foster, 2011; Penacchio, Otazu, and Dempere-Marco, 2013; Gao et al., 2015; Chariker, Shapley, and Young, 2016; Angelucci et al., 2017; Akbarinia and Parraga, 2018; Martinez-Cañada, Morillas, and Pelayo, 2018). Some of these models propose that SO and DO cells are the main ingredients for edge detection and color constancy (Yang et al., 2013; Gao et al., 2015) and that near- and far-surrounds also play an important role in these tasks (Akbarinia and Parraga, 2016; Akbarinia and Parraga, 2018). In particular, one of them proposed that type I SO and hypothetical DO cells are the ones responsible for color constancy (Gao et al., 2015). Other models are more biologically plausible but they still reproduce psychophysical results on contour integration and texture segmentation (Li, 1998; Li, 1999). Since the HVS can be considered as a unique system that performs several tasks, a model similar to the one by Li (1999) showed that it also reproduces psychophysical data on brightness induction (Penacchio, Otazu, and Dempere-Marco, 2013). These models are mainly defined by *excitatory-inhibitory networks*, which model separately the inhibitory and excitatory neurons (Wilson and Cowan, 1972). In these recurrent dynamic systems the activity of the inhibitory neurons depends on the activity of the excitatory ones, and this in turn depends on the inhibitory neurons' activity. Thus, in this kind of systems oscillations arise (Dayan and Abbott, 2001). In Section 3.2.7 we studied the temporal evolution of Penacchio et al.'s architecture (2013) when we present flashed stimuli to study color induction. We concluded that the architecture reproduces the lateral connections present in layer 2/3 because, for uniform surround, the model results were similar to the ones of psychophysics (compare Figures 3.5 and 3.7a).

Other models do not reproduce psychophysical data, but reproduce visual functions observed in electrophysiological recordings (Chariker, Shapley, and Young, 2016; Angelucci et al., 2017; Martinez-Cañada, Morillas, and Pelayo, 2018). Several computational architectures were used to study the orientation selectivity in V1

from LGN input (Ringach, Hawken, and Shapley, 1997; Sompolinsky and Shapley, 1997; McLaughlin et al., 2000; Shapley, Hawken, and Ringach, 2003; Xing et al., 2011). They concluded that both the feedforward and feedback connections are important for orientation selectivity. In particular, they point out that suppressive feedback connections from the same area sharpen the orientation tuning of V1 neurons (Sompolinsky and Shapley, 1997; McLaughlin et al., 2000; Xing et al., 2011), and that this sharpening, in output layers (layers 2/3, 4B, 5 or 6), changes with time (Ringach, Hawken, and Shapley, 1997).

Only few models focused on color processing have been published (De Valois and De Valois, 1993; Billock, 1995; Momiji et al., 2006; Momiji et al., 2007; Martinez-Cañada, Morillas, and Pelayo, 2017; Martinez-Cañada, Morillas, and Pelayo, 2018). Some of them are focused on the color processing in the retina (Momiji et al., 2006; Momiji et al., 2007; Martinez-Cañada, Morillas, and Pelayo, 2017), one models SO cells in cortical area (Billock, 1995) and the rest are multi-stage architectures (De Valois and De Valois, 1993; Martinez-Cañada, Morillas, and Pelayo, 2018). Recently, Martinez-Cañadas et al. (2018) published an extensive work where they provide a biologically plausible framework of the parvocellular pathway from the retina to V1 layer 4C β . Based on physiological and anatomical studies and a previous model of the retina (Martinez-Cañada, Morillas, and Pelayo, 2017), they modeled LGN and V1 neurons, considering the SO type I cell in LGN and both SO type II and DO simple cells in V1. To test their architecture, the authors used several visual stimuli such as light-flashes, spatially uniform squares and gratings.

Similarly to Martinez-Cañada et al. (2018), in this chapter, we provide a new firing-rate architecture of the parvocellular pathway. In this work, we have focused on the parvocellular pathway in V1 because it is the most well-understood chromatic pathway. Thus, we implemented a multilayer architecture composed by V1 layers 4C β and 2/3. Our model considers their RFs and their lateral connections. We tested our architecture using standard visual stimuli from electrophysiological recordings such as drifting gratings varying the spatial and temporal frequency, orientation and grating's size.

4.2 Methods

The proposed architecture models two layers (layers 4C β and 2/3) of the parvocellular pathway in V1. It is based on an excitatory-inhibitory network, where we have modeled both excitatory and inhibitory populations that interact between them. The model is inspired by Li's (1999) and Penacchio et al's (2013) architectures. The visual input I is decomposed by the RFs into several scales ($s = 1, 2, \dots, n_s$), orientations ($\theta = 0, \frac{\pi}{n_\theta}, \dots, \pi$) and polarities ($\phi = 1, 2, \dots, n_\phi$). The subindexes $is\theta\phi$ indicate that the neuron at the i th retinotopic position responds best to the spatial frequency of scale s , orientation θ and polarity ϕ . The provided architecture is ruled by a general equation (see Equation 4.1).

$$\begin{cases} \dot{x}_{is\theta\phi} = & -\alpha_x x_{is\theta\phi} - g_y(y_{is\theta\phi}) \\ & - \sum_{\Delta\theta} \psi(\Delta\theta) g_y(y_{is\theta+\Delta\theta\phi}) + J_o g_x(x_{is\theta\phi}) \\ & + \sum_{j \neq i, \theta'} J_{[is\theta\phi, js\theta'\phi]} g_x(x_{js\theta'\phi}) + I_{is\theta\phi} + I_o, \\ \dot{y}_{is\theta\phi} = & -\alpha_y y_{is\theta\phi} + g_x(x_{is\theta\phi}) + \sum_{j \neq i, \theta'} W_{[is\theta\phi, js\theta'\phi]} g_x(x_{js\theta'\phi}) + I_c. \end{cases} \quad (4.1)$$

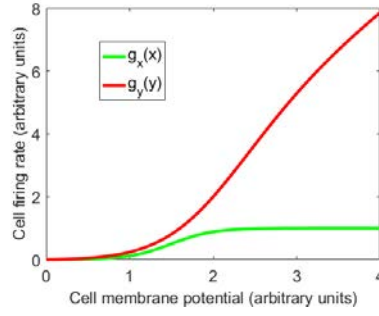


FIGURE 4.4: The membrane potentials of simple cells ($\gamma = 1$) are transformed to firing rate by the functions $g_x(x)$ (for excitatory neurons) and $g_y(y)$ (for inhibitory neurons). Similarly to Li (1999) and Penacchio et al. (2013), both functions are positive non-linear and non-decreasing. The maximum firing rate for excitatory simple neurons is $g_x(x) = 1$ and $g_y(y)$ has not maximum.

where $x_{is\theta\phi}$ is the membrane potential of the excitatory neuron and $y_{is\theta\phi}$ is the membrane potential of the inhibitory neuron at the same retinotopic position and spatial frequency, orientation and polarity preferences. The membrane potentials are transformed to firing rate by functions g_x and g_y for excitatory and inhibitory neurons, respectively (see Figure 4.4). The firing rate function for excitatory neurons is defined by $g_x(x) = (0.5\gamma)(\tanh((2/\gamma)(x - (1.5\gamma))) + 1)$ and the one for inhibitory neurons is $g_y(y) = 0.5(\text{sign}(y) + 1)y(1 + \tanh((y - (2 * \gamma))/\gamma))$, where $\gamma = 1$ when the neuron is a simple cell and $\gamma = 10$ when it is a complex cell. This γ parameter models the higher spontaneous firing rate activity of complex cells (Ringach, Shapley, and Hawken, 2002). Similarly to Li (1999) and Penacchio et al. (2013), both firing rate functions are non-linear and non-decreasing. The decay constants are $\alpha_x = 1$ and $\alpha_y = 2$, the function $\psi(y)$ models the divisive normalization defined by Carandini and Heeger (2012). Similarly to Penacchio et al. (2013), we defined it as $\psi(\Delta\theta) = \cos(\Delta\theta)^6$. J and W model the lateral connections of excitatory and inhibitory neurons, respectively, being J_0 the self-excitatory connection ($J_0 = 0.8$). I_c and I_0 model the background neural noise, where $I_c = 1.0\gamma + I_{noise}\gamma$ and $I_0 = 0.85\gamma + I_{norm} + I_{noise}\gamma$. The spatial white noise is modeled by $I_{noise} = N(\bar{x}; \sigma_t, \sigma_x) = N(0; 0.1, 0.1)$ (Li, 1999) and I_{norm} is defined in Equation 4.2, where $S_i = \{j | d(i, j) \leq 2\}$, $d(i, j)$ is the Euclidean distance between the i th and the j th neurons, $\sigma_f = FWHM/2.355$ and $FWHM = 5$ (in distance units).

$$I_{norm}(is\theta\phi) = -2 \left(\frac{\sum_{j \in S_i} f(i, j) g_x(x_{js\theta\phi})}{\sum_{j \in S_i} f(i, j)} \right), \text{ with} \quad (4.2)$$

$$f(i, j) = e^{-\frac{d(i, j)^2}{2\sigma_f^2}}$$

We have divided the section according to the two different layers and the components we have modeled, detailing the differences with respect to the architecture's general equation 4.1. In Figure 4.5, we can observe an illustrative general structure of the provided architecture.

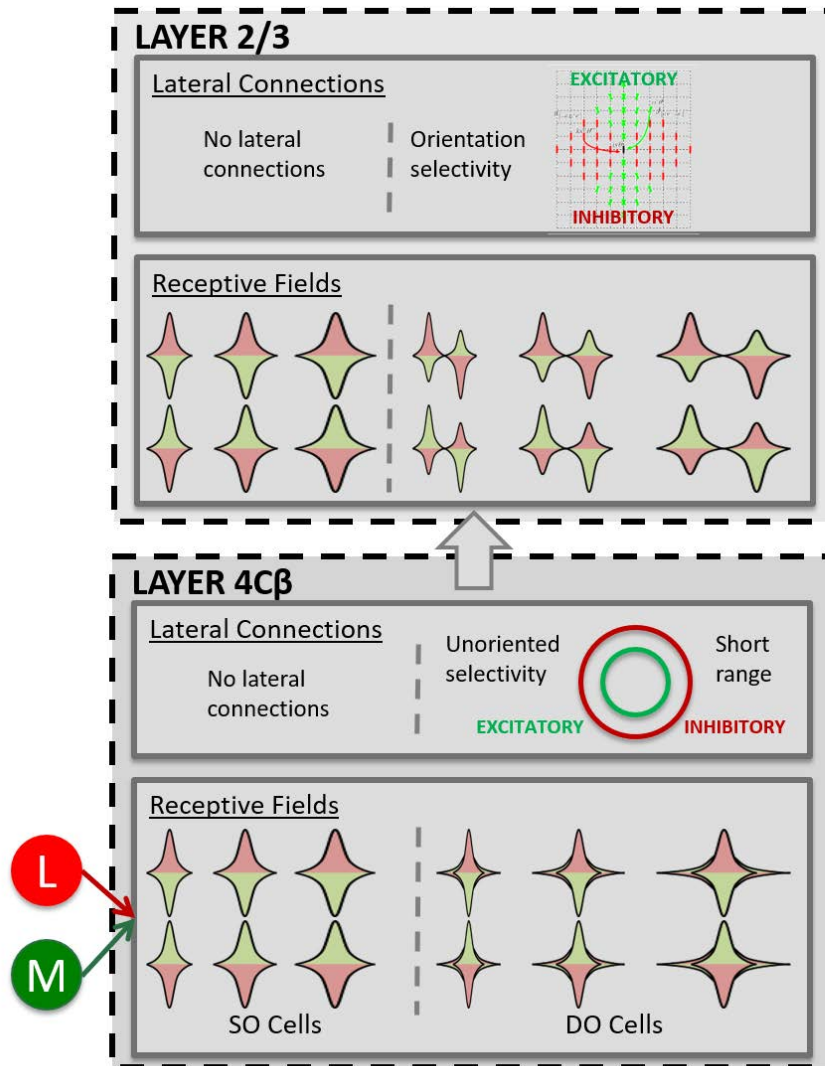


FIGURE 4.5: An illustrative scheme of the provided architecture. For sake of simplicity, here we only show the simple cells. The architecture considers two different layers of the V1 parvocellular pathway (layers 4C β and 2/3). The information in V1 arrives to layer 4C β , where SO and DO cells lack orientation selectivity. Lateral connections between DO cells only considers the physical distance between neighboring neurons and the model predicts that SO cells lack lateral connections. Then, the information is sent to layer 2/3 where DO cells are orientation selective and their lateral connections connect near neurons that have similar orientation preference (Malach et al., 1993). The layer 2/3 lateral connections scheme is adapted from (Pencchio, Otazu, and Dempere-Marco, 2013).

4.2.1 Layer 4C β

Although there are some orientation-selective cells, Color (SO cells) and Color-Lum (both DO and complex) neurons of layer 4C β lack orientation-selectivity (Blasdel and Fitzpatrick, 1984; Ringach, Shapley, and Hawken, 2002; Hubel and Wiesel, 2004). Moreover, this layer is mainly composed by simple cells instead of complex ones, but we cannot consider them non-existent (Ringach, Shapley, and Hawken, 2002). In the computational architecture, according to their properties, all the different cells obey

different equations (see below).

Simple cells

When the parvocellular pathway is activated, in layer $4C\beta$ of V1 two types of simple cells respond: SO and DO cells. As stated before, they respond to different stimuli (SO cells respond to large areas of uniform chromaticity and DO cells respond to chromatic and luminance borders). Thus, their RFs are completely different:

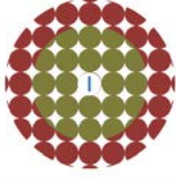
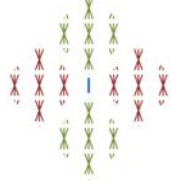
Layer	Simple		Complex
	Single-Opponent (SO)	Double-Opponent (DO)	Double-Opponent (DO)
$4C\beta$?		?
2/3	?		?

FIGURE 4.6: The cells that interact through the lateral connections depend on the cells' type and the layer. Up to our knowledge, lateral connections between SO cells have not been described, thus, we have modeled them and we have not. Then, we have compared both results in order to predict whether these connections are present between SO cells. Similarly to Li (Li, 1999) and Penacchio et al. (2013), the lateral interactions between neighboring cells depend on the cells' properties and their distance. In layer $4C\beta$, since the neurons lack orientation selectivity, these interactions only depend on the physical distance. In layer 2/3, the interactions depend on both the physical distance and the orientation preference instead. From observations published in the literature, we have assumed that complex cells lack lateral connections (see Section 4.2.1). In this figure, both sizes and ratios of the lateral connections only have an illustrative purpose. The colors indicate whether the connections are excitatory (J term of Equation 4.1, green color) or inhibitory (W term of the equation, red color) and the shape indicates the orientation selectivity. Circles indicate that the lateral connections do not depend on the orientation preference of the target neuron (indicated in blue) w.r.t. the neighbors' orientation preference. The crossed lines indicate that the lateral connections between the target (in blue) and its neighbors also depend on the orientation preference: Neurons of similar orientation preference (the same one with a certain bandwidth) interact. For illustrative purpose, the DO cell of layer 2/3 has a vertical orientation preference (vertical blue line) and interacts with neighbors that have similar orientation preferences (vertical and almost vertical red and green lines).

Single-opponent cells In layer $4C\beta$, these cells are of type II (see Figure 4.3) and are modeled as the difference of two Gaussians, one that responds to L-cones and another one that responds to M-cones (Johnson, Hawken, and Shapley, 2004; Solomon and Lennie, 2007). For the sake of simplicity and to reduce the computational cost, the architecture only considers the L-ON and M-OFF SO cells (two different polarities L-ON-center/M-OFF-surround and M-OFF-center/L-ON-surround). Thus, the RFs respond to L-cone increments and M-cone decrements. The size of the RF varies according to the different spatial frequencies. Although the RF's sizes should range from 0.1 to 1 *deg* of visual angles (Hubel and Wiesel, 1965; Schiller, Finlay, and Volman, 1976; Serre and Riesenhuber, 2004), due to computational constraints, we have reduced the biggest RF size to 0.6 visual angles. We have defined 6 different scales ranging from 0.1 to 0.6 *deg* of visual angles with a scale increment of 0.1 *deg*. Type II SO cells do not have orientation selectivity and we have not modeled lateral connections between them (see the reason in Section 4.3 and a schematic of lateral connections in Figure 4.6). Thus, the excitatory-inhibitory network of these cells do not have the lateral connections terms ($J = 0$ and $W = 0$).

Double-opponent cells In layer $4C\beta$, these cells lack orientation selectivity (Johnson, Hawken, and Shapley, 2008). To model them, we have used the hypothetical DO cells (Shapley and Hawken, 2002; Conway and Livingstone, 2006; Johnson, Hawken, and Shapley, 2008). The activation of these cells is given by two type II RFs of different sizes which overlap (see Figure 4.3). One of these type II cells is an L-ON-center/M-OFF-surround and the other one is a M-OFF-center/L-ON-surround. Again, for computational constraints, we have only modeled the L-ON-center/M-OFF-surround neurons, but the L-OFF/M-ON also exist. The modeled neurons have two different polarities (when the L-ON-center/M-OFF-surround RF is bigger than the M-OFF-center/L-ON-surround RF and the inverse). Since these neurons lack orientation selectivity, the modeled lateral connections link neurons that have the same spatial frequency preference and the same polarity preference. In particular, lateral connections in this layer are short range (Binzegger, Douglas, and Martin, 2004; Chisum and Fitzpatrick, 2004; Hirsch and Martinez, 2006; Binzegger, Douglas, and Martin, 2009; Antolík and Bednar, 2011) and inhibitory connections (W) are larger than excitatory (J) ones (Antolík and Bednar, 2011). The strength of the lateral connections between one neuron and its neighbors depends on their physical distance, according to the Gaussian function 4.3, where $\sigma_x = 0.5$, $\sigma_y = 1.5$, $d(i, j)$ is the Euclidean distance between the neighboring cells and z is a factor to normalize the lateral connections area according to Li (1999) ($z_x = 6.88$ and $z_y = 3.52$) (see summary of the lateral connections of the different components in Figure 4.6).

$$l(x_{is\theta\phi}, x_{js\theta\phi}) = z_x \frac{e^{-\frac{d(i,j)^2}{2\sigma_x^2}}}{\sum_{\forall j} e^{-\frac{d(i,j)^2}{2\sigma_x^2}}} \quad (4.3)$$

Complex cells

Complex cells respond equally to both ON and OFF light, are selective to one orientation but respond to all (Ringach, Shapley, and Hawken, 2002) and are usually modeled as a pool of simple cells. Thus, we have modeled them as a pool of simple cells of different orientations and polarities. Pooled simple cells are weighted according to both their physical distance to the complex cell ($\sigma = 2$) and their orientation preference w.r.t the orientation preference of the complex cell using Gaussian

functions ($\sigma = 0.41/(\sqrt{2 \log \sqrt{2}})$). Complex cells can be classified as DO cells because they respond to both luminance and chromatic stimuli, in fact, they are usually classified as Lum or Color-Lum neurons (Johnson, Hawken, and Shapley, 2001; Johnson, Hawken, and Shapley, 2004; Shapley, Hawken, and Johnson, 2014). Thus, in this architecture, we have only modeled complex cells that pool DO simple cells. Yeh et al. (2009) used sparse noise and Hartley subspace stimuli to study the RFs of both simple and complex neurons in layers 2/3, 4C and 5/6. It is considered that sparse noise does not activate lateral connections and Hartley subspace stimuli do. Regarding layer 4C and 2/3 results, they observed that there is interlaminar difference for simple cells (high Receptive Field Similarity -RFS- in layer 4C and low RFS in layer 2/3). The higher the RFS, the more similar the RFs when both sparse noise and Hartley subspace stimuli are used. They concluded that this difference might be explained by the activation (using the Hartley subspace stimuli) or no activation (using sparse noise) of lateral connections in layer 2/3. Moreover, they observed that the RFS for complex cells was not significantly different between both layers. Although it is highly speculative, the similarity of RFS in both layers could be due to either the lack of lateral connections between complex cells or the similarity of these connections in both layers. Considering that complex cells have an orientation preference in layer 2/3 and do not in layer 4C and that lateral connections link neighbors with similar orientation preference (Malach et al., 1993), it does not seem feasible that lateral connections between complex cells are similar in both 4C and 2/3 layers. For this reason, we have modeled complex cells without lateral connections.

4.2.2 Layer 2/3

The red-green chromatic information from layer 4C β is projected to layer 2/3. This layer is considered the output of V1 to higher visual areas such as V2. Regarding the parvocellular pathway, the input of this layer is layer 4C β , thus, orientation selectivity of layer 2/3 cells arises from the output of layer 4C β non-oriented cells (Ringach, Shapley, and Hawken, 2002; Xing et al., 2011).

Similarly to layer 4C β , this layer is also composed by simple (both SO and DO cells) and complex cells, although the number (or the density) of complex cells in this layer is higher than in layer 4C β (Ringach, Shapley, and Hawken, 2002).

Simple cells

Simple cells in layer 2/3 are either SO or DO cells. The main difference with respect to layer 4C β is that DO cells are orientation selective.

Single-opponent cells In layer 2/3, these cells are very similar to the ones of layer 4C β . They also lack orientation selectivity and they are of type II. We have used the same filters as for layer 4C β SO cells, but instead of using the visual input, they use the activity of layer 4C β excitatory cells. Thus, the activity of layer 2/3 SO cells comes from the activity of layer 4C β SO cells. In this case, the term $I_{is\theta\phi}$ is the activity of excitatory SO cells in layer 4C β and they also lack lateral connections.

Double-opponent cells These cells are very different to layer 4C β DO cells because, in this layer, they have an orientation preference. DO cells are usually modeled by Gabor filters (Daugman, 1985), but in this architecture we have only considered odd- and mixed-symmetric filters (even-symmetric filters have been removed) (Girard and Morrone, 1995; Shapley, Hawken, and Johnson, 2014). The input of these

neurons is the activity of excitatory DO cells in layer $4C\beta$. Layer $4C\beta$ DO cells are weighted according to their polarity preference w.r.t. the polarity preference of layer 2/3 DO cell. The lateral connections between these neurons depend on both the physical distance and the orientation preference of the neighboring cells (Malach et al., 1993). To model these connections, we have used the same implementation as Penacchio et al. (2013) (see Figure 4.6 and Equation 4.4), but we did not introduce a scale interaction because it was minimal.

$$\begin{aligned}
 J_{[is\theta\phi, js\theta'\phi]} &= \begin{cases} 0.126e^{-(\beta/d)^2 - 2(\beta/d)^7 - d^2/90} & \text{if } (0 < d \leq 10 \text{ and } \beta < \pi/2.69) \\ & \text{or } [(0 < d \leq 10 \text{ and } \beta < \pi/1.1) \\ & \text{and } |\theta_1| < \pi/5.9 \text{ and } |\theta_1| < \pi/5.9] \\ 0 & \text{otherwise} \end{cases} \\
 W_{[is\theta\phi, js\theta'\phi]} &= \begin{cases} 0 & \text{if } d = 0 \text{ or } d \geq 10 \text{ or } \beta < \pi/1.1 \\ & \text{or } |\Delta\theta| \geq \pi/3 \text{ or } |\theta_1| < \pi/11.999 \\ 0.14(1 - e^{-0.4(\beta/d)^{1.5}})e^{-(\Delta\theta/(\pi/4))^{1.5}} & \text{otherwise} \end{cases}
 \end{aligned} \tag{4.4}$$

Complex cells

As stated before, complex cells can be modeled as a pool of DO simple cells. An open question is whether complex cells of layer 2/3 receive an input of complex cells of layer $4C\beta$. Up to our knowledge, there are no studies in this direction. Thus, we have modeled the complex cells neurons of layer 2/3 as a pooling of DO simple cells neurons of the same layer with a small contribution of layer $4C\beta$ complex cells. Thus, the activity of complex cells in layer 2/3 is driven by DO simple cells of the same layer and complex cells of the previous one (layer $4C\beta$). For the same reason as in layer $4C\beta$, we have assumed that these cells do not have lateral connections between them.

Although the output of the architecture could be considered the excitatory activity of DO cells in layer 2/3 (similarly to the HVS), it does not have a single output, because it considers several types of neurons and several connectivities (feedforward and lateral connections). Thus, the output varies from one run to another depending on the properties to analyze.

To test our architecture, similarly to the works coauthored by Hawken and Shapley (Johnson, Hawken, and Shapley, 2001; Ringach, Shapley, and Hawken, 2002; Johnson, Hawken, and Shapley, 2008), we have defined a set of drifting gratings that allow us to study the different cells' properties (see Figure 4.7). Since we want to study the properties of parvocellular pathway in V1, the drifting gratings are sinusoidal and equiluminant. They are produced by modulating sinusoidally in antiphase the L- and M-cones activation (L and $M \in [0, 1]$). Thus, when L-cone activation is maximal ($L = 1$), M-cone activation is minimal ($M = 0$). The stimuli depend on the temporal frequency (the speed of the drift), the spatial frequency of the sinusoid (how thick are the stripes), the grating's area (how many periods are inside the circle) and the orientation. We have defined a set of values for each of those parameters and we have measured the activity of a cell for all of them. The cell preference is determined by the stimulus' parameters that produce the highest cell response (*optimal stimulus*). Once we find the preference of the cell, we systematically vary all the stimuli parameters in order to study the cells' properties. For the

sake of simplicity, we have always placed the grating in the middle of the stimulus and we have measured the activity of the cells whose RF is centered in the stimulus. We have selected the $x_{is\theta\phi}$ neuron that responds best to the stimuli.

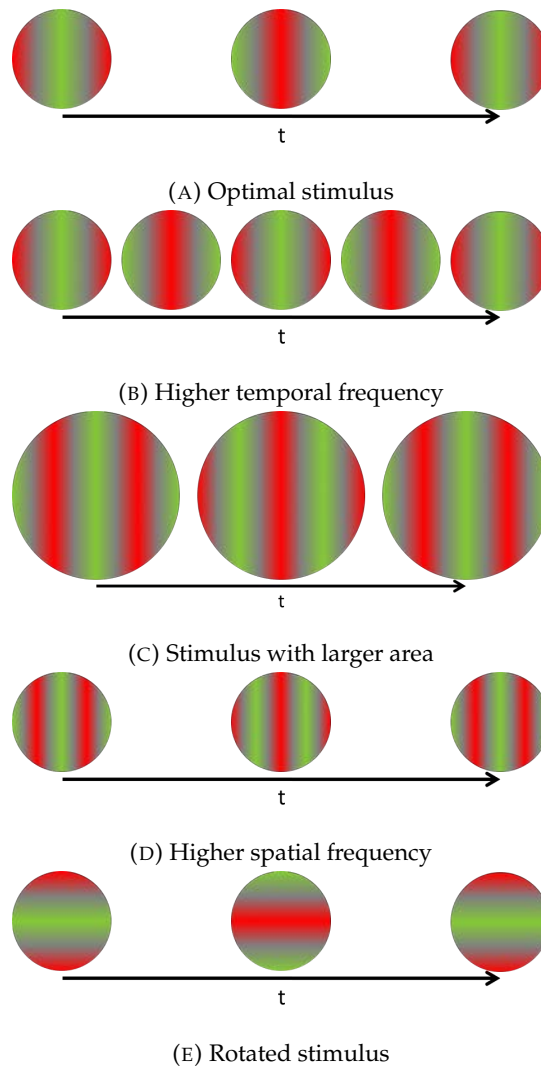


FIGURE 4.7: Sinusoidal equiluminant drifting gratings are used to study cells' properties. First, we have found the optimal stimulus, *i.e.*, the parameters (temporal and spatial frequencies, area and orientation) of the drifting grating that make the cell to respond best (A). Then, we have varied several stimulus' parameters such as the temporal frequency (B), the grating area (C), spatial frequency (D), orientation (E) to study the cells' response (Ringach, Shapley, and Hawken, 2002). The gratings are presented inside a gray square and the L-M grating is produced by modulating the L- (red color) and M-cones (green color) activation in antiphase.

To study the orientation selectivity of the cells, we have calculated the *circular variance* (CV) and the *bandwidth* which both together help to assess the orientation tuning of a cell (Johnson, Hawken, and Shapley, 2008). CV measures the response to the preferred orientation with respect to all orientations. When CV is close to 0, it means that the cell has a high orientation selectivity, whereas a CV close to 1 means that it has a broad orientation selectivity (Mardia, 1972; Ringach, Shapley, and Hawken, 2002; Johnson, Hawken, and Shapley, 2008). The bandwidth measure

shows the degrees in which the cell is selective to (standard deviation of the cell's response to different orientations). Therefore, the higher the bandwidth the less orientation selective is the cell.

Another interesting measure for orientation selectivity is the ratio between the orthogonal-to-preferred orientation and the preferred orientation (O/P) (Ringach, Shapley, and Hawken, 2002). When the cell responds similarly to the preferred orientation and to the orthogonal one, the ratio is close to 1. When the responses are completely different, its value is close to 0.

It has been observed that, when the stimulus is high contrast, lateral connections act as inhibitory, while when the stimulus is low contrast, they act as facilitatory (Ichida et al., 2007; Shushruth et al., 2009; Angelucci and Shushruth, 2014). To test the lateral connections of layer 2/3 DO cells, we have varied the grating's area in order to cover the lateral connections' region. Thus, a very small grating does not fill the cRF, but as the grating's area increases the cRF is filled and the lateral connections start to be activated.

Since, up to our knowledge, there are no studies that describe lateral connections between SO cells, we have run the model activating and deactivating them. We have compared both results in order to predict whether these connections could be present between these cells. SO cells are non-orientation selective cells, thus, similarly to layer 4C β DO cells, we have modeled their lateral connections based on the physical distance between neighboring neurons, being the inhibitory lateral connections larger than the excitatory ones (Antolík and Bednar, 2011). Using the same methodology as described above, we have studied the spatial frequency selectivity of these cells (after obtaining the optimal stimulus, the spatial frequency of the drifting gratings has been varied).

4.3 Results

This section is divided according to the studied properties. We have started studying the temporal frequency, and then we have also studied the grating area, the spatial frequency and the orientation. Moreover, we observe that the modeled lateral connections participate actively in the center-surround modulation.

4.3.1 Temporal frequency

To study the temporal properties of the different architecture's components, we vary the temporal frequency (f) of the drifting grating ($f \in [2, 4, 8, 16] \text{ Hz}$; see an illustrative example in Figure 4.7b). We observe that, in general, the modeled cells prefer low temporal frequencies such as $f = 2$ or $f = 4 \text{ Hz}$ instead of higher ones such as $f = 8$ or $f = 16 \text{ Hz}$ (see Figure 4.8).

4.3.2 Grating area

The stimulus is a gray square with a circular region in the center. The drifting grating is presented in this circular region of sharp edges. In this study we vary the size of the circular area (a), thus, the larger area, the more cycles of the drifting grating are displayed (see Figure 4.7c). The number of cycles of the drifting grating are ($a \in [1, 2, 5, 7, 10] \text{ cycles}$). In Figure 4.9, the results for SO cells are not shown because their distributions are completely flat. Since SO cells are low-pass and do not have lateral connections, they are insensitive to area size variations because the drifting

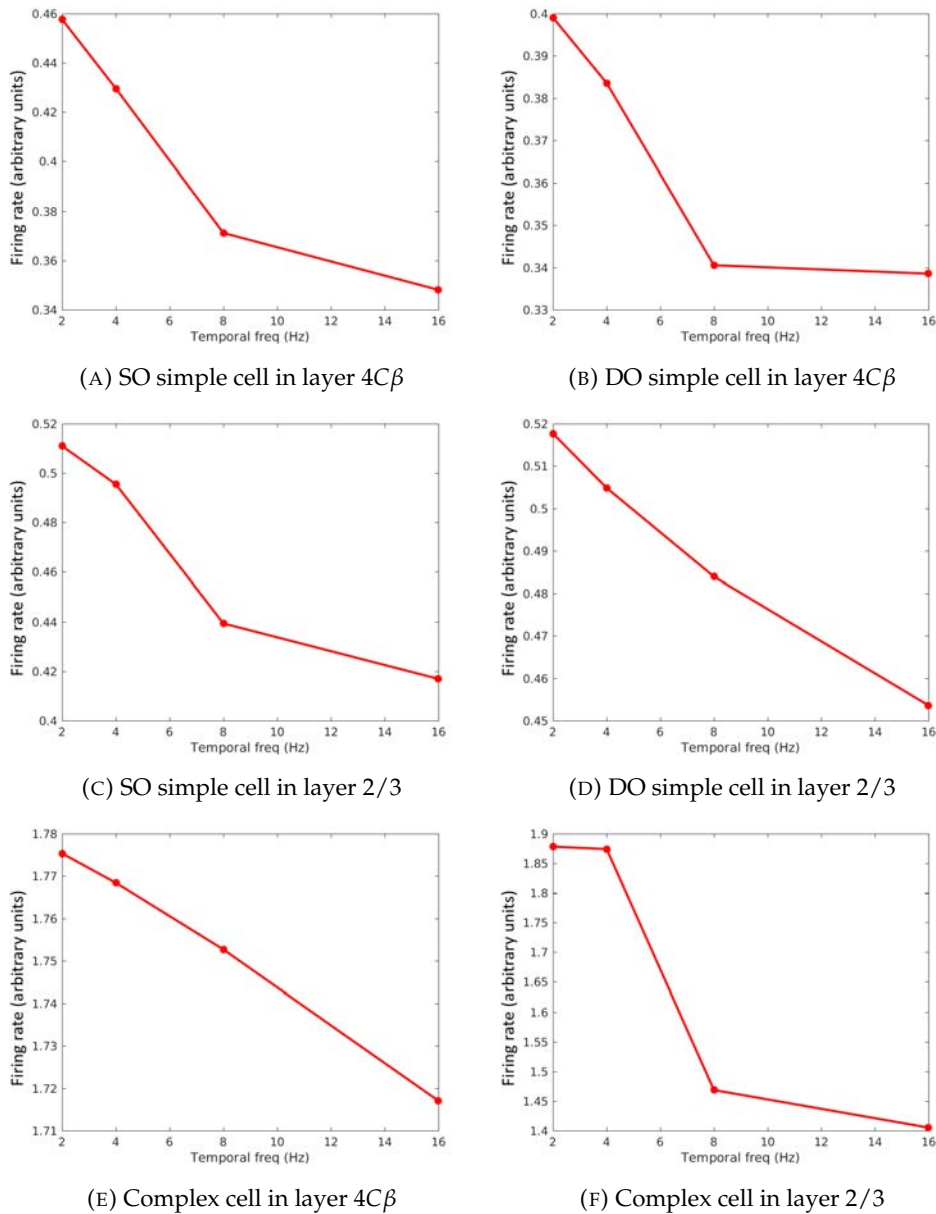


FIGURE 4.8: Study of the drifting grating's temporal frequency in different cells of the proposed architecture. The higher the temporal frequency, the faster the drift. Modeled neurons clearly respond best to slow stimuli ($f < 4$ Hz).

grating already covers their RF when $a = 1$ cycle. In contrast, we can observe that DO and complex cells have an area size preference ($a > 1$ cycles).

4.3.3 Spatial frequency

Spatial frequency selectivity is one of the major factors to distinguish between SO and DO cells. As described before, SO cells respond best to large chromatic areas and DO cells respond to both luminance and chromatic borders. Here, we vary the spatial frequency of the drifting grating while maintaining the temporal

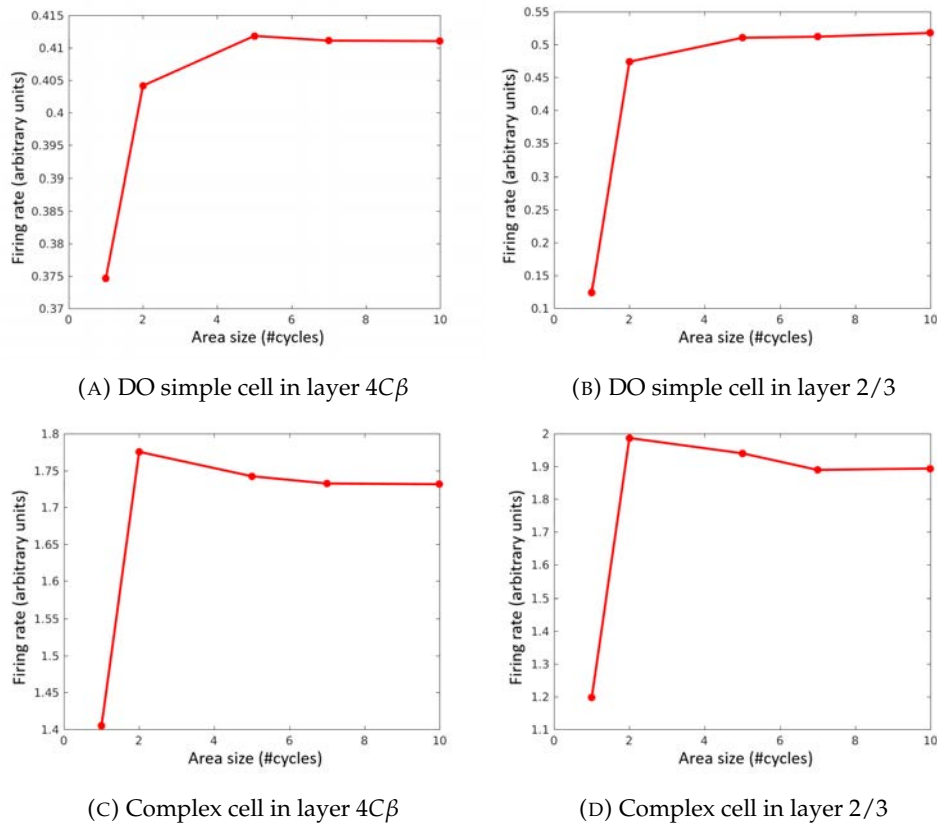


FIGURE 4.9: We vary the area of the circular region where the drifting grating is presented. Due to their low spatial frequency selectivity and their lack of lateral connections, SO cells (not shown) have a completely flat distribution, pointing out that they are insensitive to different area sizes. In contrast, DO cells' activity depends on the area of the circular region.

frequency, area size and orientation to match the optimal stimulus (see an example in Figure 4.7d). We have tested the architecture using 8 different spatial frequencies ($v \in [0.2, 0.5, 0.75, 1, 2, 3.5, 5, 10] \text{ cycles/deg}$). In Figure 4.10, we can observe that the SO cells of this architecture respond best to low spatial frequencies ($v < 1 \text{ cycles/deg}$; *i.e.*, large areas) and do not respond at all to high spatial frequencies ($v > 2 \text{ cycles/deg}$). In contrast, DO cells respond best to borders and do not respond to large chromatic areas. Similarly to DO cells, complex cells are band-pass, although they also respond to low spatial frequencies.

4.3.4 Orientation

When we vary the orientation of the drifting grating, a clear distinction between layer $4C\beta$ and layer 2/3 cells has arisen. We start from the optimal stimulus and we rotate the grating between θ_p and $\theta_p + 2\pi$, where θ_p is the preferred orientation of the cell (see Figure 4.7e). For the sake of simplicity and taking into account that the architecture does not consider motion direction, we rotate the grating from 0 to 180° in steps of 10° . In Figure 4.11, we can observe several cell responses when the drifting grating is rotated (red line). Layer $4C\beta$ and layer 2/3 SO cells distributions are almost flat, pointing out that they do not have orientation selectivity. Similarly, since complex cells in layer $4C\beta$ pool non-oriented DO neurons, they do not have

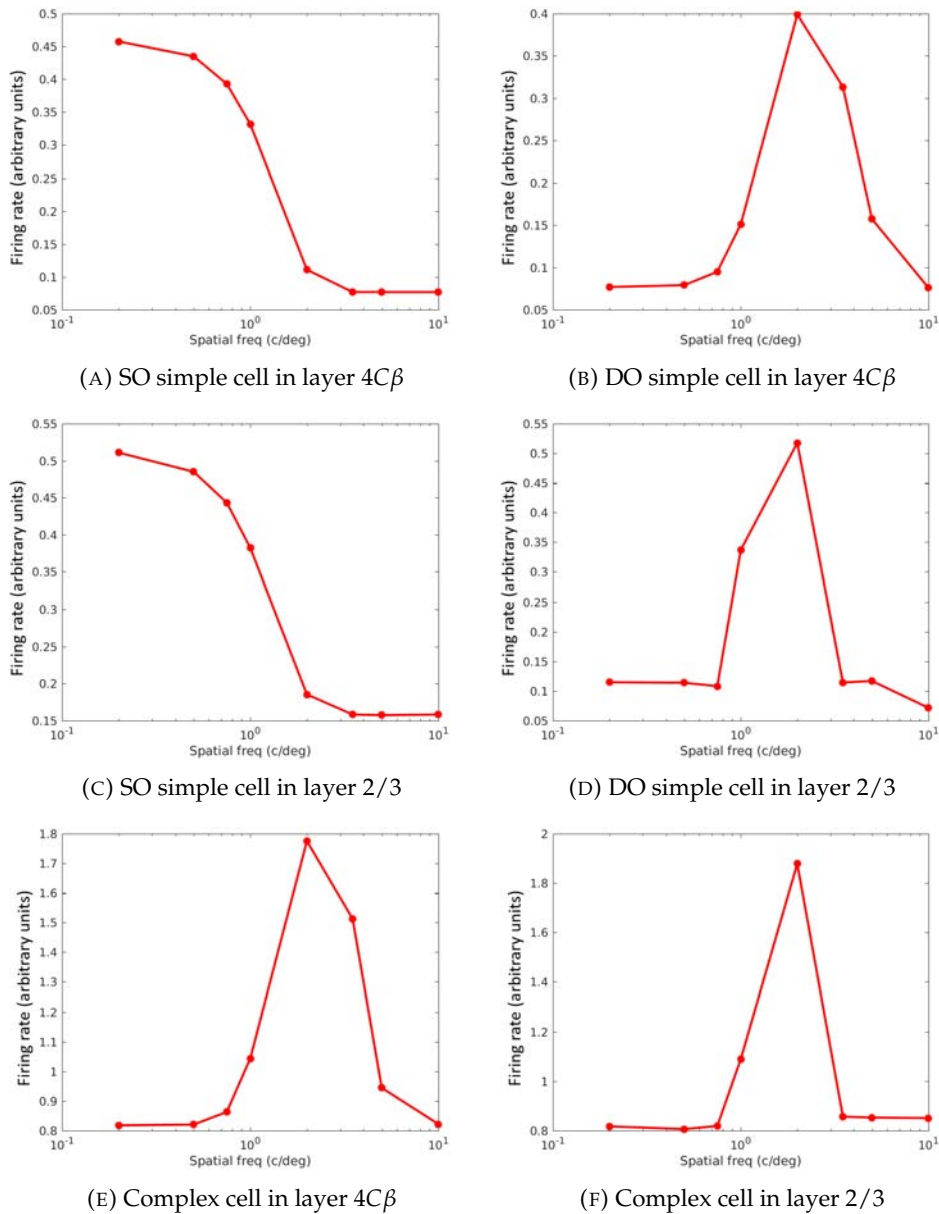


FIGURE 4.10: The abscissa shows different spatial frequencies for the drifting grating and the ordinate shows the firing rate activity (in arbitrary units) for different cells (SO, DO and complex cells) in different layers. We can observe that SO cells of this model respond best to uniform chromatic areas whereas DO and complex cells respond best to chromatic borders.

orientation selectivity neither. In contrast, layer 2/3 DO and complex cells have a high orientation selectivity. All these observations are captured in the measures: CV values are high for layer $4C\beta$ cells and layer 2/3 SO cells and low for layer 2/3 DO and complex cells; bandwidth values are around 10° in orientation selective cells. In addition, we can observe that orientation non-selective cells (layer $4C\beta$ cells and layer 2/3 SO cells) have a high O/P value, while selective ones (layer 2/3 DO simple and complex cells) have a low O/P ratio. Notice that layer 2/3 DO cells respond to a determined orientation and bandwidth and, outside this range, they do not respond at all. Layer 2/3 complex cells have a stronger response when the stimulus matches

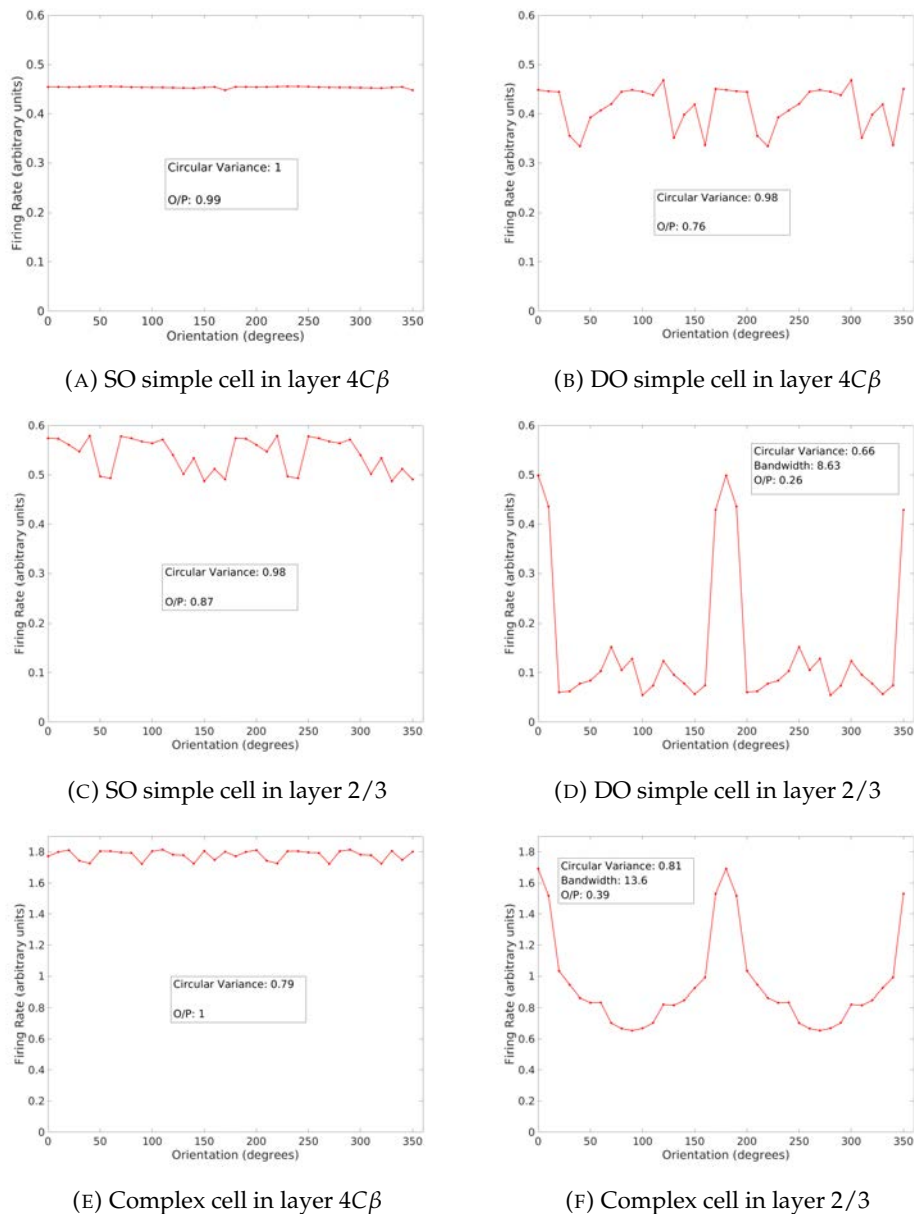


FIGURE 4.11: The x axis corresponds to the orientation of the grating (in degrees) and the y axis is the firing rate (in arbitrary units) of the neuron which is centered in the stimulus (the cell response). The bandwidth (not shown for non-oriented cells) together with circular variance (CV), help to assess the orientation tuning of the cell. When CV is high it means that the cell has a broad orientation selectivity, while a low value means that the cell has a narrow orientation selectivity. The bandwidth measures the number of degrees in which the cell is responsive to. Finally, the ratio between the orthogonal-to-preferred orientation and the preferred orientation (O/P) shows how the cell responds to the orthogonal-to-preferred orientation with respect to its preferred one. Thus, when the ratio is high (close to 1), it means that the cell responds similarly to both oriented gratings and when the ratio is low the cell's response is completely different.

their preferred orientation, but they respond to all orientations (as the stimulus is rotated, their firing rate never is close to 0).

4.3.5 Center-surround modulation

In Figure 4.12, we show the response of a layer 2/3 DO cell for a high contrast stimulus (blue line) and for a low contrast stimulus (red line). In this study, the contrast of the high contrast stimulus is 5 times higher than the contrast of the low one ($c_h = 2$ and $c_l = 0.4$, where c_h is the high contrast and c_l is the low contrast). We can observe that, as expected, the response is weaker when a low contrast stimulus is presented. When the lateral connections are activated (around $a = 5$), the high contrast response decreases (it is suppressed) but the low contrast response keeps increasing (it is facilitated). Therefore, the modeled lateral connections act as facilitatory when a low contrast stimulus is presented and act as inhibitory when a high contrast one is presented.

4.3.6 Lateral connections between SO cells

The results of SO cells in Figure 4.10 have been calculated assuming no lateral connections between these cells. When these lateral connections are activated, the results are quite different (see Figure 4.13). They show a band-pass cell for low spatial frequencies, instead of a low-pass one (see Figure 4.10).

4.4 Discussion

In Section 4.2.1, we have assumed that SO cells lack lateral connections. As stated before, the computational models are especially interesting when they fail. When these lateral connections are activated, SO cells are not low-pass, they are band-pass (see Figure 4.13). Thus, based on our results and the lack (up to our knowledge) of studies that describe the lateral connections between SO cells in V1, we assume that no lateral connections exist between these cells.

To test our architecture, we compare our results to electrophysiological studies. In particular, we have studied the spatial frequency and orientation properties of different types of neurons (both SO and DO cells) in different layers (layer $4C\beta$ and 2/3) of the parvocellular pathway in V1. In Figure 4.14 (Figure adapted from (Johnson, Hawken, and Shapley, 2001; Johnson, Hawken, and Shapley, 2008)), we can observe the response of different cells when drifting grating's spatial frequency is varied. Our results (see Figure 4.10) reproduce these electrophysiological observations: SO cells are low-pass and DO cells are band-pass. Moreover, we can observe that, similarly to our results, complex cells are also band-pass and their response to low spatial frequencies is not zero. Unfortunately, we have not found results for layer $4C\beta$ SO simple cell and simple cells in layer 2/3, but these studies point out that they are not different from the ones shown in Figure 4.14.

Comparing Figures 4.11 and 4.15 (adapted from (Johnson, Hawken, and Shapley, 2008)), we can observe that our results also reproduce electrophysiological observations in terms of orientation selectivity: layer $4C\beta$ cells are non-orientation selective and DO and complex cells in layer 2/3 are. Especially interesting is the layer $4C\beta$ DO cell (see Figure 4.15b) because, although it is a DO cell, it lacks orientation selectivity. Their RF has not been mapped, but some of their properties have been observed. In our architecture we have modeled the hypothetical RF defined by Shapley and Hawken (2002). We can observe that accepting the existence of this DO cell, both spatial frequency and orientation selectivity results can be reproduced.

Similarly to spatial frequency selectivity, layer 2/3 complex cells, although being orientation selective, respond to a broad band of orientations (see Figure 4.15d).

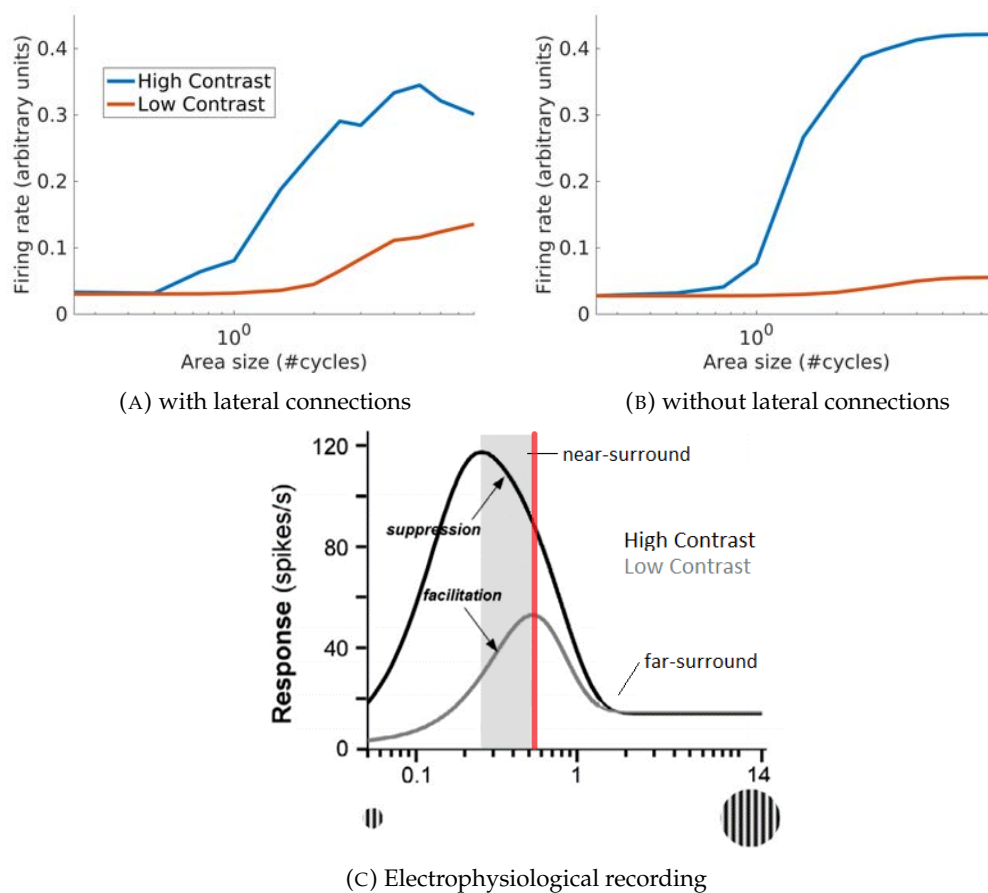


FIGURE 4.12: As the area of the grating is increased, the cRF and the lateral connections are activated. We presented both high contrast and low contrast stimuli and we studied the response of the same cell (a layer 2/3 DO cell). **(A)** We can observe that, due to the lateral connections, around $a = 5$ cycles, the response to the high contrast stimulus decreases, while the response to the low one increases. This points out that the lateral connections act as facilitatory or inhibitory depending on the stimulus contrast. **(B)** To test that the center-surround modulation is due to modeled lateral connections between layer 2/3 DO cells we cut off these connections and we studied the cell's response. We can observe that the response increases as the cRF is filled, but when it is completely filled, the response remains constant (there are not lateral connections that modulates the cell response). **(C)** Electrophysiology recordings show that the result of the lateral connections depends on the stimulus' contrast. When the stimulus is high contrast, the result is inhibitory, while it is facilitatory when the stimulus is low contrast. Far-surround always suppresses the cells' response instead. The vertical red line indicates the limit of our architecture (it models up to the near-surround). Thus, in Figures **(A, B)** we do not observe the suppression due to the far-surround (feedback connections). Figure adapted from (Nurminen and Angelucci, 2014).

Thus, these cells have a high CV but a low bandwidth. Layer 2/3 complex cells of our architecture have the same properties, they respond to all orientation, although they respond best to the one of their preference and, with respect to layer 2/3 DO cells, their CV is higher and their bandwidth is similar (Ringach, Shapley, and Hawken, 2002).

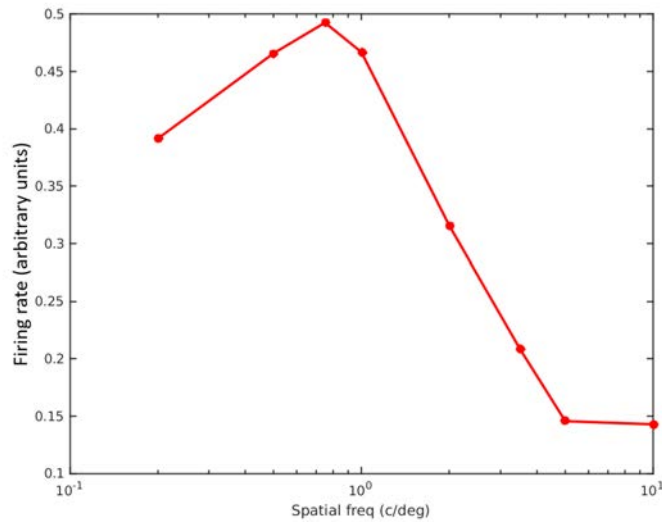


FIGURE 4.13: In the proposed architecture we assume that SO cells do not have lateral connections because if we activate them, these cells are band-pass (the model fails).

In Figure 4.12, we observed that due to the lateral connections between layer 2/3 DO cells, the cells' response to a high contrast stimulus is suppressed (for $a > 5$ cycles), while the response to a low contrast stimulus is facilitated. In several works coauthored by Angelucci (Ichida et al., 2007; Shushruth et al., 2009; Angelucci and Shushruth, 2014; Angelucci et al., 2017), the authors have observed this lateral connections' property (see Figure 4.12c, adapted from (Nurminen and Angelucci, 2014)). Moreover, they have observed that the far-surround (composed by feedback connections) always suppresses the cells' response, regardless of the stimulus' contrast (Angelucci and Shushruth, 2014; Angelucci et al., 2017). In our architecture we did not model these feedback connections, thus, the cell's response for low contrast stimulus in Figure 4.12 is not suppressed.

4.5 Conclusions

In this work, we have implemented a new firing rate neurodynamical model of the parvocellular pathway (red-green chromatic information) in V1. To do so, it considers two different layers of this cortical areal: layers $4C\beta$ (where LGN information is projected to) and 2/3 (from where the information is sent to higher visual areas such as V2). Both layers are connected through feedforward connections and each layer is modeled as a recurrent network composed by both excitatory and inhibitory cells. Layer $4C\beta$ is composed by two types of simple cells: SO and DO cells; and complex cells. As observed in electrophysiological recordings, all of them lack orientation selectivity and respond to different spatial frequencies (Johnson, Hawken, and Shapley, 2001; Ringach, Shapley, and Hawken, 2002; Johnson, Hawken, and Shapley, 2008). To model non-oriented DO simple cells we have to suppose the existence of the hypothetical DO cells, which have not been mapped but some of their properties have been observed (Shapley and Hawken, 2002). Moreover, to reproduce electrophysiological recordings we have to assume a lack of lateral connections between SO simple cells because otherwise they are not low-pass (see Figure 4.13). To reproduce their properties, complex cells have been modeled as a pool of DO simple cells.

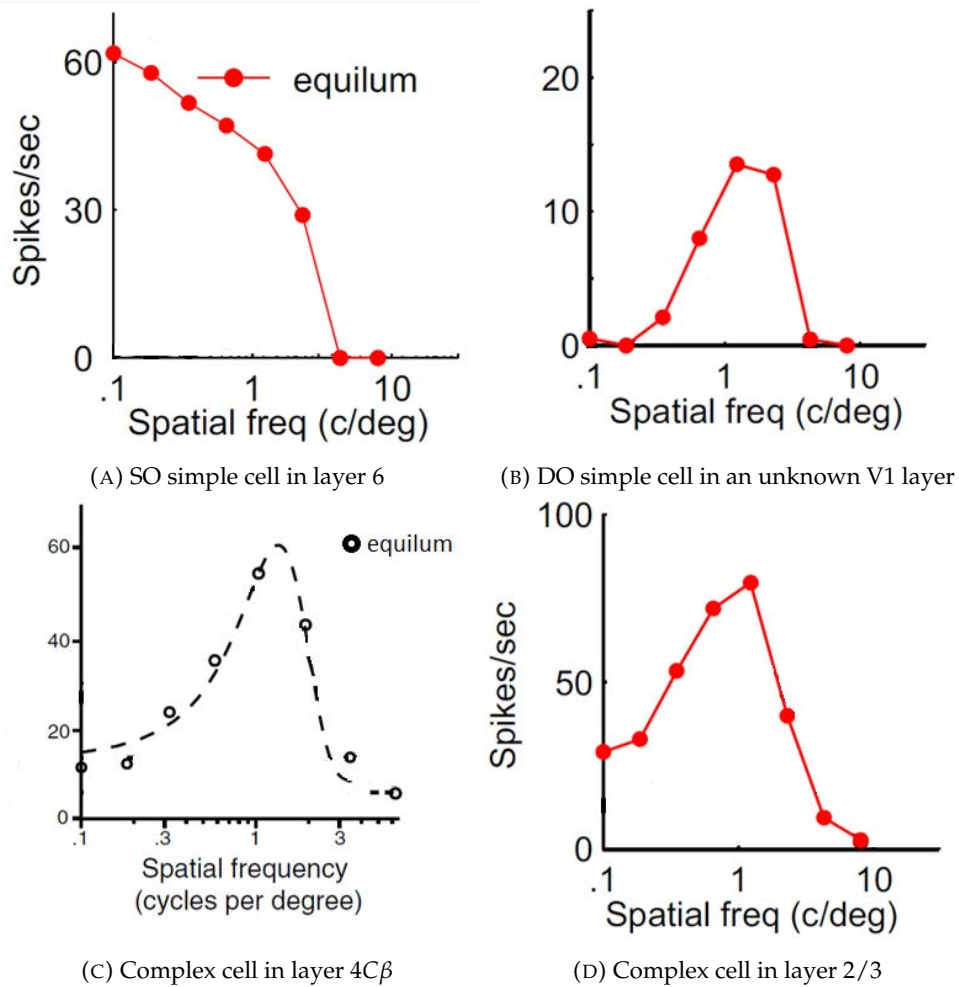


FIGURE 4.14: Several works have studied the spatial frequency properties of different cells located in different layers. Similarly to Figure 4.10, the x axis indicates the spatial frequency of the stimulus and the y axis shows the cell's response. Figures adapted from (Johnson, Hawken, and Shapley, 2001; Johnson, Hawken, and Shapley, 2008).

The cells in layer $4C\beta$ serve as input of cells in layer 2/3. In the architecture, layer 2/3 is also composed by two types of simple cells: SO and DO cells; and complex cells. Thus, the input of layer 2/3 SO and DO simple cells are layer $4C\beta$ SO and DO simple cells, respectively. In contrast, complex cells from layer 2/3 receive input from layer 2/3 DO simple cells (they pool them) and a small contribution of layer $4C\beta$ complex cells. Layer 2/3 DO cells receive input from non-orientation selective cells but they are orientation selective (see Figure 4.11). Complex cells in layer 2/3 show orientation selectivity although they respond to all orientations. To test our architecture, we have simulated electrophysiological studies (Johnson, Hawken, and Shapley, 2001; Ringach, Shapley, and Hawken, 2002; Johnson, Hawken, and Shapley, 2008) and we have reproduced the cells' response when several stimuli properties are varied.

To test the lateral connections between layer 2/3 DO cells, we have simulated the study performed by Ichida et al. (2007). We presented two different stimuli, one of high contrast and one of low contrast. We observe (see Figure 4.12) that lateral connections are mandatory to modulate the cell's response and that their result is

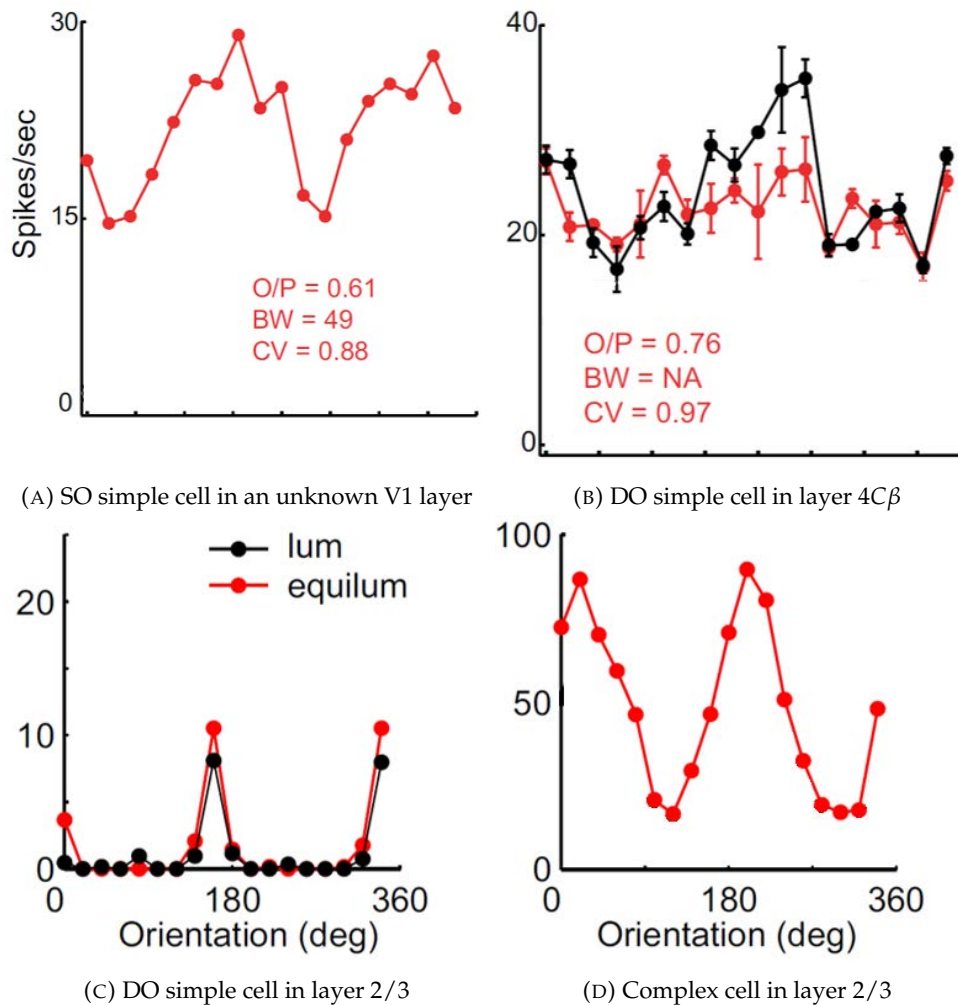


FIGURE 4.15: As well as spatial frequency, cells' orientation selectivity has been widely studied using electrophysiological recordings (Johnson, Hawken, and Shapley, 2001; Ringach, Shapley, and Hawken, 2002; Johnson, Hawken, and Shapley, 2008). Here, we show several recordings, adapted from (Johnson, Hawken, and Shapley, 2008), of different cells when the orientation of the grating varied. As stated before, SO cells and layer 4C β DO simple cells (A, B) lack orientation selectivity and layer 2/3 DO simple and complex cells do not (C-E). Thus, our results in Figure 4.11 reproduce these observations.

facilitatory for low contrast stimulus and inhibitory for high contrast stimulus. Although Ichida et al. (2007) used achromatic stimuli, other works showed that, the same is true (but reduced) for color selective cells and chromatic stimuli (Solomon, Peirce, and Lennie, 2004).

4.6 Future work

This architecture can be extended considering feedback connections which are one of the main ingredients in the HVS processing. There are several feedback connections that could be modeled: the inter-area connections (*i.e.*, feedback connections to LGN or from V2) and intra-area (*i.e.*, feedback connections in the same V1 area). Both have

to be modeled together with layer 5/6, which plays an important role in feedback functionality in V1.

Moreover, in the previous chapter, we have observed that luminance and chromatic channels (*i.e.*, magno- and parvo- or koniocellular pathways) interact in V1 and that these interactions have an important role in color perception, or at least in color induction. Although magno-parvo interactions have not the influence of magno-konio interactions, it will be interesting to include the magnocellular pathway in this architecture.

And last, but not least, this architecture could be used as saliency map estimator (Li, 2002). Especially interesting would be the study of complex cells in these tasks. Since they respond to a broad range of spatial frequencies and they respond to all orientations, regardless of stimulus polarity, they could estimate well the saliency map.

4.7 Related publications

- Brightness and colour induction through contextual influences in V1 (Otazu, Penacchio, and Cerda-Company, 2015b), *Scottish Vision Group (SVG)*, 2015.
- A multi-task neurodynamical model of lateral interactions in V1: chromatic induction (Cerda-Company and Otazu, 2016a), *European Conference on Visual Perception (ECPV)*, 2016.
- A new dynamical firing rate model of the parvocellular pathway in V1 (Cerda-Company, Otazu, and Penacchio, 2018), *Barcelona Computational, Cognitive and Systems Neuroscience (BARCCSYN)*, 2018.

Chapter 5

General Conclusions

In this chapter, we have summed up the conclusions along all the chapters of this PhD:

1. When tone-mapping operators are compared, the used criteria is fundamental.
2. Local tone-mapping operators perform best when local criteria is used and global tone-mapping operators perform best when a global one is considered.
3. There is ample room to define a tone-mapping operator that considers both local and global perceptual properties.
4. Since humans are the users of tone-mapping operators, a perceptual metric based on psychophysics should be defined for a proper and fair comparison among them.
5. Color induction depends on the inducers' chromaticities and the luminance differences between the target and the inducers.
6. Color contrast, but not color assimilation, could occur in equiluminant stimuli.
7. Color contrast, induced by flashed stimuli, depends on the flash duration.
8. When the stimulus is either equibrightness or equiluminant, no color assimilation effect occurs.
9. When luminance is varied, color induction depends on the varied element. The spatially further the varied element with respect to the target, the weaker the induced color in the target.
10. A luminance-chromatic interaction is necessary to induce color assimilation and it depends on the chromatic pathway and their polarities. This luminance-chromatic interaction could be explained by a mutual-inhibition mechanism.
11. Maybe due to natural evolution, color assimilation never occurs when the surround is green.
12. There is no computational model that reproduces color induction effects. None of the defined models consider the inducers' chromaticities and the luminance differences.
13. We defined a computational model that reproduces electrophysiological recordings in terms of spatial frequency, orientation selectivity and center-surround modulation.

14. To reproduce the electrophysiological recordings, the provided architecture has to assume the existence of the hypothetical double-opponent cells defined by (Shapley and Hawken, 2002).
15. Our computational model predicts that no lateral connections are present between single-opponent cells because otherwise it fails to reproduce electrophysiological observations.

During this PhD, several articles have been published and other ones are in preparation, but during this period of almost 3.5 years not only the articles have been important. I have also tried to acquire other "alternative" skills that I believe they will be very useful in my future academic and research life. I think that maybe the most relevant ones are: psychophysics methodology and computational modeling, but there are more which are as important such as analysis, comprehension and synthesis capabilities, oral and written communications, article writing, searching, perform a mid-term project, networking, consider alternatives, etc. I think that my PhD is not only the publications and the new concepts that I have learned, but the mosaic of all of them together with these "alternative" skills.

Appendix A

Statistical Analysis of Section 3.3

TABLE A.1: Summary of the nested ANOVA results for both luminance and brightness experiments. The first column indicates the experiment (luminance or brightness), the second one the varied element, the third the chromatic condition, the fourth the effect (between groups, within groups and the error), the fifth the degrees of freedom, the sixth the sum of squares (SS), the seventh the mean square (MS) and the last two the F and p values. These results show that, in all conditions of both experiments, color induction depends on the luminance/brightness differences

Experiment	Element	Chromatic Condition	Source	df	SS	MS	F	p
Luminance	Test ring	red-green	Luminance Cond	4	0.16	0.04	6.31	<0.001
			Subject(Luminance Cond)	43	1.10	0.03	3.96	<0.001
		green-red	Error	426	2.75	0.00		
			Luminance Cond	4	1.35	0.34	68.5	<0.001
		purple-lime	Subject(Luminance Cond)	43	1.44	0.03	6.79	<0.001
			Error	426	2.10	0.00		
	lime-purple	purple-lime	Luminance Cond	4	11.5	2.88	248	<0.001
			Subject(Luminance Cond)	44	12.0	0.27	23.5	<0.001
		lime-purple	Error	437	5.06	0.01		
			Luminance Cond	4	9.41	2.35	173	<0.001
		lime-purple	Subject(Luminance Cond)	44	10.0	0.23	16.7	<0.001
			Error	438	5.96	0.01		

Continued from previous page

Experiment	Element	Chromatic Condition	Source	<i>df</i>	<i>SS</i>	<i>MS</i>	<i>F</i>	<i>p</i>
Luminance	1 st inducer	red-green	Luminance Cond	4	0.48	0.12	34.5	<0.001
			Subject(Luminance Cond)	34	2.88	0.08	24.5	<0.001
			Error	349	1.21	0.00		
		green-red	Luminance Cond	4	2.56	0.64	206	<0.001
			Subject(Luminance Cond)	34	1.79	0.05	17.0	<0.001
			Error	347	1.08	0.00		
		purple-lime	Luminance Cond	4	2.71	0.68	102	<0.001
			Subject(Luminance Cond)	34	3.49	0.10	15.4	<0.001
			Error	350	2.32	0.01		
		lime-purple	Luminance Cond	4	3.88	0.97	124	<0.001
			Subject(Luminance Cond)	35	6.04	0.17	22.2	<0.001
			Error	359	2.79	0.01		
	2 nd inducer	red-green	Luminance Cond	4	0.12	0.03	12.4	<0.001
			Subject(Luminance Cond)	34	1.17	0.03	14.5	<0.001
			Error	349	0.83	0.00		
		green-red	Luminance Cond	4	0.16	0.04	17.7	<0.001
			Subject(Luminance Cond)	34	1.33	0.04	17.1	<0.001
			Error	350	0.80	0.00		
		purple-lime	Luminance Cond	4	0.13	0.03	5.52	<0.001
			Subject(Luminance Cond)	35	5.66	0.16	27.9	<0.001
Error			360	2.08	0.01			
lime-purple		Luminance Cond	4	0.18	0.05	7.40	<0.001	
		Subject(Luminance Cond)	34	2.28	0.07	11.0	<0.001	
		Error	349	2.13	0.01			

Continued from previous page

Experiment	Element	Chromatic Condition	Source	<i>df</i>	<i>SS</i>	<i>MS</i>	<i>F</i>	<i>p</i>
Luminance	Both inducers	red-green	Luminance Cond	4	0.12	0.03	12.4	<0.001
			Subject(Luminance Cond)	34	1.17	0.03	14.5	<0.001
			Error	349	0.83	0.00		
		green-red	Luminance Cond	4	0.16	0.04	17.7	<0.001
			Subject(Luminance Cond)	34	1.33	0.04	17.1	<0.001
			Error	350	0.80	0.00		
	purple-lime	Luminance Cond	4	0.13	0.03	5.52	<0.001	
		Subject(Luminance Cond)	35	5.66	0.16	27.9	<0.001	
		Error	360	2.08	0.01			
	lime-purple	Luminance Cond	4	0.18	0.05	7.40	<0.001	
		Subject(Luminance Cond)	34	2.28	0.07	11.0	<0.001	
		Error	349	2.13	0.01			
Brightness	Test ring	red-green	Brightness Cond	4	0.35	0.09	40.5	<0.001
			Subject(Brightness Cond)	40	1.48	0.04	17.1	<0.001
			Error	403	0.87	0.00		
		green-red	Brightness Cond	4	1.16	0.29	131	<0.001
			Subject(Brightness Cond)	38	1.07	0.03	12.8	<0.001
			Error	386	0.85	0.00		
	purple-lime	Brightness Cond	4	2.12	0.53	78.0	<0.001	
		Subject(Brightness Cond)	40	5.18	0.13	19.0	<0.001	
		Error	404	2.75	0.01			
	lime-purple	Brightness Cond	4	1.32	0.33	62.4	<0.001	
		Subject(Brightness Cond)	40	3.69	0.09		<0.001	
		Error	402	2.12	0.00			

Continued from previous page

Experiment	Element	Chromatic Condition	Source	<i>df</i>	<i>SS</i>	<i>MS</i>	<i>F</i>	<i>p</i>
Brightness	1 st inducer	red-green	Brightness Cond	4	0.15	0.04	35.9	<0.001
			Subject(Brightness Cond)	29	0.84	0.03	27.1	<0.001
			Error	304	0.33	0.00		
		green-red	Brightness Cond	4	1.07	0.27	211	<0.001
			Subject(Brightness Cond)	30	1.26	0.04	33.1	<0.001
			Error	310	0.39	0.00		
		purple-lime	Brightness Cond	4	0.85	0.21	72.0	<0.001
			Subject(Brightness Cond)	29	1.95	0.07	22.9	<0.001
			Error	303	0.89	0.00		
		lime-purple	Brightness Cond	4	2.90	0.73	255	<0.001
			Subject(Brightness Cond)	27	1.52	0.06	19.8	<0.001
			Error	285	0.81	0.00		
	2 nd inducer	red-green	Brightness Cond	4	0.08	0.02	24.4	<0.001
			Subject(Brightness Cond)	25	0.47	0.02	22.3	<0.001
			Error	266	0.22	0.00		
		green-red	Brightness Cond	4	0.20	0.05	57.3	<0.001
			Subject(Brightness Cond)	30	0.95	0.03	35.9	<0.001
			Error	311	0.28	0.00		
		purple-lime	Brightness Cond	4	0.11	0.03	9.99	<0.001
			Subject(Brightness Cond)	30	3.86	0.13	46.4	<0.001
Error			311	0.86	0.00			
lime-purple		Brightness Cond	4	0.18	0.05	15.98	<0.001	
		Subject(Brightness Cond)	26	1.03	0.04	13.8	<0.001	
		Error	277	0.79	0.00			

Continued from previous page

Experiment	Element	Chromatic Condition	Source	<i>df</i>	<i>SS</i>	<i>MS</i>	<i>F</i>	<i>p</i>
Brightness	Both inducers	red-green	Brightness Cond	4	0.12	0.03	31.4	<0.001
			Subject(Brightness Cond)	28	0.67	0.02	24.2	<0.001
			Error	297	0.29	0.00		
		green-red	Brightness Cond	4	0.57	0.14	152	<0.001
			Subject(Brightness Cond)	30	0.48	0.02	17.0	<0.001
			Error	313	0.29	0.00		
		purple-lime	Brightness Cond	4	0.47	0.12	45.9	<0.001
			Subject(Brightness Cond)	30	1.51	0.05	19.9	<0.001
			Error	315	0.80	0.00		
		lime-purple	Brightness Cond	4	1.86	0.47	195	<0.001
			Subject(Brightness Cond)	27	1.03	0.04	16.0	<0.001
			Error	287	0.69	0.00		

Bibliography

- Akbarinia, A. (Aug. 2017). "Computational model of visual perception: from colour to form". PhD thesis. Barcelona, Spain: Computer Science Department, Univeritat Autònoma de Barcelona.
- Akbarinia, A. and C. A. Parraga (2016). "Biologically-inspired edge detection through surround modulation". In: *Proceedings of the British Machine Vision Conference (BMVC)*, pp. 1–13.
- (2018). "Colour constancy beyond the classical receptive field". In: *IEEE Transactions on Pattern Analysis and Machine Intelligence* 40.9, pp. 2081–2094.
- Akyüz, A. O. et al. (2007). "Do HDR Displays Support LDR Content? A Psychophysical Evaluation". In: *ACM Transactions on Graphics* 26.3, pp. 38–1–38–7.
- Andoni, S., A. Tan, and N. J. Priebe (2014). "The cortical assembly of visual receptive fields". In: *The New Visual Neurosciences*. Ed. by J. S. Werner and L. M. Chalupa. Cambridge, Massachusetts: The MIT Press, pp. 367–379.
- Angelucci, A. and S. Shushruth (2014). "Beyond the Classical Receptive Field: Surround Modulation in Primary Visual Cortex". In: *The New Visual Neurosciences*. Ed. by J. S. Werner and L. M. Chalupa. Cambridge, Massachusetts & London, England: The MIT Press, pp. 425–444.
- Angelucci, A. et al. (2017). "Circuits and mechanisms for surround modulation in visual cortex". In: *Annual Review of Neuroscience* 40, pp. 425–451.
- Anstis, S., B. Rogers, and J. Henry (1978). "Interactions between simultaneous contrast and coloured afterimages". In: *Vision Research* 18, pp. 899–911.
- Antolík, J. and A. J. Bednar (2011). "Development of maps of simple and complex cells in the primary visual cortex". In: *Frontiers in Computational Neuroscience* 5.17, pp. 1–19.
- Ashikhmin, M. (2002). "A tone mapping algorithm for high contrast images". In: *13th Eurographics Workshop on Rendering*.
- Ashikhmin, M. and J. Goyal (2006). "A Reality Check for Tone-Mapping Operators". In: *ACM Transactions on Applied Perception* 3.4, pp. 399–411.
- Aydin, T. O. et al. (2008). "Dynamic Range Independent Image Quality Assessment". In: *ACM Transactions on Graphics* 27.3, 69:1–69:10.
- Banterle, F. et al. (2011). *Advanced High Dynamic Range Imaging: Theory And Practice*. Natick, MA, US: AK Peters, Ltd.
- Barlow, H. B. (1953). "Summation and Inhibition in the Frogs Retina". In: *The Journal of Physiology* 119.1, pp. 69–88.
- Beck, J. (1966). "Contrast and assimilation in lightness judgments". In: *Perception & Psychophysics* 1.5, pp. 342–344.
- Billock, V. A. (1995). "Cortical simple cells can extract achromatic information from the multiplexed chromatic and achromatic signals in the parvocellular pathway". In: *Vision Research* 35.16, pp. 2359–2369.
- Bimler, D. L., G. V. Paramei, and C. A. Izmailov (2009). "Hue and saturation shifts from spatially induced blackness". In: *Journal of the Optical Society of America A* 26.1, pp. 163–172.

- Binzegger, T., R. J. Douglas, and K. A. C. Martin (2004). "A quantitative map of the circuit of cat primary visual cortex". In: *The Journal of Neuroscience* 24.39, pp. 8441–8453.
- (2009). "Topology and dynamics of the canonical circuit of cat V1". In: *Neural Networks* 22.8, pp. 1071–1078.
- Blakemore, C. and F. W. Campbell (1969). "On the existence of neurons in the human visual system selectively sensitive to the orientation and size of retinal images". In: *The Journal of Physiology* 203, pp. 237–260.
- Blakemore, C. and E. A. Tobin (1972). "Lateral inhibition between orientation detectors in the cat's visual cortex". In: *Experimental Brain Research* 15, pp. 439–440.
- Blakeslee, B. and M. E. McCourt (1977). "Similar mechanisms underlie simultaneous brightness contrast and grating induction". In: *Vision Research* 37.20, pp. 2849–2869.
- (1999). "A multiscale spatial filtering account of the White effect, simultaneous brightness contrast and grating induction". In: *Vision Research* 39.26, pp. 4361–4377.
- (2004). "A unified theory of brightness contrast and assimilation incorporating oriented multiscale spatial filtering and contrast normalization". In: *Vision Research* 44.21, pp. 2483–2503.
- Blasdel, G. G. and D. Fitzpatrick (1984). "Physiological organization of layer 4 in macaque striate cortex". In: *The Journal of Neuroscience* 4.3, pp. 880–895.
- Bosking, W. H. et al. (1997). "Orientation selectivity and the arrangement of horizontal connections in tree shrew striate cortex". In: *The Journal of Neuroscience* 17.6, pp. 2112–2127.
- Boynton, R. M. (1973). "Implications of the minimally distinct border". In: *Journal of the Optical Society of America* 63.9, pp. 1037–1043.
- (1986). "A system of photometry and colorimetry based on cone excitations". In: *Color Research and Applications* 11, pp. 244–252.
- (1996). "History and current status of a physiologically based system of photometry and colorimetry". In: *Journal of the Optical Society of America A* 13, pp. 1609–1621.
- Boynton, R. M. and P. K. Kaiser (1968). "Vision: The additivity Law made to work for heterochromatic photometry with bipartite fields". In: *Science* 161.3839, pp. 366–368.
- Bradley, A., X. Zhang, and L. Thibos (1992). "Failures of isoluminance caused by ocular chromatic aberrations". In: *Applied Optics* 31.19, pp. 3657–3667.
- Bredfeldt, C. E. and D. L. Ringach (2002). "Dynamics of spatial frequency tuning in macaque V1". In: *The Journal of Neuroscience* 22.5, pp. 1976–1984.
- Bressan, P. (1995). "A closer look at the dependence of neon colour spreading on wavelength and illuminance". In: *Vision Research* 35.3, pp. 375–379.
- Briggs, F. and W. M. Usrey (2008). "Emerging views of corticothalamic function". In: *Current Opinion in Neurobiology* 18.4, pp. 403–407.
- (2009). "Parallel processing in the corticogeniculate pathway of the macaque monkey". In: *Neuron* 62, pp. 135–146.
- (2014). "Functional Properties of Cortical Feedback to the Primate Lateral Geniculate Nucleus". In: *The New Visual Neurosciences*. Ed. by J. S. Werner and L. M. Chalupa. Cambridge, Massachusetts: The MIT Press, pp. 315–322.
- Brill, M. H. (2014). "Minimally Distinct Border". In: *Encyclopedia of Color Science and Technology*. Ed. by M. R. Luo. Berlin, Heidelberg: Springer Berlin Heidelberg, pp. 1–3.

- Brown, R. O. and D. I. A. MacLeod (1997). "Color appearance depends on the variance of surround colors". In: *Current Biology* 7.11, pp. 844–849.
- Cadik, M. et al. (2006). "Image Attributes and Quality for Evaluation of Tone Mapping Operators". In: *14th Pacific Conference on Computer Graphics and Applications*, pp. 35–44.
- (2008). "Evaluation of HDR Tone Mapping Methods using Essential Perceptual Attributes". In: *Computers & Graphics* 32, pp. 330–349.
- Callaway, E. M. (1998). "Local circuits in primary visual cortex of the macaque monkey". In: *Annual Review of Neuroscience* 21, pp. 47–74.
- (2014). "Cells types and local circuits in primary visual cortex of the macaque monkey". In: *The New Visual Neurosciences*. Ed. by J. S. Werner and L. M. Chalupa. Cambridge, Massachusetts & London, England: The MIT Press, pp. 353–365.
- Camera Calibration Methods*. www.cvc.uab.es/color_calibration/CameraCal2.htm. Accessed: 2018-02-06.
- Cao, D. and S. K. Shevell (2005). "Chromatic assimilation: spread light or neural mechanism?" In: *Vision Research* 45, pp. 1031–1045.
- Carandini, M. and D. J. Heeger (2012). "Normalization as a canonical neural computation". In: *Nature Reviews Neuroscience* 13, pp. 51–62.
- Carew, T. J. (2000). *Behavioral neurobiology: the cellular organization of natural behavior*. Massachusetts, USA: Sinauer Associates Publishers. Chap. 1.
- Casagrande, V. et al. (2007). "The morphology of the koniocellular axon pathway in the macaque monkey". In: *Cerebral Cortex* 17.10, pp. 2334–2345.
- Cerda-Company, X. and X. Otazu (2016a). "A multi-task neurodynamical model of lateral interactions in V1: chromatic induction". In: *European Conference on Visual Perception (EVP) Abstract Book*, pp. 52–53.
- (2016b). "Dynamic colour induction can be reproduced by a neurodynamical model of lateral interactions in V1". unpublished conference abstract.
- (2017a). "Equiluminant colour induction in flashed and static stimuli". unpublished conference abstract.
- (2017b). "Is luminance a key factor for static and flashed chromatic assimilation?" In: *European Conference on Visual Perception (EVP) Abstract Book*, pp. 17–18.
- (2019). "Color induction in equiluminant flashed stimuli". In: *Journal of the Optical Society of America A* 36.1, pp. 22–31.
- Cerda-Company, X., X. Otazu, and O. Penacchio (2018). "A new dynamical firing rate model of the parvocellular pathway in V1". In: *Barcelona Computational, Cognitive and Systems Neuroscience (BARCCSYN)*, p. 29.
- Cerda-Company, X., C. A. Parraga, and X. Otazu (2018). "Which tone-mapping operator is the best? A comparative study of the perceptual quality". In: *Journal of the Optical Society of America A* 35.4, pp. 626–638.
- Cerda-Company, X. et al. (2018a). "Colour induction in migraine". In: *Applied Vision Association (AVA) Christmas Meeting*.
- Cerda-Company, X. et al. (2018b). "Luminance spatial distribution plays a major role in color assimilation". unpublished conference abstract.
- (2018c). "The effect of luminance differences on color assimilation". In: *Journal of Vision* 18.10, pp. 1–23.
- Cerda, X., C. A. Parraga, and X. Otazu (2014). "Which tone-mapping is the best? A comparative study of tone-mapping perceived quality". In: *European Conference on Visual Perception (EVP) Abstract Book*, p. 106.
- Chariker, L., R. Shapley, and L. Young (2016). "Orientation selectivity from very sparse LGN inputs in a comprehensive model of macaque V1 cortex". In: *The Journal of Neuroscience* 36.49, pp. 12368–12384.

- Chatterjee, S. and E. M. Callaway (2003). "Parallel colour-opponent pathways to primary visual cortex". In: *Nature* 426, pp. 668–671.
- Chevreul, M. E. (1839). *De la loi du contraste simultane des couleurs*. Paris: Chez Pitois-Levrault et Ce.
- Chiel, H. J. and R. D. Beer (1997). "The brain has a body: adaptive behavior emerges from interactions of nervous system, body and environment". In: *Trends in Neuroscience* 20.12, pp. 553–557.
- Chisum, H. J. and D. Fitzpatrick (2004). "The contribution of vertical and horizontal connections to the receptive field center and surround in V1". In: *Neural Networks* 17.5-6, pp. 681–693.
- Choudhury, P. and J. Tumblin (2003). "The trilateral filter for high contrast images and meshes". In: *Proceedings of the Eurographics Symposium on Rendering*, pp. 186–196.
- Conway, B. R. and M. S. Livingstone (2006). "Spatial and temporal properties of cone signals in alert macaque primary visual cortex". In: *The Journal of Neuroscience* 26.42, pp. 10826–10846.
- Courtney, S. M., L. H. Finkel, and G. Bachsbaum (1995). "A multistage neural network for color constancy and color induction". In: *IEEE Transactions on Neural Networks* 6.4, pp. 972–985.
- Dacey, D. and B. B. Lee (1984). "The blue-ON pathway in primate retina originates from a distinct bistratified ganglion cell type". In: *Nature* 367, pp. 731–735.
- Daugman, J. G. (1985). "Uncertainty relation for resolution in space, spatial frequency, and orientation optimized by two-dimensional visual cortical filters". In: *Journal of the Optical Society of America A* 2.7, pp. 1160–1169.
- Dayan, P. and L. F. Abbott (2001). "Network Models". In: *Theoretical Neuroscience: Computational and Mathematical Modeling of Neural Systems*. Cambridge, Massachusetts, USA: The MIT Press. Chap. 7, pp. 229–278.
- De Valois, R. L., D. G. Albrecht, and L. Thorell (1982). "Spatial-frequency selectivity of cells in macaque visual cortex". In: *Vision Research* 22.5, pp. 545–559.
- De Valois, R. L. and K. K. De Valois (1988a). "Sensitivity to Color Variations". In: *Spatial Vision*. Oxford Psychology Series. New York, Oxford: Oxford University Press, Clarendon Press. Chap. 7, pp. 212–239.
- (1988b). *Spatial Vision*. Oxford Psychology Series. New York, Oxford: Oxford University Press, Clarendon Press.
- (1993). "A multi-stage color model". In: *Vision Research* 33.8, pp. 1053–1065.
- De Valois, R. L., M. A. Webster, and K. K. De Valois (1986). "Temporal properties of the brightness and color induction". In: *Vision Research* 26.6, pp. 887–897.
- De Valois, R. L. et al. (2000). "Spatial and temporal receptive fields of geniculate and cortical cells and directional selectivity". In: *Vision Research* 40.27, pp. 3685–3702.
- De Weert, C. M. and N. A. Kruysbergen (1997). "Assimilation: central and peripheral effects". In: *Perception* 26.10, pp. 1217–1224.
- De Weert, C. M. and L. Spillmann (1995). "Assimilation: Asymmetry between brightness and darkness?" In: *Vision Research* 35.10, pp. 1413–1419.
- DeAngelis, G. C. and A. Anzai (2014). "A Modern View of the Classical Receptive Field: Linear and Nonlinear Spatiotemporal Processing by V1 Neurons". In: *The New Visual Neurosciences*. Ed. by J. S. Werner and L. M. Chalupa. Cambridge, Massachusetts & London, England: The MIT Press, pp. 704–719.
- DeAngelis, G. C., I. Ohzawa, and R. D. Freeman (1993a). "Spatiotemporal organization of simple-cell receptive fields in the cat's striate cortex. I. General characteristics and postnatal development". In: *The Journal of Neurophysiology* 69.4, pp. 1091–1117.

- (1993b). “Spatiotemporal organization of simple-cell receptive fields in the cat’s striate cortex. II. Linearity of temporal and spatial summation”. In: *The Journal of Neurophysiology* 69.4, pp. 1118–1135.
- (1995). “Receptive-field dynamics in the central visual pathways”. In: *Trends in Neurosciences* 18.10, pp. 451–458.
- Derrington, A. M., J. Krauskopf, and P. Lennie (1984). “Chromatic mechanisms in lateral geniculate nucleus of macaque”. In: *Journal of Physiology* 357, pp. 241–265.
- Devinck, F., B. Pinna, and J. S. Werner (2014). “Chromatic assimilation in visual art and perception”. In: *Perception Beyond Gestalt*. Ed. by A. Geremek, M. W. Greenlee, and S. Magnussen. Hove, UK: Psychology Press, pp. 1–3.
- Devinck, F. et al. (2005). “The watercolor effect: quantitative evidence for luminance-dependent mechanisms of long-range color assimilation”. In: *Vision Research* 45, pp. 1413–1424.
- Devinck, F. et al. (2006). “Spatial profile of contours inducing long-range color assimilation”. In: *Visual Neuroscience* 23, pp. 573–577.
- Disraeli, B. (1996). “General summary statistics”. In: *Understanding statistics*. Ed. by G. Upton and I. Cook. New York, Oxford: Oxford University Press. Chap. 2, pp. 36–83.
- Dominy, N. J. and P. W. Lucas (2001). “Ecological importance of trichromatic vision to primates”. In: *Nature* 410, pp. 363–366.
- Dougherty, P. (1997). “Homeostasis and Higher Brain Functions”. In: *Neuroscience Online: An Electronic Textbook for the Neurosciences*. Ed. by J. H. Byrne. Houston, USA: The University of Texas Health Science Center at Houston. Chap. 4. URL: <http://nba.uth.tmc.edu/neuroscience/> (visited on 11/26/2018).
- Drago, F. et al. (2003a). “Adaptive Logarithmic Mapping for Displaying High Contrast Scenes”. In: *Proceedings of Eurographics*. Vol. 22.
- Drago, F. et al. (2003b). “Perceptual Evaluation of Tone Mapping Operators”. In: *ACM SIGGRAPH Conference Abstracts and Applications*.
- Dresp, B. and S. Fischer (2001). “Asymmetrical contrast effects induced by luminance and color configurations”. In: *Perception & Psychophysics* 63.7, pp. 1262–1270.
- Durand, F. and J. Dorsey (2002). “Fast Bilateral Filtering for the Display of High Dynamic-Range Images”. In: *Proceedings of ACM SIGGRAPH*. ACM Press, pp. 257–266.
- Ehrenstein, W. (1941). “Über Abwandlungen der L. Hermannschen Helligkeitserscheinung”. In: *Zeitschrift für Psychologie* 150, pp. 83–91.
- Ejima, Y. et al. (1984). “The neon color effect in the Ehrenstein pattern. Dependence on wavelength and illuminance”. In: *Vision Research* 24.12, pp. 1719–1726.
- Fach, C. and L. T. Sharpe (1986). “Assimilative hue shifts in color gratings depend on bar width”. In: *Perception & Psychophysics* 40.6, pp. 412–418.
- Fairchild, M. D. and G. M. Johnson (2000). “Rendering HDR Images”. In: *11th Color Imaging Conference*. IS&T/SID, pp. 108–111.
- Farnsworth, D. (1947). *The Farnsworth dichotomous test for color blindness: panel D-15*. Psychological Corporation.
- Fattal, R., D. Lischinski, and M. Werman (2002). “Gradient Domain High Dynamic Range Compression”. In: *Proceedings of ACM SIGGRAPH*. ACM Press, pp. 249–256.
- Faul, F., V. Ekroll, and G. Wendt (2008). “Color appearance: the limited role of chromatic surround variance in the ‘gamut expansion effect’”. In: *Journal of Vision* 8.30, pp. 1–20.

- Ferradans, S. et al. (2011). "An Analysis Of Visual Adaptation and Contrast Perception for Tone Mapping". In: *IEEE Transactions on Pattern Analysis and Machine Intelligence* 33.10.
- Ferwerda, J. A. and S. Luka (2009). "A high resolution, high dynamic range display system for vision research". In: *Journal of Vision* 9.8.
- Ferwerda, J. A. et al. (1996). "A Model of Visual Adaptation for Realistic Image Synthesis". In: *Proceedings of ACM SIGGRAPH*. ACM Press, pp. 249–258.
- Festinger, L., S. Coren, and G. Rivers (1970). "Effect of attention on brightness contrast and assimilation". In: *American Journal of Psychology* 83.2, pp. 189–207.
- Field, D. J., J. R. Golden, and A. Hayes (2014). "Contour integration and the association field". In: *The New Visual Neurosciences*. Ed. by J. S. Werner and L. M. Chalupa. Cambridge, Massachusetts: The MIT Press, pp. 627–638.
- Field, D. J., A. Hayes, and R. F. Hess (1993). "Contour integration by the human visual system: Evidence for a local". In: *Vision Research* 33.2, pp. 173–193.
- Foster, D. H. (2011). "Color constancy". In: *Vision Research* 51.7, pp. 674–700.
- Freeman, J. and E. P. Simoncelli (2011). "Metamers of the ventral stream". In: *Nature Neuroscience* 14, pp. 1195–1201.
- Friedman, H. S., H. Zhou, and R. von der Heydt (2003). "The coding of uniform colour figures in monkey visual cortex". In: *The Journal of Physiology* 548.2, pp. 593–613.
- Gao, S. et al. (2015). "Color constancy using double-opponency". In: *IEEE Transactions on Pattern Analysis and Machine Intelligence* 37.10, pp. 1973–1985.
- Garcia-Marin, V., J. G. Kelly, and M. J. Hawken (2017). "Major feedforward thalamic input into layer 4C of primary visual cortex in primate". In: *Cerebral Cortex*, pp. 1–16.
- Gegenfurtner, K. R. (2003). "Cortical mechanisms of colour vision". In: *Nature Reviews Neuroscience* 4, pp. 563–572.
- Gegenfurtner, K. R., D. C. Kiper, and S. B. Fenstemaker (1996). "Processing of color, form, and motion in macaque area V2". In: *Visual Neuroscience* 13.1, pp. 161–172.
- Gilchrist, A. et al. (1999). "An anchoring theory of lightness perception". In: *Psychological Review* 106.4, pp. 795–834.
- Girard, P. and M. C. Morrone (1995). "Spatial structure of chromatically opponent receptive fields in the human visual system". In: *Visual Neuroscience* 12.1, pp. 103–116.
- Gordon, J. and R. M. Shapley (2006). "Brightness contrast inhibits color induction: evidence for a new kind of color theory". In: *Spatial Vision* 19, pp. 133–146.
- Granger, E. M. and J. C. Heurtley (1973). "Visual chromaticity-modulation transfer function". In: *Journal of the Optical Society of America* 63.9, pp. 1173–1174.
- Hamada, J. (1984). "Lightness decrease and increase in square-wave grating". In: *Perception & Psychophysics* 35.1, pp. 16–21.
- Helson, H. (1963). "Studies of anomalous contrast and assimilation". In: *Journal of the Optical Society of America* 53.1, pp. 179–184.
- Henry, C. A. et al. (2013). "Functional characterization of the extraclassical receptive field in macaque V1: contrast, orientation, and temporal dynamics". In: *The Journal of Neuroscience* 33.14, pp. 6230–6242.
- Hirsch, J. A. and L. M. Martinez (2006). "Laminar processing in the visual cortical column". In: *Current Opinion in Neurobiology* 16.4, pp. 377–384.
- Hong, S. W. and S. K. Shevell (2004). "Brightness contrast and assimilation from patterned inducing backgrounds". In: *Vision Research* 44.1, pp. 35–43.
- Horiuchi, K. et al. (2014). "Chromatic induction from surrounding stimuli under perceptual suppression". In: *Visual Neuroscience* 31.6, pp. 387–400.

- Horton, J. C. and D. H. Hubel (1981). "Regular distribution of cytochrome oxidase staining in primary visual cortex of macaque monkey". In: *Nature* 292, pp. 762–764.
- Hubel, D. H. and T. N. Wiesel (1959). "Receptive fields of single neurones in the cat's striate cortex". In: *The Journal of Physiology* 148.3, pp. 574–591.
- (1962). "Receptive fields, binocular interaction and functional architecture in the cat's visual cortex". In: *The Journal of Physiology* 160.1, pp. 106–154.
- (1965). "Receptive fields and functional architecture in two nonstriate visual areas (18 and 19) of the cat". In: *The Journal of Neurophysiology* 28.2, pp. 229–289.
- (2004). *Brain and Visual Perception: The Story of a 25-Year Collaboration*. New York, USA: Oxford University Press. Chap. 14.
- Hupe, J. M. et al. (1998). "Cortical feedback improves discrimination between figure and background by V1, V2 and V3 neurons". In: *Nature* 394, pp. 784–787.
- Hurlbert, A. and K. Wolf (2004). "Color contrast: a contributory mechanism to color constancy". In: *Progress in Brain Research* 144, pp. 145–160.
- Ichida, J. M. et al. (2007). "Response facilitation from the 'suppressive' receptive field surround of macaque V1 neurons". In: *The Journal of Neurophysiology* 98, pp. 2168–2181.
- Ishihara, S. (1972). *Tests for colour-blindness*. Tokyo, Japan: Kanehara Shippan Co., Ltd.
- Johnson, E. N., M. J. Hawken, and R. M. Shapley (2001). "The spatial transformation of color in the primary visual cortex of the macaque monkey". In: *Nature Neuroscience* 4.4, pp. 409–416.
- (2004). "Cone inputs in macaque primary visual cortex". In: *The Journal of Neurophysiology* 91, pp. 2501–2514.
- (2008). "The orientation selectivity of color-responsive neurons in macaque V1". In: *The Journal of Neuroscience* 28.32, pp. 8096–8106.
- Kaiser, P. (1971). "Minimally distinct border as a preferred psychophysical criterion in visual heterochromatic photometry". In: *Journal of the Optical Society of America A* 61.7, pp. 966–971.
- Kaiser, P. et al. (1990). "The physiological basis of the minimally distinct border demonstrated in the ganglion cells of the macaque retina". In: *Journal of Physiology* 422, pp. 153–183.
- Kamermans, M., D. A. Kraaij, and H. Spekreijse (1998). "The cone/horizontal cell network: a possible site for color constancy". In: *Visual Neuroscience* 15.5, pp. 787–797.
- Kamermans, M. and H. Spekreijse (1999). "The feedback pathway from horizontal cells to cones: A mini review with a look ahead". In: *Vision Research* 39.15, pp. 2449–2468.
- Kaneko, S. and I. Murakami (2012). "Flashed stimulation produces strong simultaneous brightness and color contrast". In: *Journal of Vision* 12.1, pp. 1–18.
- Kaplan, E. (2014). "The M, P, and K pathways of the primate visual system revisited". In: *The New Visual Neurosciences*. Ed. by J. S. Werner and L. M. Chalupa. Cambridge, Massachusetts: The MIT Press, pp. 215–226.
- Kelly, D. H. and E. Martinez-Uriegas (1993). "Measurements of chromatic and achromatic afterimages". In: *Journal of Optical Society of America A* 10.1, pp. 29–37.
- Kendall, M. G. and B. Babington-Smith (1940). "On the Method of Paired Comparisons". In: *Biometrika* 31.3/4, pp. 324–345.
- Khan, F. S. et al. (2012). "Color attributes for object detection". In: *2012 IEEE Conference on Computer Vision and Patter Recognition*, pp. 3306–3313.

- Kim, M. H. and J. Kautz (2008). "Consistent Tone Reproduction". In: *Proceedings of Computer Graphics and Imaging*.
- Kingdom, F. A. A. (2011). "Lightness, brightness and transparency: A quarter century of new ideas, captivating demonstrations and unrelenting controversy". In: *Vision Research* 51.7, pp. 652–673.
- Kirschmann, A. (1891). "Ueber die quantitativen Verhältnisse des simultanen Helligkeits- und Farben-Contrastes". In: *Philosophische Studien* 6, pp. 417–491.
- Kitaoka, A. (2007). "Tilt illusions after Oyama (1960): a review". In: *Japanese Psychological Research* 49.1, pp. 7–19.
- Kolb, H. (2005). "Feedback Loops in the Retina". In: *Webvision: The Organization of the Retina and Visual System [Internet]*. Ed. by H. Kolb, R. Fernandez, and R. Nelson. Salt Lake City, USA: University of Utah Health Sciences Center, pp. 1–13.
- Krawczyk, G., K. Myszkowski, and H. Seidel (2005). "Lightness Perception in Tone Reproduction for High Dynamic Range Images". In: *Proceedings of Eurographics*. 3.
- Kuang, J., G. M. Johnson, and M. D. Fairchild (2007). "iCAM06: A Refined Image Appearance Model for HDR Image Rendering". In: *Journal of Visual Communication And Image Representation* 18, pp. 404–414.
- Kuang, J. et al. (2004). "Testing HDR Image Rendering Algorithms". In: *IS&T/SID 12th Color Imaging Conference*.
- Kuang, J. et al. (2007). "Evaluating HDR Rendering Algorithms". In: *ACM Transactions on Applied Perception* 4.2.
- Land, E. H. (1964). "The Retinex". In: *American Scientist* 52.2, pp. 247–253, 255–264.
- Land, E. H. and J. J. McCann (1971). "Lightness and retinex theory". In: *Journal of the Optical Society of America* 61.1, pp. 1–11.
- Landy, M. S. (2014). "Texture analysis and perception". In: *The New Visual Neurosciences*. Ed. by J. S. Werner and L. M. Chalupa. Cambridge, Massachusetts: The MIT Press, pp. 639–652.
- Ledda, P. et al. (2005). "Evaluation of Tone Mapping Operators using a High Dynamic Range Display". In: *ACM Transactions on Graphics* 24.3, pp. 640–648.
- Lee, B. B. (2014). "Color coding in the primate visual pathway: a historical review". In: *Journal of the Optical Society of America A* 31.4, A103–A112.
- Lennie, P., J. Krauskopf, and G. Sclar (1990). "Chromatic mechanisms in striate cortex of macaque". In: *The Journal of Neuroscience* 10, pp. 649–669.
- Leventhal, A. G. et al. (1995). "Concomitant sensitivity to orientation, direction, and color of cells in layers 2, 3, and 4 of monkey striate cortex". In: *The Journal of Neuroscience* 15.3, pp. 1808–1818.
- Levitt, J. B., D. C. Kiper, and J. A. Movshon (1994). "Receptive fields and functional architecture of macaque V2". In: *The Journal of Neurophysiology* 71.6, pp. 2517–2542.
- Levitt, J. B. and J. S. Lund (1997). "Contrast dependence of contextual effects in primate visual cortex". In: *Nature* 387, pp. 73–76.
- Li, Y., L. Sharan, and E. H. Adelson (2005). "Compressing and Companding High Dynamic Range Images with Subband Architectures". In: *ACM Transactions on Graphics* 24.3, pp. 836–844.
- Li, Z. (1998). "A neural model of contour integration in the primary visual cortex". In: *Neural Computation* 10.4, pp. 903–940.
- (1999). "Visual segmentation by contextual influences via intra-cortical interactions in the primary visual cortex". In: *Network: Computation in Neural Systems* 10.2, pp. 187–212.

- (2002). “A saliency map in primary visual cortex”. In: *Trends in Cognitive Sciences* 6.1, pp. 9–16.
- Livingstone, M. S. and D. H. Hubel (1988). “Segregation of form, color, movement, and depth: anatomy, physiology, and perception”. In: *Science* 240.4853, pp. 740–749.
- Loffler, G. (2008). “Perception of contours and shapes: Low and intermediate stage mechanisms”. In: *Vision Research* 48.20, pp. 2106–2127.
- Lotto, R. B. and D. Purves (1999). “The effects of color on brightness”. In: *Nature Neuroscience* 2.11, pp. 1010–1014.
- Lu, H. D. and A. W. Rose (2007). “Functional organization of color domains in V1 and V2 of macaque monkey revealed by optical imaging”. In: *Cerebral Cortex* 18.3, pp. 516–533.
- Lucas, P. W. et al. (1998). “Colour cues for leaf food selection by long-tailed macaques (*Macaca fascicularis*) with a new suggestion for the evolution of trichromatic colour vision”. In: *Folia Primatologica* 69.3, pp. 139–154.
- Lucas, P. W. et al. (2003). “Evolution and function of routine trichromatic vision in primates”. In: *Evolution* 57.11, pp. 2636–2643.
- MacEvoy, B. (2016). *HandPrint website*. URL: <https://www.handprint.com> (visited on 10/19/2018).
- MacLeod, D. A. and R. M. Boynton (1979). “Chromaticity diagram showing cone excitation by stimuli of equal luminance”. In: *Journal of the Optical Society of America* 69.8, pp. 1183–1186.
- Malach, R. et al. (1993). “Relationship between intrinsic connections and functional architecture revealed by optical imaging and in vivo targeted biocytin injections in primate striate cortex”. In: *Proceedings of the National Academy of Sciences of United States of America* 90.22, pp. 10469–10473.
- Malone, B. J., V. R. Kumar, and D. L. Ringach (2007). “Dynamics of receptive field size in primary visual cortex”. In: *The Journal of Neurophysiology* 97.1, pp. 407–414.
- Mardia, K. V. (1972). “Probability and mathematical statistics: statistics of directional data”. In: *London: Academic*.
- Martinez-Cañada, P., C. Morillas, and F. Pelayo (2017). “A conductance-based neuronal network model for color coding in the primate foveal retina”. In: *Natural and Artificial Computation for Biomedicine and Neuroscience: International Work-Conference on the Interplay Between Natural and Artificial Computation (IWINAC)*, pp. 63–74.
- (2018). “A neuronal network model of the primate visual system: color mechanisms in the retina, LGN and V1”. In: *International Journal of Neural Systems* 28.0, pp. 1850036–1–1850036–22.
- Martinez, L. M. and J. M. Alonso (2003). “Complex receptive fields in primary visual cortex”. In: *Neuroscientist* 9.5, pp. 317–331.
- Mazer, J. A. et al. (2002). “Spatial frequency and orientation tuning dynamics in area V1”. In: *Proceedings of the National Academy of Sciences of the United States of America* 99.3, pp. 1645–1650.
- McCann, J. J. (1999). “Lessons learned from Mondrians applied to real images and color gamuts”. In: *7th Color Imaging Conference: Color Science, Systems and Applications*. Proc. IS&T/SID, pp. 1–8.
- (2004). “Capturing a black cat in shade: past and present of Retinex color appearance models”. In: *Journal of Electronic Imaging* 13.1, pp. 36–47.
- (2007). “Art, Science, and Appearance in HDR Images”. In: *Journal of the Society for Information Display* 15.9, pp. 709–719.

- McCann, J. J. (2017). "Retinex at 50: color theory and spatial algorithms, a review". In: *Journal of Electronic Imaging* 26.3.
- McCann, J. J., C. Parraman, and A. Rizzi (2014). "Reflectance, illumination, and appearance in color constancy". In: *Frontiers in Psychology* 5.5, pp. 1–17.
- McCann, J. J. and A. Rizzi (2012). "The Art and Science of HDR Imaging". In: First. West Sussex, UK: WILEY. Chap. 13, pp. 119–121.
- McCourt, M. E. (1982). "A spatial frequency dependent grating-induction effect". In: *Vision research* 22.5, pp. 119–123, 125–134.
- McIntyre, D. (2002). *Colour blindness: Causes and effects*. Chester, UK: Dalton Publishing.
- McLaughlin, D. et al. (2000). "A neuronal network model of macaque primary visual cortex (V1): Orientation selectivity and dynamics in the input layer 4C α ". In: *Proceedings of the National Academy of Sciences of the United States of America* 97.14, pp. 8087–8092.
- Mechler, F. and D. L. Ringach (2002). "On the classification of simple and complex cells". In: *Vision Research* 42.8, pp. 1017–1033.
- Mees, C. E. K. (1921). "The fundamentals of photography". In: Second. Rochester, N.Y.: Eastman Kodak Company.
- Mertens, T., J. Kautz, and F. Van Reeth (2007). "Exposure Fusion". In: *15th Pacific Conference on Computer Graphics and Applications*, pp. 382–390.
- Meylan, L., D. Alleysson, and S. Süsstrunk (2007). "Model of Retinal Local Adaptation for the Tone Mapping Color Filter Array Images". In: *Journal of the Optical Society of America A* 24.9.
- Miller, N. J., Ngai P. Y., and Miller D. D. (1984). "The Application of Computer Graphics in Lighting Design". In: *Journal of the Illuminating Engineering Society* 14.1, pp. 6–26.
- Mollon, J. D. (1989). "Tho' she kneel'd in that place where they grew... The uses and origins of primate colour vision". In: *Journal of Experimental Biology* 146.1, pp. 21–38.
- Momiji, H. et al. (2006). "Numerical study of short-term afterimages and associate properties in foveal vision". In: *Vision Research* 46.3, pp. 365–381.
- Momiji, H. et al. (2007). "A numerical study of red-green colour opponent properties in the primate retina". In: *European Journal of Neuroscience* 25.4, pp. 1155–1165.
- Monnier, P. and S. K. Shevell (2003). "Large shifts in color appearance from patterned chromatic backgrounds". In: *Nature Neuroscience* 6, pp. 801–802.
- (2004). "Chromatic induction from S-cone patterns". In: *Vision Research* 44, pp. 849–856.
- Montage, E. D. (2004). "Louis Leon Thurstone in Monte Carlo: Creating Error Bars for the Method of Paired Comparison". In: *Proceedings of SPIE-IS&T Electronic Imaging*. Vol. 5294, pp. 222–230.
- Mullen, K. T. (1985). "The contrast sensitivity of human colour vision to red-green and blue-yellow chromatic gratings". In: *The Journal of Physiology* 359.1, pp. 381–400.
- Nassi, J. J. and E. M. Callaway (2009). "Parallel processing strategies of the primate visual system". In: *Nature Reviews Neuroscience* 10, pp. 360–372.
- Nunez, V., R. M. Shapley, and J. Gordon (2018). "Cortical double-opponent cells in color perception: perceptual scaling and chromatic visual evoked potentials". In: *i-Perception* 9.1, pp. 1–16.
- Nurminen, L. and A. Angelucci (2014). "Multiple components of surround modulation in primary visual cortex: Multiple neural circuits with multiple functions?" In: *Vision Research* 104, pp. 47–56.

- Otazu, X. (2012). "Perceptual Tone-Mapping Operator based on Multiresolution Contrast Decomposition". In: *European Conference on Visual Perception Abstract Book*, p. 86.
- Otazu, X., C. A. Parraga, and M. Vanrell (2010). "Toward a unified chromatic induction model". In: *Journal of Vision* 10.12, pp. 1–24.
- Otazu, X., O. Penacchio, and X. Cerda-Company (2015a). "An excitatory-inhibitory firing rate model accounts for brightness induction, color induction and visual discomfort". unpublished conference abstract.
- (2015b). "Brightness and colour induction through contextual influences in V1". In: *Scottish Vision Group (SVG)*. Vol. 12, 9, pp. 1208–2012.
- Otazu, X., M. Vanrell, and C. A. Parraga (2008). "Multiresolution wavelet framework models brightness induction effects". In: *Vision Research* 48.5, pp. 733–751.
- Otazu, X. et al. (2018). "Stronger colour induction in migraine". unpublished conference abstract.
- Parraman, C. (2010). "The drama of illumination: artist's approaches to the creation of HDR in paintings and prints". In: *Proc.SPIE*. Vol. 7527, 75270U–1–75270U–12.
- Penacchio, O., X. Otazu, and L. Dempere-Marco (2013). "A neurodynamical model of brightness induction in V1". In: *PLOS One* 8.5, pp. 1–14.
- Pinna, B. (1987). "Un effetto di colorazione". In: *Il laboratorio e la città. XXI Congresso degli Psicologi Italiani*. Ed. by V. Majer, M. Maeran, and M. Santinello, p. 158.
- Pinna, B., G. Brelstaff, and L. Spillmann (2001). "Surface color from boundaries: a new 'watercolor' illusion". In: *Vision Research* 41, pp. 2669–2676.
- Pinna, B., L. Spillmann, and J. S. Werner (2003). "Anomalous induction of brightness and surface qualities: A new illusion due to radial lines and chromatic rings". In: *Perception* 32, pp. 1289–1305.
- Ramon y Cajal, S. (1894). "The Croonian lecture: La fine structure des centres nerveux". In: *Proceedings of the Royal Society of London* 55.331–335, pp. 444–468.
- Reagan, B. C. et al. (1998). "Frugivory and colour vision in *Alouatta seniculus*, a trichromatic platyrrhine monkey". In: *Vision Research* 38.21, pp. 3321–3328.
- Reagan, B. C. et al. (2001). "Fruits, foliage and the evolution of primate colour vision". In: *Philosophical Transactions of the Royal Society B* 356.1407, pp. 229–283.
- Redies, C. and L. Spillmann (1981). "The neon color effect in the Ehrenstein illusion". In: *Perception* 10, pp. 667–681.
- Reinhard, E. and K. Devlin (2005). "Dynamic Range Reduction Inspired by Photoreceptor Physiology". In: *IEEE Transactions on Visualization and Computer Graphics* 11.1, pp. 13–24.
- Reinhard, E. et al. (2002). "Photographic Tone Reproduction for Digital Images". In: *ACM Transactions on Graphics* 21.3, pp. 267–276.
- Reinhard, E. et al. (2005). "High Dynamic Range Imaging: Acquisition, Display and Image-Based Lighting". In: *First*. San Francisco, CA, US: Morgan Kaufmann Publishers Inc. Chap. 6, pp. 187–221.
- Ringach, D. L., M. J. Hawken, and R. M. Shapley (1997). "Dynamics of orientation tuning in macaque primary visual cortex". In: *Nature* 387, pp. 281–284.
- Ringach, D. L. and R. M. Shapley (2004). "Reverse correlation in neurophysiology". In: *Cognitive Science* 28.2, pp. 147–166.
- Ringach, D. L., R. M. Shapley, and M. J. Hawken (2002). "Orientation selectivity in macaque V1: diversity and laminar dependence". In: *The Journal of Neuroscience* 22.13, pp. 5639–5651.
- Robinson, A., P. Hammon, and V. de Sa (2007). "Explaining brightness illusions using spatial filtering and local response normalization". In: *Vision Research* 47.12, pp. 1631–1644.

- Rodieck, R. W. (1988). "The primate retina". In: *Neurosciences - Comparative primate biology*. Ed. by H. D. Steklis and J. Brown. Vol. 4. New York, US: Alan R. Liss, pp. 203–278.
- Rolls, E. T. and G. Deco (2002). "The primary visual cortex". In: *Computational Neuroscience of Vision*. New York, Oxford: Oxford University Press. Chap. 2, pp. 36–56.
- Rossi, A. F., C. D. Rittenhouse, and M. A. Paradiso (1996). "The representation of brightness in primary visual cortex". In: *Science* 273.5278, pp. 1104–1107.
- Roufs, J. A. J. (1978). *Light as a true visual quantity: Principles of measurement*. Tech. rep. 41 (TC-1.4). Bureau Central de la CIE, Paris, France: Commission Internationale de l'Éclairage.
- Ruppertsberg, A. I. et al. (2007). "Displaying colourimetrically calibrated images on a high dynamic range display". In: *Journal of Visual Communication and Image Representation* 18.5, pp. 429–438.
- Sabbah, S. et al. (2013). "Feedback from horizontal cells to cones mediates color induction and may facilitate color constancy in rainbow trout". In: *PLoS ONE* 8.6, pp. 1–11.
- Sagi, D. and S. Hochstein (1985). "Lateral inhibition between spatially adjacent spatial-frequency channels?" In: *Perception & Psychophysics* 37.4, pp. 315–322.
- Schachar, R. A. (1976). "The 'pincushion grid' illusion". In: *Science* 192.4237, pp. 389–390.
- Schiller, P. H., B. L. Finlay, and S. F. Volman (1976). "Quantitative studies of single-cell properties in monkey striate cortex. I. Spatiotemporal organization of receptive fields". In: *The Journal of Neurophysiology* 39.6, pp. 1288–1319.
- Schober, H. and H. Munker (1967). "Untersuchungen zu den Übertragungseigenschaften des Gesichtsinns für die Farbinformation". In: *Vision Research* 7.11-12, pp. 1015–1026.
- Science Photo Library (2018). *Refraction in a glass of water*. URL: www.sciencephoto.com (visited on 10/25/2018).
- Serre, T. and M. Riesenhuber (2004). *Realistic modeling of simple and complex cell tuning in the HMAX model, and implications for invariant object recognition in cortex*. Tech. rep. AI-MEMO-2004-017. Massachusetts Inst. of Tech. Cambridge Computer Science and Artificial Intelligence Lab., pp. 1–11.
- Serre, T. et al. (2007). "Robust object recognition with cortex-like mechanisms". In: *IEEE Transactions on Pattern Analysis and Machine Intelligence* 29.3, pp. 411–426.
- Shapley, R. M. and M. J. Hawken (2002). "Neural mechanisms for color perception in the primary visual cortex". In: *Current Opinion in Neurobiology* 12.4, pp. 426–432.
- (2011). "Color in the Cortex: single- and double-opponent cells". In: *Vision Research* 51.7, pp. 701–717.
- Shapley, R. M., M. J. Hawken, and E. N. Johnson (2014). "Color in the Primary Visual Cortex". In: *The New Visual Neurosciences*. Ed. by J. S. Werner and L. M. Chalupa. Cambridge, Massachusetts: The MIT Press, pp. 569–586.
- Shapley, R. M., M. J. Hawken, and D. L. Ringach (2003). "Dynamics of orientation selectivity in the primary visual cortex and the importance of cortical inhibition". In: *Neuron* 38.5, pp. 689–699.
- Sherman, S. M. and R. W. Guillery (1998). "On the actions that one nerve cell can have on another: Distinguishing 'drivers' from 'modulators'". In: *Proceedings of the National Academy of Sciences of the United States of America* 95.12, pp. 7121–7126.
- Shevell, S. K. and T. J. Burroughs (1988). "Light spread and scatter from some common adapting stimuli: computations based on the point-source light profile". In: *Vision Research* 28.5, pp. 605–609.

- Shushruth, S. et al. (2009). "Comparison of spatial summation properties of neurons in macaque V1 and V2". In: *The Journal of Neurophysiology* 102, pp. 2069–2083.
- Sincich, L. C. and J. C. Horton (2005). "The circuitry of V1 and V2: integration of color, form, and motion". In: *Annual Review of Neuroscience* 28, pp. 303–326.
- Singer, B. and M. D'Zmura (1994). "Color contrast induction". In: *Vision Research* 34.23, pp. 3111–3126.
- Singh, I. (2006). "A Brief Review of the Techniques Used in the Study of Neuroanatomy". In: *Textbook of Human Neuroanatomy*. New Delhi, India: Jaypee Brothers Medical Publishers.
- Skottun, B. C. (2013). "On using isoluminant stimuli to separate magno- and parvocellular responses in psychophysical experiments - A few words of caution". In: *Behavior Research Methods* 45, pp. 637–645.
- Smith, V. C., P. Q. Jin, and J. Pokorny (2001). "The role of spatial frequency in color induction". In: *Vision Research* 41.8, pp. 1007–1021.
- Smith, V. C. and J. Pokorny (1975). "Spectral sensitivity of the foveal cone photopigments between 400 and 500 nm". In: *Vision Research* 15, pp. 161–171.
- Snowden, R., P. Thompson, and T. Troscianko (2006). *Basic Vision an Introduction to Visual Perception*. New York, Oxford: Oxford University Press.
- Solomon, S. G. and P. Lennie (2007). "The machinery of colour vision". In: *Nature Reviews Neuroscience* 8.4, pp. 276–286.
- Solomon, S. G., J. W. Peirce, and P. Lennie (2004). "The impact of suppressive surround on chromatic properties of cortical neurons". In: *The Journal of Neuroscience* 24.1, pp. 148–160.
- Sompolinsky, H. and R. M. Shapley (1997). "New perspectives on the mechanisms for orientation selectivity". In: *Current Opinion in Neurobiology* 7.4, pp. 514–522.
- Spitzer, H. and Y. Barkan (2005). "Computational adaptation model and its predictions for color induction of first and second orders". In: *Vision Research* 45.27, pp. 3323–3342.
- Stemmler, M., M. Usher, and E. Niebur (1995). "Lateral interactions in primary visual cortex: a model bridging physiology and psychophysics". In: *Science* 269.5232, pp. 1877–1880.
- Stettler, D. D. et al. (2002). "Lateral connectivity and contextual interactions in macaque primary visual cortex". In: *Neuron* 36.4, pp. 739–750.
- Stockman, A. and D. H. Brainard (2010). "Color vision mechanisms". In: *The Optical Society of America Handbook of Optics*. Ed. by M. Bass et al. Vol. 3: Vision and Vision Optics. New York: McGraw Hill. Chap. 11, pp. 11.1–11.84.
- Sumner, P. and J. D. Mollon (2003). "Did primate trichromacy evolve for frugivory or folivory?" In: *Normal and defective colour vision* 4.3, pp. 21–30.
- Thorell, L. G., R. L. de Valois, and D. G. Albrecht (1984). "Spatial mapping of monkey V1 cells with pure color and luminance stimuli". In: *Vision Research* 24, pp. 751–769.
- Todorovic, D. M. (2017). "A computational account of a class of orientation illusions". In: *ModVis, Computational and Mathematical Models in Vision*.
- Tolhurst, D. J. and L. P. Barfield (1978). "Interactions between spatial frequency channels". In: *Vision Research* 18.8, pp. 951–958.
- Tumblin, J. and H. Rushmeier (1993). "Tone Reproduction for Realistic Images". In: *IEEE Computer Graphics and Applications* 13.6, pp. 42–4.
- Van Kleef, J. P., S. L. Cloherty, and M. R. Ibbotson (2010). "Complex cell receptive fields: evidence for a hierarchical mechanism". In: *The Journal of Physiology* 588.18, pp. 3457–3470.

- Van Tuijl, H. F. J. M. (1975). "A new visual illusion: neonlike color spreading and complementary color induction between subjective contours". In: *Acta Psychologica* 39, pp. 441–445.
- Van Tuijl, H. F. J. M. and C. M. De Weert (1979). "Sensory conditions for the occurrence of the neon spreading illusion". In: *Perception* 8, pp. 211–215.
- Van de Sande, K., T. Gevers, and C. Snoek (2010). "Evaluating color descriptors for object and scene recognition". In: *IEEE Transactions on Pattern Analysis and Machine Intelligence* 32.9, pp. 1582–1596.
- VanLeeuwen, M. T. et al. (2007). "The contribution of the outer retina to color constancy: A general model for color constancy synthesized from primate and fish data". In: *Visual Neuroscience* 24.3, pp. 277–290.
- Verweij, J., M. Kamermans, and H. Spekreijse (1996). "Horizontal cells feed back to cones by shifting the cone calcium-current activation range". In: *Vision Research* 36.24, pp. 3943–3953.
- Von Bezold, W. (1876). *The theory of color and its relation to art and art-industry*. Boston: L. Prang and Company.
- Wagner, G. and R. Boynton (1972). "Comparison of four methods of heterochromatic photometry". In: *Journal of Optical Society of America A* 62.12, pp. 1508–1515.
- Ward, G. (1994). "A contrast-based scalefactor for luminance display". In: *Graphics gems IV*. San Diego, CA: Academic Press Professional, Inc, pp. 415–421.
- Watanabe, T. and T. Sato (1989). "Effects of luminance contrast on color spreading and illusory contour in the neon color spreading effect". In: *Perception & Psychophysics* 45.4, pp. 427–430.
- Watson, N. V. and S. M. Breedlove (2015). "Vision: From Eye to Brain". In: *The Mind's Machine: Foundations of Brain and Behavior*. Massachusetts, USA: Sinauer Associates. Chap. 7.
- Weisstein, E. W. (2018). *Fourier Series–Square Wave*. URL: <http://mathworld.wolfram.com/FourierSeriesSquareWave.html> (visited on 06/25/2018).
- White, M. (1979). "A new effect of pattern on perceived lightness". In: *Perception* 8.4, pp. 413–416.
- Wiesel, T. N. and D. H. Hubel (1966). "Spatial and chromatic interactions in the lateral geniculate body of the rhesus monkey". In: *The Journal of Neurophysiology* 29.6, pp. 1115–1156.
- Williams, D. R. et al. (1994). "Double-pass and interferometric measures of the optical quality of the eye". In: *Journal of the Optical Society of America A* 11.12, pp. 3123–3134.
- Wilson, H. R. and J. D. Cowan (1972). "Excitatory and inhibitory interactions in localized populations of model neurons". In: *Biophysical Journal* 12.1, pp. 1–24.
- Wong-Riley, M. (1979). "Changes in the visual system of monocularly sutured or enucleated cats demonstrable with cytochrome oxidase histochemistry". In: *Brain Research* 171.1, pp. 11–28.
- Xing, D. et al. (2005). "Effect of stimulus size on the dynamics of orientation selectivity in macaque V1". In: *The Journal of Neurophysiology* 94.1, pp. 799–812.
- Xing, D. et al. (2011). "Untuned suppression makes a major contribution to the enhancement of orientation selectivity in macaque V1". In: *The Journal of Neuroscience* 31.44, pp. 15972–15982.
- Xing, D. et al. (2015). "Brightness-color interactions in human early visual cortex". In: *The Journal of Neuroscience* 35.5, pp. 2226–2232.
- Yang, K. et al. (2013). "Efficient color boundary detection with color-opponent mechanisms". In: *The IEEE Conference on Computer Vision and Pattern Recognition (CVPR)*, pp. 2810–2817.

- Yeganeh, H. and Z. Wang (2012). "Objective Quality Assessment of Tone-Mapped Images". In: *IEEE Transactions on Image Processing* 22.2, pp. 657–667.
- Yeh, C. et al. (2009). "Stimulus ensemble and cortical layer determine V1 spatial receptive fields". In: *Proceedings of the National Academy of Sciences of the United States of America* 106.34, pp. 14652–14657.
- Yoshida, A. et al. (2005). "Perceptual Evaluation of Tone Mapping Operators with Real-World Scenes". In: *Human Vision & Electronic Imaging X*. SPIE.
- (2007). "Testing Tone Mapping Operators with Human-Perceived Reality". In: vol. 16. 1.
- Zaidi, Q. (1999). "Color and brightness induction: from Mach bands to three-dimensional configurations". In: *Color Vision: From genes to perception*. Ed. by K. R. Gegenfurtner and L. T. Sharpe. Cambridge, UK: Cambridge University Press, pp. 317–344.
- Zaidi, Q. et al. (1992). "Lateral interactions within color mechanism in simultaneous induced contrast". In: *Vision Research* 32.9, pp. 1695–1707.